TGA-FTIR study of the vapours released by volatile corrosion inhibitor model systems

by

Nontete Suzan Nhlapo

A thesis submitted in partial fulfilment

of the requirements for the degree

Doctor of Philosophy

in the

Department of Chemical Engineering

Faculty of Engineering, the Built Environment and Information Technology

University of Pretoria

Pretoria

July 2013

TGA-FTIR study of the vapours released by volatile corrosion inhibitor model systems

Author: Nontete Suzan Nhlapo

Supervisor: Prof. Walter W. Focke

Co-supervisor: Dr Eino Vuorinen

Degree: PhD (Chemical Technology)

Department: Chemical Engineering

ABSTRACT

Proprietary mixtures of amines and carboxylic acids are used as volatile corrosion inhibitors (VCIs) for the protection of steel and iron components against atmospheric corrosion during storage and transportation. Interactions between amines and carboxylic acids have been comprehensively reported in the literature. However, little is known about the nature of the vapours these mixtures emit. The present study focused on the development of the evolved gas analysis method which will help in the characterisation of the vapours released by VCIs. In the method, the evaporation of various amine-carboxylic acid binary mixtures was monitored by thermogravimetric analysis (TGA). The nature and the composition of the released vapours was followed by Fourier transform infrared (FTIR) spectroscopy. Mixtures consisting of triethylamine (TEA) and acetic acid were studied as a model compound using TGA-FTIR at 50 °C to validate the TGA-FTIR method. As vaporisation progressed, the composition of the remaining liquid and the emitted vapour converged to a fixed amine content of ca. 27 mol %. This is just above the composition expected for the 1:3 amine: carboxylic acid complex. Mixtures close to this composition also featured the lowest volatility. TGA-FTIR proved to be a convenient method for studying the evaporation of TEA-acetic acid mixtures, and the nature and composition of the released vapours.

Amine addition leads to the dissociation of carboxylic acid dimers in favour salt formation. The formation of an ion pair between the amine and carboxylic acid was confirmed by the

FTIR spectra of the liquid phase. The resulting amine-carboxylic acid mixtures showed a slow mass loss rate on TGA when compared with the pure amines and pure carboxylic acids. This indicated that the mixtures have low volatility, hence low vapour pressure compared with the pure components. The low vapour pressure of the mixtures was confirmed by the calculated gas permeability values. These values were much higher for the pure amines and the pure carboxylic acids. However, they dropped significantly on amine addition. The strong amine-carboxylic acid interaction is responsible for the suppressed volatility of the mixtures. No interaction is observed between amine and carboxylic acid molecules in the vapour phase at 230 °C.

The method developed was applied to characterise the model compounds simulating the amine-carboxylic acid-based volatile corrosion inhibitors. These model systems contained the primary, secondary and tertiary amines (hexylamine, morpholine and triethylamine), as well as carboxylic acids with different chain lengths (acetic, propanoic, hexanoic and octanoic). These systems are usually employed as equimolar mixtures to protect ferrous metals against atmospheric corrosion. The key finding of the study was that the vapours released by such equimolar mixtures initially contain almost exclusively free amine. After prolonged vaporisation, a steady-state “azeotrope”-like composition is approached. It contains excess acid and features impaired corrosion-inhibition efficiencies according to the Skinner test. In part, this behaviour can be attributed to the mismatch between the volatilities of the amine and carboxylic acid constituents.

Keywords: Amines, carboxylic acids, VCIs, atmospheric corrosion, evaporation, vapour pressure, gas permeability, corrosion efficiency, TGA-FTIR

DEDICATION

This dissertation is dedicated to my late father Nopagatha Daniel Nhlapo, my mom Ntsoaki Lizbeth Moshoadiba (Masephoso), and my brother Molendazo Simon Nhlapo for their understanding and encouragement, and for being my great source of inspiration and motivation during all these years of study. Most of all, for believing in me …!

"In the confrontation between the river and the rock, the river always wins...not by strength, but by perseverance."-Unknown

ACKNOWLEDGEMENTS

Financial support for this research, from the National Metrology Institute of South Africa (NMISA), the Institutional Research Development Programme (IRDP) of the National Research Foundation of South Africa, the University of Pretoria and Xyris Technology CC, is gratefully acknowledged.

I am greatly indebted to the following people since without their support this study would not have been possible:

- Prof Walter W. Focke for his great supervision, guidance and encouragement throughout the study.
- Dr Eino Vuorinen from NMISA for his mentorship, valuable suggestions and encouragement throughout the study, and the organic chemistry group of NMISA for their support (Dr Maria Fernandes-Whaley, thank you).
- Ollie del Fabbro and Isbe van der Westerhuizen from the Institute of Applied Materials (IAM) for their patience during experimental setups and TGA runs.
- Dr Liezel van der Merwe for giving me time on the DSC instrument.
- Suzette Seymore for ordering the reagents, among others – thank you very much Suzette.
- My colleagues at IAM, University of Pretoria: Shepherd Tichapondwa, Washington Mhike, Mthokozisi Sibanda, Herminio Muiambo and Hendrik Oosthuizen for their valuable inputs.
- My dearest friends: Lumbidzani Moyo, Jabu Mabena, Sibusiso Jozela and Sechaba Masiteng for their inputs, constant support, and for being my great source of motivation during my down-times.
- My family: My sisters (Nozika, Nomthemba and Nonhlupheko, Mpolokeng Makhanya) and brothers (Mphikeleli and Mfokazana) for being there for me throughout the duration of the study.

Last but not least, God Almighty for his strength and protection … Most of all for bringing me this far...(*To Him be the Glory Forever: Romans: 11:33-37*)

DECLARATION

I, the undersigned, declare that the dissertation, which I hereby submit for the PhD degree at the University of Pretoria, is my own work and has not previously been submitted by me for the degree at this or any other tertiary institution.

……

Nontete Suzan Nhlapo

Contents

Abstract ..... **i**

Dedication ..... **iii**

Acknowledgements ..... **iv**

Declaration ..... **v**

List of Figures ..... **ix**

List of Tables ..... **xiv**

List of Schemes ..... **xv**

List of Abbreviations ..... **xvi**

List of Symbols ..... **xviii**

1 Introduction and Aim of Study **1**

1.1 Introduction 1

1.2 Brief history of VCIs 3

1.3 Problem statement 4

1.4 Aims and objectives 5

1.5 Dissertation outline 7

2 Literature review **8**

2.1 VCI formulations 11

2.2 VCI mechanism of action 12

2.3 Compounds used as VCIs 13

2.4 Review of the methods used to test the effectiveness of VCIs 14

2.4.1 Skinner's test method 14

2.4.2 Conical flask method 16

2.4.3 Electrochemical measurement methods 16

2.4.4 Eschke's test method 17

2.4.5 Other corrosion inhibition test methods 17

2.5 Factors affecting the effectiveness of VCIs 17

2.5.1 pH of the system 18

2.5.2 Concentration of an inhibitor 18

2.5.3 Temperature and humidity 19
2.5.4 Vapour pressure 19
2.5.5 Other factors 20
2.6 Amine-carboxylic acid interactions 21
2.7 The effect of water 26
2.8 Review of amine-carboxylic acid characterisation methods 27
2.8.1 Ultraviolet visible (UV-Vis) spectroscopy 28
2.8.2 Nuclear magnetic resonance (NMR) spectroscopy 28
2.8.3 Fourier transform infrared (FTIR) spectroscopy 28
2.8.4 Thermo-gravimetric analysis (TGA) 30
2.8.5 Coupling TGA with FTIR 31

3 Experimental 34

3.1 Reagents and suppliers 34
3.2 Experimental methods 35
3.3 Instrumentation 37

4 Results 40

Part 1: Method Development 40

4.1 Liquid phase FTIR 41
4.2 DSC 43
4.3 TGA-FTIR 44

Part 2: Method Application 54

4.4 Liquid phase FTIR and refractive index 54
4.5 Liquid phase DSC 58
4.6 TGA 62
4.7 Vapour phase FTIR 71
4.8 Corrosion tests 79

5 Discussion 81

6 Conclusion 89

References 91

Publications 101

Appendices **102**

Appendix A: The refractive index values of the pure components and the mixtures determined at 20 °C 102

Appendix B: Liquid phase FTIR spectra 103

Appendix C: Time evolution FTIR spectra of binary amine-carboxylic acids 108

Appendix D: Calibration curves 111

Appendix E: Shape functions 113

Appendix F: PiD_{Ai} profiles of pure amines, pure carboxylic acids and their mixtures 115

LIST OF FIGURES

Figure 1: Mechanism of the atmospheric corrosion process of iron.....9

Figure 2: Corrosion test method developed by Skinner (1993) (diagram adopted from Skinner, 1993) 15

Figure 3: TGA pan dimensions (where d refers to the diameter and h the height) 38

Figure 4: Phase diagram of TEA-acetic acid binary mixtures; ◊ indicates LLE data obtained by Kohler *et al*. (1972), ○ indicates LLE data, ♦ and Δ VLE data obtained by Van Klooster & Douglas (1945) at atmospheric pressure, and ● LLE data obtained in the present study.....40

Figure 5: Liquid phase and vapour phase spectra of (a) pure acetic acid and (b) pure TEA..42

Figure 6: Liquid phase FTIR spectra of binary acetic acid-TEA mixtures in comparison with pure acetic acid and pure TEA 43

Figure 7: DSC profiles of acetic acid-TEA binary mixtures in comparison with pure acetic acid and pure TEA.....44

Figure 8: TGA-FTIR data for heating sodium bicarbonate from 25 °C to 400 °C at a scan rate of 20 °C min^{-1} in nitrogen gas flowing at a rate of 50 mL min^{-1}. The maximum absorbance of the band located near 2300 wavenumbers in the FTIR spectrum (□) and the TGA derivative mass signal shifted by a time interval of 0.56 min (▲) are shown 45

Figure 9: TGA evaporation profiles of selected acetic acid-TEA binary mixtures compared with pure acetic acid and pure TEA 45

Figure 10: Time evolution of the gas phase FTIR spectra for a mixture with initial composition z_A = 0.33 (a) and z_A = 0.20 (b) as a function of mass fraction evaporated. The arrows indicating the time direction and the spectra for pure TEA and pure acetic acid are shown for comparison.....46

Figure 11: TEA and acetic acid calibration curves used for the determination of the proportionality constants 47

Figure 12: Shape function profiles α for pure acetic acid, pure TEA and experimental data (Δ) for a vapour mixture. The solid line for the mixture was generated using Equation (7) with the β_{mix} = 0.638 value determined via a least squares curve fit. According to calculations using Equations (8) and (9), this indicates that the mixture contained approximately 25 mol % amine.....48

Figure 13: Time dependence of the mole fraction of TEA present in the released vapour. The indicated TEA concentrations refer to the initial TEA content of the liquid phase 50

Figure 14: Mole fraction of TEA released into the vapour phase as a function of the fraction of VCI released. The indicated TEA concentrations refer to the initial TEA content of the liquid phase.....51

Figure 15: Evaporation trend obtained for TEA-acetic acid binary mixtures 52

Figure 16: Calculated mole fractions of TEA in the liquid phase as a function of the initial mixture composition and the fraction of VCI released. The indicated TEA concentrations refer to the initial content of the liquid phase 53

Figure 17: Liquid phase FTIR spectra of binary mixtures of triethylamine and hexanoic acid. The absorption maximum at ca. 1560 cm^{-1} is attained at a composition corresponding to the A_1C_3 complex, i.e. z_A = 0.25.....54

Figure 18: The effect of amine addition on the position of the FTIR absorption bands due to carboxylic acid (C=O), carboxylate ion (COO^-) and the protonated amine in the mixtures with amines (hexylamine and TEA) with octanoic acid 55

Figure 19: The effect of amine addition on the position of the FTIR absorption bands due to carboxylic acid (C=O), carboxylate ion (COO^-) and the protonated amine in the mixtures of morpholine with octanoic acid.....56

Figure 20: The effect of liquid phase composition on the absorbance maximum near 1560 cm^{-1} in the FTIR spectra of binary mixtures of the various amines with octanoic acid. The absorption maximum at ca. 1560 cm^{-1} is attained at a composition corresponding to the A_1C_3 complex for TEA, but for the other two amines it corresponds to the A_2C_2 complex, i.e. z_A = 0.50 57

Figure 21: The effect of liquid phase composition on the refractive index of amine-propanoic (A) and amine-hexanoic acid (B) mixtures at 20 °C. The 1:1 and 2:1 (mole basis) mixtures of hexanoic acid and the 1:1 mixture of propanoic acid with morpholine are not reported because they were solids at this temperature 57

Figure 22: DSC traces of pure amines (A) and pure carboxylic acids (B) 58

Figure 23: DSC traces of binary hexylamine and (A) acetic, (B) propanoic, (C), hexanoic and (D) octanoic acid mixtures in comparison with pure hexylamine and pure carboxylic acids 59

Figure 24: DSC traces of secondary amine, morpholine, with octanoic acid mixtures.....60

Figure 25: DSC scans of binary TEA systems with (a) hexanoic and (b) octanoic acid mixtures 61

Figure 26: DSC results for liquid mixtures: —Δ— DSC melting peak temperatures for hexylamine-octanoic acid mixtures; – –○ – – vaporisation enthalpies; and — □ — vaporisation peak temperatures for triethylamine-octanoic acid mixtures.....61

Figure 27: TGA evaporation rates for the neat amines and carboxylic acids measured at 50 °C.....62

Figure 28: TGA evaporation profiles of hexylamine and (A) acetic, (B) propanoic, (C) hexanoic and (D) octanoic acid binary mixtures compared with those of pure hexylamine and pure carboxylic acids 63

Figure 29: Time it takes to reach the selected fractional mass loss values as a function of composition of the mixtures for (A) hexylamine-acetic, (B) hexylamine-propanoic, (C) hexylamine-hexanoic and (D) hexylamine-octanoic acid.....64

Figure 30: TGA evaporation profiles of morpholine and (A) acetic, (B) propanoic, (C) hexanoic and (D) octanoic acid binary mixture compared to pure morpholine and pure carboxylic acids.....66

Figure 31: Time it takes to reach the selected fractional mass loss values as a function of composition of the mixture for (A) morpholine-acetic, (B) morpholine-propanoic, (C) morpholine-hexanoic and (D) morpholine-octanoic acid 67

Figure 32: TGA evaporation profiles of TEA and the (A) acetic, (B) propanoic, (C) hexanoic and (D) octanoic acid binary mixtures compared with pure morpholine and pure carboxylic acids 69

Figure 33: Time it takes to reach the selected fractional mass loss values as a function of the composition of the mixture for (A) TEA-acetic, (B) TEA-propanoic, (C) TEA-hexanoic and (D) TEA-octanoic acid 70

Figure 34: Time evolution of the vapour phase FTIR spectra for binary TEA-propanoic acid mixtures with initial composition (A) z_A = 0.20, (B) 0.25, (C) 0.50 and (D) 0.75 as a function of mass fraction evaporated. The arrows indicate the time direction. The spectra for pure TEA and pure propanoic acid are shown for comparison 72

Figure 35: Time evolution of the vapour phase FTIR spectra for (A) binary morpholine-hexanoic acid mixtures with initial composition z_A = 0.67 and (B) binary morpholine-octanoic acid mixtures with initial composition z_A = .0.50 as a function of mass fraction evaporated. The arrows indicate the time direction. The spectra for pure morpholine and pure carboxylic acids are shown for comparison 74

Figure 36: Mole fraction of TEA released into the vapour phase as a function of the percentage weight fraction released by the TEA-formic acid binary mixture with an initial composition of 33.3 mol % TEA 76

Figure 37: Mole fraction of amine in the released vapour (y_A) and the calculated amine mole fraction in the liquid phase (x_A) for the TEA-propanoic acid mixture with an initial composition (a) 33.3 and (b) 50 mol % TEA 77

Figure 38: Mole fraction of TEA released into the vapour phase as a function of the percentage weight fraction released by the TEA-propanoic acid binary mixture with an initial composition of 80 mol % TEA 78

Figure 39: Vapour-liquid “equilibrium” at 50 °C in the TEA-propanoic acid and morpholine-propanoic acid systems 78

Figure 40: Skinner corrosion test results on copper and mild steel for the amine-octanoic acid mixtures with amine contents of z_A = 0.25 and 0.50 79

Figure 41: Product of vapour pressure and diffusion coefficient of the morpholine-propanoic acid binary mixture compared with pure morpholine and pure propanoic acid.....84

LIST OF TABLES

Table 1: Reagents, molecular mass, melting and boiling points, and the suppliers.....34

Table 2: Experimentally determined proportionality constants for the neat amines and the neat carboxylic acids 75

Table 3: Experimental densities (ρ) of the neat amines, the neat carboxylic acids and the least volatile binary mixtures in the amine-carboxylic acid systems at 50 °C. The number in brackets indicates the concentration of the amine in the mixture in mol %.....83

Table 4: Gas permeability ($S_i = P_i D_{Ai}$) of the neat amines, the neat carboxylic acids and the least volatile binary mixtures in the amine-carboxylic acid systems at 50 °C. The number in brackets indicates the concentration of the amine in the mixture in mol % .85

Table 5: The experimental pH values for 5 wt.% solutions, in deionised water, of 1:1 and 1:3 mixtures of the amines with octanoic acid. 88

LIST OF SCHEMES

Scheme I: Schematic presentation of acetic acid dimer ring 22

Scheme II: Schematic presentation of (A) molecular and (B) ionic amine-carboxylic acid (A_1C_1) complex (Tamada & King, 1990).....22

Scheme III: Schematic presentation of the 1:3 amine-carboxylic acid complex (Tamada & King, 1990).....24

Scheme IV: Schematic presentation of the 1:2 amine-carboxylic acid complex (Tamada & King, 1990).....24

Scheme V: Schematic presentation of an amine-carboxylic acid mixture. A and C represent an amine and a carboxylic acid, while C···C and A^+C^- represent a hydrogen bonded carboxylic acid dimer and an amine-carboxylic acid salt respectively. 86

LIST OF ABBREVIATIONS

^{13}C-NMR	carbon-13-nuclear magnetic resonance spectroscopy
^{1}H-NMR	hydrogen-1-nuclear magnetic resonance spectroscopy
A	amine
C	carboxylic acid
DAHC	diaminohexane cinnamate
DAHM	diaminohexane maleate
DAHN	diaminohexane nitrobenzene
DAHO	diaminohexane orthophosphate
DAHP	diaminohexane phthalate
DEAP	1,3-bis-diethylamino-propan-2-ol
DICHAN	dicyclohexylammonium nitrite
DMP	1,3-di-morpholin-4-yl-propan-2-ol
DSC	differential scanning calorimetry
DTG	derivative thermogravimetry
EGA	evolved gas analysis
FTIR	Fourier transform infrared spectroscopy
FT-Raman	Fourier transform Raman spectroscopy
LLE	liquid-liquid equilibrium
Near-IR	near infrared spectroscopy
NMR	nuclear magnetic resonance spectroscopy
TEA	triethylamine
TGA	thermogravimetric analysis
UV	ultraviolet radiation
UV-Vis	ultraviolet visible spectroscopy
VCI(s)	volatile corrosion inhibitor(s)

VLE	vapour-liquid equilibrium
VpCI(s)	vapour phase corrosion inhibitors

LIST OF SYMBOLS

Beer's law equation

A	absorbance [-]
T	transmittance [-]
ε	absorptivity [-]
λ	wavelength [m]

Integrated area equation

A	dimensionless absorbance [-]
a_i	integrated area under the absorbance curve [cm^{-1}]
k_i	characteristic constant for component i [min mg^{-1} cm^{-1}]
l	layer thickness [m]
M_i	molecular mass of component i [kmol kg^{-1}]
m_i	mass of component i in liquid phase [kg]
$\dot{m}_i$	TGA mass flux (i.e. dm_i/dt) of component i entering gas phase [mg min^{-1}]
w_i	mass fraction component i in the vapour phase [-]
t	time [s]
x_i	mole fraction of component i in the liquid phase [-]
y_i	mole fraction of component i in the vapour phase [-]
z	distance from top of pan to liquid meniscus [m]
z_i	initial mole fraction of component i [-]
α_i	shape function for component i [-]
α_{mix}	shape function for a mixture [-]
β_i	characteristic measure of the mixture composition, equation 7 [-]
σ	wavenumber [cm^{-1}]

Corrosion efficiency equation

C_R	corrosion rate [µm $year^{-1}$]

Vapour pressure and diffusion coefficient equation

A	vaporisation surface area [m^2]
D_{Ai}	diffusion coefficient of component *i* in air [$m^2\ s^{-1}$]
M	molecular mass [$kg\ mol^{-1}$]
P_i	vapour pressure of component *i* [Pa]
R	universal gas constant [$J\ mol^{-1}\ K^{-1}$]
S	gas permeability [$Pa\ m^2\ s^{-1}$]
T	temperature [K] or [°C]
ρ	density of the liquid [$kg\ m^{-3}$]

Subscripts

A	Amine
C	Carboxylic acid
mix	mixture

1 INTRODUCTION AND AIM OF STUDY

1.1 Introduction

Atmospheric corrosion is defined as a natural process resulting from the individual or combined action of oxygen, moisture and contaminants (e.g. acid rain, hydrogen sulphide, chlorides) present in air with the metallic surface (Rozenfeld, 1981; Sastri, 1998; Roberge *et al.*, 2002; Andreev & Kuznetsov, 2005). Protection of metals against atmospheric corrosion with corrosion inhibitors is an intensively developing method. Corrosion inhibitors are compounds that when added to corrosive environments in relatively small quantities, drastically reduce the corrosion rate (Sastri, 1998; Vuorinen *et al.*, 2004). Corrosion inhibitors find application in a wide variety of industries such as petroleum, gas and water systems, engine coolants, construction and packaging (Sanyal, 1981; Ahmad, 2006).

The present study focuses on volatile corrosion inhibitors (VCIs), also referred to as vapour phase corrosion inhibitors (VpCIs) (Estevão & Nacimento, 2001; Bastidas *et al.*, 2005; Andreev & Kuznetsov, 2005). This subclass of VCIs is used to protect metal substrates against atmospheric corrosion during storage and transportation (Skinner, 1993; Roberge, 2000; Estevão & Nacimento, 2001; Vuorinen *et al.*, 2004; Andreev & Kuznetsov, 2005; Bastidas *et al.*, 2005; Choi *et al.*, 2012). The inhibitive mechanism comprises adsorption on the metal surface, followed by the formation of a passive film or a protective barrier layer which limits the penetration of corrosion-causing contaminants (Vuorinen *et al.*, 2004; Bastidas *et al.*, 2005; Andreev & Kuznetsov, 2005). The protective barrier layer does not alter the bulk properties of the metal (Bastidas *et al.*, 2005).

For an inhibitor to be classified as a VCI it must be sufficiently volatile to allow fast migration to the metal surface and rapid development of the protective layer (Vuorinen *et al.*, 2004; Bastidas *et al.*, 2005). The vapour must also be able to retard the corrosion rate (Ramachandran *et al.*, 1996; Bastidas *et al.*, 2005). Thus volatility is the main property of VCIs that distinguishes them from other corrosion inhibitors (Vuorinen & Skinner, 2002; Vuorinen *et al.*, 2004; Bastidas *et al.*, 2005). VCIs provide an effective, simple and reliable way of controlling corrosion in closed systems and environments (Skinner, 1993; Vuorinen *et al.*, 2004; Andreev & Kuznetsov, 2005). They volatilise at temperatures typical of tropical climates. They should be non-toxic and safe to use (Skinner, 1993; Vuorinen & Skinner, 2002). Proper use of VCIs considerably lengthens the service life of machinery without

promoting any other forms of corrosion, such as pitting (a localised form of corrosion that results in excessive metal loss or holes in the metal (Skinner, 1993).

The efficiency of VCIs is affected by the ambient temperature and humidity, the concentration of the inhibitor and the method of application. It is also influenced by the presence of corrosive contaminants. Generally, VCIs prevent atmospheric corrosion, as long as the chemicals remain active (Dutton, 2004; Bastidas *et al.*, 2005). Metal packaging materials should therefore be chosen carefully to retain the VCIs and to prevent deactivation due to ultraviolet (UV) exposure (Badran *et al.*, 1982; Hassan *et al.*, 1990; Skinner *et al.*, 1999; Vuorinen & Skinner, 2002; Vuorinen *et al.*, 2004; Bastidas *et al.*, 2005; Cano *et al.*, 2005; Vuorinen & Focke, 2006).

A wide range of chemical compounds have been proposed as VCIs (Vuorinen & Skinner, 2002; Quraishi & Jamal, 2002; Andreev & Kuznetsov, 2005; Bastidas *et al.*, 2005; Rammelt *et al.*, 2011). Amines, carboxylic acids and, in particular, their mixtures are used as VCIs to protect steel and ferrous metals against atmospheric corrosion during storage and transportation (Vuorinen & Skinner, 2002; Bastidas *et al.*, 2005; Vuorinen & Focke, 2006; Kondo, 2008; Rammelt *et al.*, 2009). Suitable combinations show a synergistic effect that is attributed to the development of a thicker barrier layer on the metal surface, which limits the penetration of corrosion-causing contaminants (Bommersbach *et al.*, 2005). The interactions between amines (A) and carboxylic acids (C) are therefore particularly relevant to this class of VCIs. These interactions have been comprehensively investigated in many studies (Kohler *et al.*, 1972; Kohler & Hyskens, 1976; Hyskens *et al.*, 1980; Kohler *et al.*, 1981a & b; Karlsson *et al.*, 2001; Orzechowski *et al.*, 2000). Carboxylic acids have a strong tendency to dimerise as each pair can form two hydrogen bonds in a planar ring formation (Kohler *et al.*, 1981a & b). Amines and carboxylic acids can also interact strongly via Brønsted-Lowry acid-base reactions and hydrogen bonding interactions to form a series of AC_n complexes, with n ranging from 1 to 3 (Kohler *et al.*, 1972; Kohler & Hyskens, 1976; Bobik, 1977; Kubilda & Schreiber, 1978; Kohler *et al.*, 1981a; Pajdowska & Sobczyk, 1982; Wiezejewska-Hnat *et al.*, 1980; Friberg *et al.*, 1990; Karlsson *et al.*, 2001; Päivärinta *et al.*, 2001). The A_1C_1 ionic complex requires stabilisation. *Ab initio* calculations have shown that, at equimolar mixing ratios, the formation of an A_2C_2 complex is more likely (Kohler *et al.*, 1981a; Päivärinta *et al.*, 2001; Karlsson *et al.*, 2001). In the absence of water and in the presence of excess carboxylic acid, the A_1C_1 complex of tertiary amines is stabilised by reacting with the cyclic dimers of the carboxylic acid, forming the A_1C_3 complex (Kohler & Hyskens, 1976; Bobik,

1977; Päivärinta *et al.*, 2001). However, when the tertiary amine is replaced with a secondary or a primary amine, the situation changes and the 1:1 complex becomes increasingly important. In the case of primary amines, there is a tendency for these to form large clusters (Kohler *et al.*, 1981a & b).

In commercial practice amine-carboxylic acid-based VCIs are generally incorporated into polymeric films, coatings, greases, functional fluids, cleaning systems, hydro-testing solutions and concrete, and in capsules. In some instances VCIs have also been adsorbed onto diatomaceous earth and zeolites for controlled release (Estevão & Nacimento, 2001; Vuorinen & Skinner, 2002; Boyle, 2004; Vuorinen & Focke, 2006; Rammelt *et al.*, 2009; Choi *et al.*, 2012). The VCI-containing film is then used to wrap metallic equipment during storage and transportation (Vuorinen & Skinner, 2002; Bastidas *et al.*, 2005; Rammelt *et al.*, 2009). The efficiency of amine-based corrosion inhibitors results from their ability to form a hydrophobic adsorption layer to shield the metal surface from corrosive contaminants (Rammelt *et al.*, 2011).

1.2 Brief history of VCIs

In the past a protective oil coating was utilised to protect metallic equipment from atmospheric corrosion during storage and transportation (Vuorinen *et al.*, 2004; Vuorinen & Focke, 2006). The problem with this was that it was necessary to remove the oily coating from the surface of the metal before applying paint or welding. This extra step increases costs and the method was also not practical enough (Pereira & Tavares, 2004; Vuorinen & Focke, 2006).

The discovery of VCIs dates back to the early 1900s. During this period VCIs were developed for the protection of ferrous metals in tropical environments (Miksic, 1975). Shell patented the use of VCIs for corrosion inhibition in the 1940s (Andreev & Kuznetsov, 2005). The first VCI chemical to be discovered was dicyclohexylammonium nitrite, abbreviated to DICHAN. Following this discovery, DICHAN was then utilised to protect military equipment in the Second World War. However, the approach proved limiting because of the incompatibility of these VCIs with non-ferrous metals (Miksic, 1975). The use of VCIs was later adopted and modified by other companies as a powder and paper coating to protect other metallic parts from corrosion as well. The main challenge at the time was that the nitrite only protects iron and aluminium, but attacks copper and bronze. The disposal of nitrites was also

causing environmental problems and it was difficult to calculate the exact application dose (VCI-2000).

Solutions to some of these problems were devised in the 1950s (VCI-2000). Continued research provided new methods and new products with improved inhibition efficiencies. Nitrites are still acceptable in most countries, e.g. the United States, and Japan and Germany continue to produce sodium nitrite products because they are inexpensive. In addition, sodium nitrites have performed well in number of tests. The result is that the environmental implications are largely ignored. From the 1970s to date research into alternative VCIs for different metallic surfaces has received considerable attention. New methods have been developed and alternative VCIs are now commercially available in a wide variety of forms. Recent investigations revealed that the active ingredient in VCIs includes products of the reaction between a volatile amine (or amine derivative) and an organic acid. These VCI products are referred to as 'amine carboxylates'. Widely used amines in VCIs include cyclohexylamine, dicyclohexylamine, guanidine and other primary, secondary and tertiary amines (Kuznetsov *et al.*, 2007).

1.3 Problem statement

Corrosion products may form away from the surface of the corroding metal, resulting in an uneven surface. This makes it difficult to control the atmospheric corrosion process and later results in metals developing holes and even in metal failure. When this happens, problems such as fires, explosions, leakages, factory blasts, collapse of bridges, pollution and environmental catastrophe may occur (Bastidas *et al.*, 2005; Hays, 2010). The direct cost of corrosion worldwide is estimated to be between 1.3 and 1.4 trillion Euros, i.e. approximately 3.1 to 3.5% of annual worldwide gross domestic product (GDP) (Hays, 2010). This figure does not include environmental damage, waste of resources, loss of production and personal injuries caused by corrosion (Hays, 2010). A study conducted by the University of the Witwatersrand estimated that the direct cost of corrosion to the South African economy was R154 billion in 2005. The metals most affected are iron and steel (Hays, 2010).

A sound knowledge and study of the corrosion process will help in choosing the design and materials necessary for maintaining high standards in the metals industry. In order to produce metals from their ores, an input energy is required (Myles & Associates, 1995) and energy is an expensive commodity (Hays, 2010). Corrosion prevention will increase the service life of the metal, reduce the unnecessary costs caused by corrosion and result in energy saving. The

VCIs method of protection provides a reliable way of controlling atmospheric corrosion in a closed system/environment.

By definition, a VCI is a volatile compound (or mixture of such compounds) capable of forming a relatively stable bond at the metal interface, thus limiting atmospheric corrosion (Bastidas *et al.*, 2006). Vapour pressure is an important parameter in determining the effectiveness of VCIs. A vapour pressure that is too low leads to the slow establishment of corrosion protection, which may result in it being insufficient. On the other hand, if the vapour pressure is too high, the effectiveness of VCIs will be limited to a short period of action due to high consumption rates. Therefore the VCIs must have enough vapour pressure in order to ensure rapid protection of metals because too high a volatility may lead to an early loss of and inhibitor's activity (Estevão & Nacimento, 2001; Bastidas *et al.*, 2005; Andreev & Kuznetsov, 2005; Pieterse *et al.*, 2006).

Amines and carboxylic acid mixtures are used as VCIs to protect metals such as iron and steel from atmospheric corrosion, as already mentioned. The vapour pressure of amine-carboxylic acid mixtures at ambient temperature is very low (Pieterse *et al.*, 2006). Therefore studies in the gas phase pose many difficulties because the experiments have to be carried out at high temperatures. A solution to some of these problems was devised by using the infrared matrix isolation technique (Wiezejewska-Hnat *et al.*, 1980). However, it is difficult to avoid the adsorption of carboxylic acids on the surface of the needle valves during the deposition of the gas mixture when using the matrix isolation technique. This makes determining the actual mixture composition in the gas phase complicated. Kubilda & Schreiber (1978) used Fourier transform infrared spectroscopy (FTIR) to study trimethylamine mixtures with acetic acid and trifluoroacetic acid at high temperatures. However, they did not disclose how the gaseous spectra were collected. Due to the complications encountered, excess amine was used frequently to prevent formation of carboxylic acid dimer and to avoid contamination, making it possible to study only the A_1C_1 complex.

1.4 Aims and objectives

The study of the vaporisation of amine-carboxylic acid-based VCI model systems may provide a solution to some of the problems encountered when using VCIs. It is therefore of importance to understand the nature, the mechanism of action and the implications of volatile actives. The considerable work done in the area of amine carboxylic acid has focused mainly on determining the density, viscosity and melting and boiling points, on volumetric

measurements, ultrasonic relaxation and on the Raman, nuclear magnetic resonance (NMR) and FTIR spectra (Kohler *et al.*, 1972; 1974; Bobik, 1977; Kohler *et al.*, 1981a & b; Hafaiedh *et al.*, 2009).

The literature on the characterisation of the vapours released by VCIs is limited. The aim of the present study is to develop a thermo-gravimetric analysis (TGA) method that will help in the characterisation of the composition of the vapours released by VCIs. This characterisation method may provide reasons for the strange behavioural reports that corrosion is enhanced when non-stoichiometric amounts or too little are used. In spite of the fact that VCIs have been used for many years for inhibiting atmospheric corrosion, their mechanism of action is still not completely clear and this study may also help to clarify the mechanism of action of VCIs.

The present study is divided into two parts. The first part introduces the proposed VCI characterisation method. In this part triethylamine (TEA)-acetic acid mixtures were used as the model compound to validate the method because much data was available on this system. The method involved studying the evaporation of amine-carboxylic acid binary mixtures using TGA, and examining the nature of the vapours released by FTIR. In addition, the released vapours were quantified in order to find out how much of each component was present in the vapour phase. The TGA-FTIR method was selected in this study because of the relatively low costs of the instrumentation, and the simplicity of these two techniques. The thesis also provides information on the individual layers of liquid-liquid phase-separated amine-carboxylic acid binary mixtures.

The second part of this study focuses on the application of the developed TGA-FTIR method of analysis to a series of VCI model systems containing primary, secondary and tertiary amines (hexylamine, morpholine and triethylamine) and aliphatic carboxylic acids with different chain lengths (acetic, propanoic, hexanoic and octanoic). Corrosion tests were also performed on these model systems to determine their effectiveness as VCIs on mild steel, galvanised steel and copper metals. As mentioned earlier, vapour pressure is an important parameter in the effectiveness of the VCI. Therefore the study also involved determining the products of vapour pressure and the diffusion coefficient of the model systems.

1.5 Dissertation outline

This dissertation is divided into five chapters. Chapter 1 gives a general overview of atmospheric corrosion, a brief introduction to corrosion inhibition, as well as the range of industries where corrosion inhibitors are used. This is followed by the classification of corrosion inhibitors and a brief background on volatile corrosion inhibitors. The chapter also discusses the problems encountered when corrosion is not controlled. This is followed by the aims and objectives of the present study.

Chapter 2 is the literature review. It starts by giving a detailed explanation of the corrosion process. This is followed by information on the commercially available forms of VCI, with the advantages and disadvantages of using a particular form. The mechanism of action of VCIs is also discussed. The chapter also reviews the different methods that are used to test the efficiency of VCIs, the factors affecting their effectiveness, amine carboxylic acid mixtures, and the effect of water on mixtures of amines and carboxylic acids. A brief review of the techniques used to characterise amine-carboxylic acid mixtures is presented. The chapter concludes by briefly discussing the coupling of thermo-gravimetric analysis (TGA) with Fourier transform infrared spectroscopy (FTIR).

Chapter 3 gives the information on all the experimental work carried out in the study, including the reagents and their properties. This chapter also gives the details on how the mixtures were prepared for the present study, the experimental conditions and the instrumentation used for characterisation.

Chapter 4 presents the results. This chapter is divided into two parts. The first part gives information on the development of the TGA-FTIR method using TEA (triethylamine)-acetic acid as the model compound. This chapter gives the liquid phase FTIR and DSC (differential scanning calorimetry) results, after which the results of the TGA study on the evaporation of mixtures and on following the emitted vapours by FTIR, are presented. The quantification procedure is fully described. The second part of the chapter focuses on the application of the developed TGA-FTIR method to the series of amine-carboxylic acid mixtures and also provides information on the corrosion tests that were performed.

Chapter 5 presents the discussion of the results. This chapter gives detailed discussions of all the results presented in Chapter 4.

This is followed by the conclusions in Chapter 6, the references and the appendices.

2 LITERATURE REVIEW

Atmospheric corrosion is an electrochemical process that involves acid-base interactions between the metal ions formed and other species present in the electrolyte (Ramachandran *et al.,* 1996; Roberge *et al.,* 2002). (An electrolyte is a solution containing free ions capable of conducting electrical current, such as moisture.) The rate of any given electrochemical corrosion process depends largely on the rate of an anodic and a cathodic reaction at the metal surface (Rozenfeld, 1981). Anodic reactions entail oxidation and consist of transferring a metal ion from the lattice to the solution, with the liberation of electrons (Rozenfeld, 1981).

Atmospheric corrosion is divided into two types: dry and wet corrosion (Du Preez, 1998). Dry atmospheric corrosion is a result of the direct chemical reaction of the metal with the environment, thereby forming the oxide layer on the surface of the metal. Wet corrosion is an electrochemical process and it takes place in neutral or acidic environments (Myles & Associates, 1995). The presence of an electrolyte is essential in wet corrosion (Du Preez, 1998).

Atmospheric corrosion occurs due to the high concentrations of oxygen in air, water or moisture droplets (from air) and of dissolved ions present on the surface of the metal (Kui *et al.,* 2008). If one considers metallic iron as an example (see Figure 1), iron is oxidised in the anodic region, resulting in the formation of soluble ferrous ions (Fe^{2+}), while the dissolved oxygen is reduced in the cathodic region to form OH^- ions. The ferrous ions and OH^- ions then combine to form a solid deposit $Fe(OH)_2$ on the metal surface. As the solubility of this solid deposit is relatively high, the dissolved $Fe(OH)_2$ can be further oxidised by access to dissolved atmospheric oxygen to form ferric ions (Fe^{3+}). These unstable ferric ions later convert to form an insoluble ferric oxide (Fe_2O_3) layer on the surface of the corroding iron metal (Roberge *et al,* 2002; Kui *et al.,* 2008; Tamura, 2008). This layer is commonly known as *rust*. The ferric ions in rust can be further reduced in the cathodic region to form FeO-Fe_2O_3 product, which contains both ferrous and ferric ions. The reduction of ferric ions is a cyclical process that can be speeded up by variations in the temperature and in the moisture coverage (Roberge *et al.,* 2002; Kui *et al.,* 2008). This results in the metal having an uneven surface and holes, which makes it difficult to stop the atmospheric corrosion process. The main factors that accelerate the atmospheric corrosion of metals are relative humidity, acid rain and trace volatile contaminants (pollutants), such as hydrochloric acid (Roberge *et al.,* 2002).

Relative humidity

Atmospheric corrosion requires a critical relative humidity level, below which corrosion does not occur (Syed, 2006). This level varies, depending largely on the nature of the corroding material and the tendency of the corrosion products and surface deposits to absorb moisture (Sastri, 1998; Roberge *et al.,* 2002). Values for the critical humidity level also differ for various pollutants. For example, the value is 60% for sulphur dioxide but higher for chloride pollutants (Sastri, 1998). The thin electrolyte layer that forms on the metallic surface is an essential requirement for the atmospheric corrosion process to occur when the metal is exposed to a critical level of humidity (Roberge *et al.,* 2002; Hœrlé *et al.,* 2004). The corrosion rate of the metal increases sharply beyond the threshold level of a critical relative humidity (Hœrlé *et al.,* 2004; Ahmad, 2006). In the presence of thin-film electrolytes, atmospheric corrosion proceeds by balanced anodic and cathodic reactions, where the anodic reaction involves attack of the metal and the cathodic reaction is oxygen reduction (Roberge *et al.,* 2002; Hœrlé *et al.,* 2004).

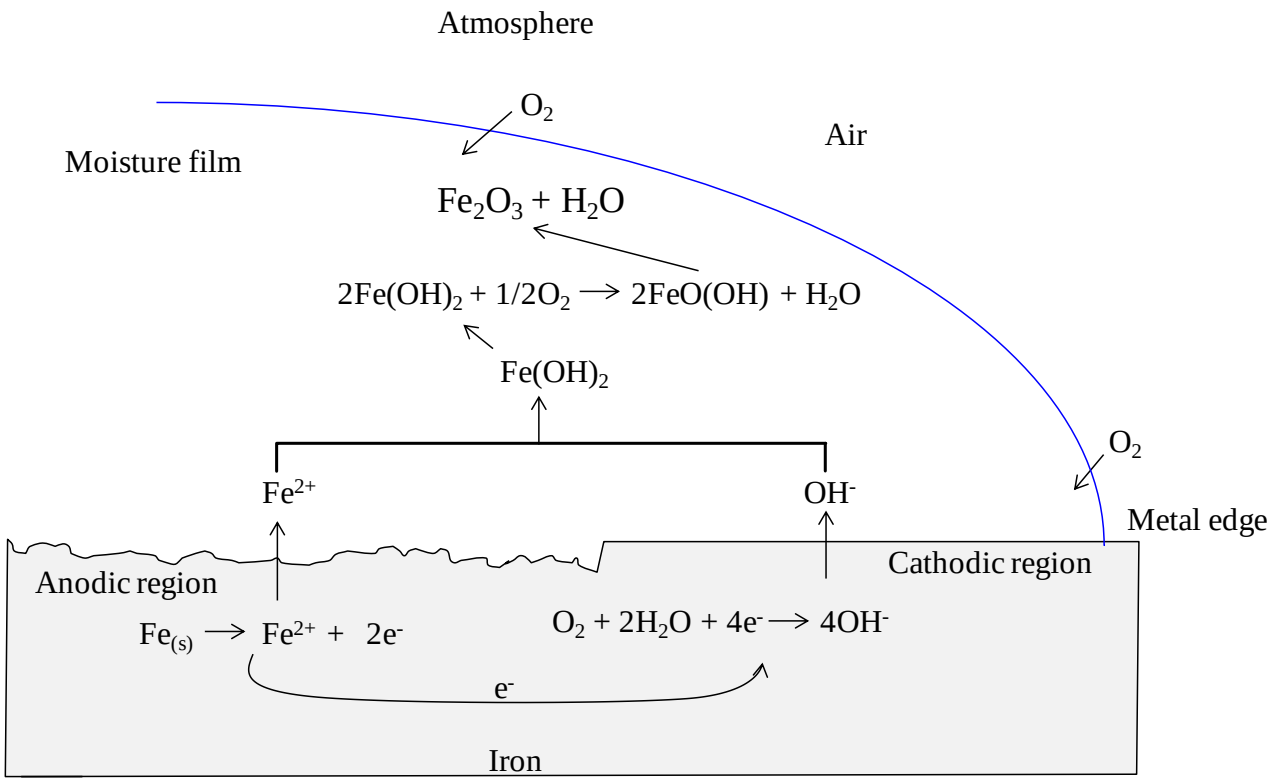

Figure 1: Mechanism of the atmospheric corrosion process of iron

Acid rain

Acid rain is a rain that possesses elevated levels of hydrogen ions (has low pH values). In the presence of atmospheric gaseous pollutants such as sulphur dioxide, atmospheric corrosion increases considerably. Atmospheric pollutants such as sulphur dioxide dissolve in water and upon oxidation it produces sulphuric acid by the following reaction sequence (Sastri, 1998; Du Preez, 1998; Kui *et al.*, 2008):

$SO_2 + H_2O \rightarrow H_2SO_3$ (sulphurous acid)

$SO_2 + 2Fe_2O_3 \rightarrow FeSO_4 + Fe_3O_4$

The acids that form further facilitate the atmospheric corrosion process of the metal; this phenomenon is known as the *acid-rain effect* (Sastri, 1998). Acid rain increases the rate of atmospheric corrosion of metals considerably because it promotes the formation of a thicker electrolyte layer on the metal surface (Ahmad, 2006).

Contaminants (pollutants)

Among the various contaminants present in salt, chloride has the greatest effect on atmospheric corrosion. Once chloride is adsorbed, tenacity of adherence is so great that it cannot be desorbed by using only simple surface-cleaning techniques (Sastri, 1998). Chlorides accelerate atmospheric corrosion by being oxidised in the metallic anode region due to the presence of atmospheric oxygen in air (Tamura, 2008):

$Fe + 2HCl \rightarrow FeCl_2 + H_2O$

$FeCl_2 + (1/4)O_2 + (5/2)H_2O \rightarrow Fe(OH)_{3(s)} + 2HCl$

In general, a combination of high relative humidity, high temperature and high levels of pollutants increases the rate of atmospheric corrosion of metals.

Atmospheric corrosion can be prevented by using VCIs, as mentioned in the previous chapter. VCIs function by changing the kinetics of the electrochemical reactions causing the corrosion process (Rozenfeld, 1981). In general, corrosion inhibitors restrict the anodic and or cathodic processes by blocking the active sites on the metal surface. Alternatively, an inhibitor may work by increasing the potential of the metal surface so that the metal enters the passivation region where a protective oxide film forms. Some corrosion inhibitors inhibit

corrosion by contributing to the formation of a thin protective film on the metallic surface. In summary, the performance of corrosion inhibitors is often related to (Sanyal, 1981):

- The chemical structure and physicochemical properties of the compound that is used as an inhibitor
- The adsorption of molecules or their ions on anodic and or cathodic sites
- An increase in cathodic and/or anodic over-voltage
- The formation of protective barrier films, consisting of complexes or films produced as a result of the interaction between the metal, its ions and ions available in the surroundings.

2.1 VCI formulations

VCIs are commercially available in different forms, i.e. liquids, powders, sachets, tablets, films and emitters (Bastidas *et al.*, 2005). Some available VCI forms are briefly summarised below:

VCI powders

Powders are the cheapest form of VCI among all the available forms. The powder forms of VCIs are easily transported. The disadvantage of some VCI powders is that they are flammable and the suspension of flammable powder in air during usage can be explosive (Myles & Associates, 1995). While the vapours preventing corrosion may be non-toxic, powders may be toxic when inhaled in dust form. Difficulties are also experienced with the removal of VCI dust after usage.

VCI tablets

VCI tablets are made by compressing the VCI powder together with a polymer binder material (Myles & Associates, 1995). The use of a polymer binder is reported to add strength and form a thin-walled matrix in the tablet to regulate the evaporation of a volatile corrosion inhibitor (Goldade *et al.*, 2005). Unlike powder, tablets do not generate any dust and can be easily removed after usage (Myles & Associates, 1995).

VCI plastic film and VCI paper

There are two types of impregnated wrapping that are mainly used: the cellulose paper type and the polyethylene plastic type (Myles & Associates, 1995; Vuorinen & Skinner, 2002; Pieterse *et al.*, 2006; Rammelt *et al.*, 2009). These VCI-containing plastics and/or papers are generally used to wrap the metallic parts during storage and transportation (Vuorinen & Skinner, 2002; Rammelt *et al.*, 2009). VCI-impregnated polymeric materials are economical, easy to use, reliable and do not pose any health hazard. Despite the considerable differences in the physical and chemical parameters, films modified by VCIs are able to retain their critical characteristics (Goldade *et al.*, 2005). This method of applying VCIs is therefore a promising type of corrosion inhibition process in the packaging industries.

VCI foam pads

A large variety of VCI foam pads are available commercially. The foam pad generally used consists of a piece of polyurethane or polyethylene impregnated with the VCI. These pads are normally found stuck to the inside surface of the container. However, they are only effective for a certain period of time and they are only used for small metallic parts (Myles & Associates, 1995).

VCI paint

This method of application involves incorporating the VCI in a paint mixture. The method is used to protect components that are too large to be wrapped or boxed, such as vehicles. VCI paints are generally clear varnishes that dry to form a clear film of approximately 5 µm thickness on the metal surface. On application, the VCI diffuses through the film to reach the targeted metal surface (Myles & Associates, 1995).

The commercially available VCIs differ in respect of volatility and the pH of the aqueous solution (Shreir *et al.*, 1994). The common characteristic of VCIs, despite the different forms that they are in, is that they are intended to provide protection from atmospheric corrosion in closed environments (Skinner, 1993; Myles & Associates, 1995; Vuorinen & Skinner, 2002; Pieterse *et al.*, 2006).

2.2 VCI mechanism of action

VCIs are transported to the metal surface that is to be protected via the gas phase at ambient temperatures (Vuorinen *et al.*, 2004). The VCI is transported to the metal surface by means of

evaporation or sublimation, diffusion and adsorption (Vuorinen & Focke, 2006; Pieterse *et al.*, 2006). The VCIs' mechanism of action is not clearly understood, although the literature suggests that the transportation can take place in two ways (Cano *et al.*, 2005; Bastidas *et al.*, 2005; Rawat & Quraishi, 2003):

- The inhibitor is dissociated before arriving at the metallic surface and saturates the air in contact with the metal with the protective groups, or
- The molecules are volatilised intact, without dissociating, and are only dissociated when they reach the metallic surface

The inhibition process starts when the VCI vapour comes in contact with the metal surface. The vapours distribute themselves within an enclosed space until equilibrium is reached (Boyle, 2004). The equilibrium is determined by the vapour pressure of the VCI compound. In the presence of moisture, the released non-dissociated molecules undergo hydrolysis of the salts into carboxylate anions and organic cations (Rawat & Quraishi, 2003). The VCI protective ions are then adsorbed onto the metal surface. During the adsorption process, the anions are adsorbed on the anodic site of a metal to inhibit anodic reaction, while the organic cations are adsorbed on the cathodic site, thereby preventing the cathodic reaction. It is claimed that the presence of π-electrons and a lone pair of electrons on the nitrogen and oxygen atoms facilitates the adsorption of an inhibitor onto the metal surface (Quraishi & Jamal, 2002; Rawat & Quraishi, 2003; Quraishi *et al.*, 2005). This results in the interruption of the electrochemical process as the ions create a protective barrier that limits the diffusion of corrosion-causing contaminants, such as oxygen, chlorides, water and others (Boyle, 2004).

2.3 Compounds used as VCIs

A wide range of chemical compounds has been proposed for use as VCIs:

Amines: Octylamine is a good inhibitor for carbon steel, copper and brass (Subramanian *et al.*, 2002) and 1,3-di-morpholin-4-yl-propan-2-ol (DMP) and 1,3-bis-diethylamino-propan-2-ol (DEAP) are good inhibitors for carbon steel (Cano *et al.*, 2005; Gao *et al.*, 2007).

Organic nitrites: This includes the nitrites of dicyclohexylamine (DICHAN), cyclohexylamine, isopropylamine, disiobutylamine, triethylamine, octylamine, hexylamine

and dibenzylamine (Shreir *et al.*, 1994; Bastidas *et al.*, 2005; Cano *et al.*, 2005). DICHAN is an excellent inhibitor for carbon steel (Cano *et al.*, 2005; Gao *et al.*, 2007).

Organic carbonates: Carbonates of cyclohexylamine, ethylamine, guanidine and dibutylamine are good inhibitors for steel (Fiaud, 1994).

Organic carboxylates: Benzoates of cyclohexylamine, diethylamine, triethylamine, dibutylamine, dibenzylamine and ethylamine and the acetate of cyclohexylamine are good inhibitors for mild steel and iron (Rammelt *et al.*, 2011). Diaminohexane nitrobenzoate (DAHN) is a good corrosion inhibitor for zinc, aluminium and mild steel (Quraishi & Jamal, 2002). Skinner *et al.* (1999) and Vuorinen & Skinner (2002) list many others.

Organic chromates: This group has certain environmental limitations, but some chromates are good VCIs, e.g. cyclohexylamine chromate is a VCI for brass (Shreir *et al.*, 1994).

Organic phosphates: Phosphates of alkyl and hexymethylamine are good inhibitors for aluminium; diaminohexane phthalate (DAHP) and diaminohexane orthophosphate (DAHO) have been found to be good corrosion inhibitors for aluminium, zinc and mild steel (Quraishi & Jamal, 2002).

2.4 Review of the methods used to test the effectiveness of VCIs

Numerous laboratory techniques have been described in the literature for evaluating the effectiveness of VCIs. These include, but are not limited to, Skinner's test method, the conical flask method, Eschke's test method and various electrochemical measurement methods (Duprat *et al.*, 1981; Hassan *et al.*, 1990). Some of these methods are described in Sections 2.4.1 to 2.4.5.

2.4.1 Skinner's test method

Skinner (1993) developed a quantitative method for the evaluation of VCIs. The method involves placing a known quantity of VCI in a glass and then placing the glass in a jar (see Figure 2). Metal specimens are mounted on the inside lids of the jar. The jar is then closed, with the lid containing the metal specimen attached on the upper inner surface or mounted as shown in Figure 2. This is followed by placing the jar in a heated water bath at a known temperature and humidity. After an appropriate inhibitor film-forming period, an electrolyte is added to the system. In this method condensation occurs at the upper inner surface of the metal specimens. After the required duration of the test, the metal specimens are removed for

evaluation by visual inspection and weight loss determination. The corrosion rate (CR) is then determined as (Skinner, 1993, Quraishi & Jamal, 2002; Vuorinen & Skinner, 2002; Vuorinen *et al.*, 2004; Quraishi *et al.*, 2005):

$$C_R = \frac{8.76 \times 10^7 \times mass\ loss\ (g)}{corrosion\ period\ (h) \times specimen\ area\ (cm^2) \times metal\ density\ (gcm^{-3})} \mu m\ a^{-1} \quad (1)$$

The effectiveness of the VCI is then determined by measuring the improvement (Skinner, 1993):

$$\text{Inhibitor effectiveness} = \frac{C_{R0} - C_{RI}}{C_{R0}} \times 100\% \quad (2)$$

where C_{R0} and C_{RI} are the corrosion rates in µm per year determined in the absence of and in the presence of the inhibitor respectively.

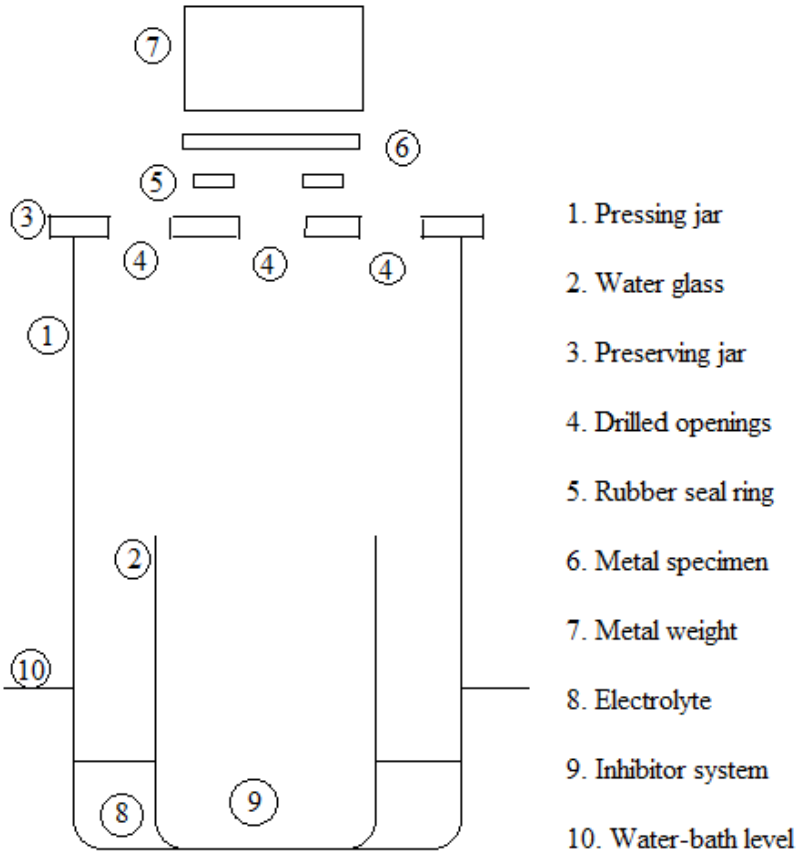

Figure 2: Corrosion test method developed by Skinner (1993) (diagram adopted from Skinner, 1993)

Skinner's test method was recently used to evaluate the effectiveness of VCIs using the metal specimens zinc, copper, iron and mild steel (Skinner, 1999; Vuorinen & Skinner, 2002; Vuorinen *et al.,* 2004; Vuorinen & Focke, 2006). Accurate and reproducible results were obtained using this method. The success is attributed to the fact that the method completely eliminates equipment contamination (Skinner, 1999; Vuorinen & Skinner, 2002).

2.4.2 Conical flask method

In this method the metal specimens to be tested are suspended in conical flasks using nylon tags (Quraishi & Jamal, 2002). The weighed amount of VCI is placed below the suspended metals in a glass container, avoiding contact with the liquid inside the conical flask. The concentration of the VCI used in this method depends on the size of the conical flask (Quraishi *et al.,* 2005). The conical flask is kept at the required temperature and relative humidity. The samples are removed at night to allow condensation of moisture on the metals. The cycle can be repeated for the required duration of the test. When the cycle is complete, the metal specimens are placed in an acid bath to remove oxides. They are then weighed and the effectiveness is calculated by using Equations (1) and (2) (Quraishi & Jamal, 2002; Quraishi *et al.,* 2005).

2.4.3 Electrochemical measurement methods

In this type of method the polarisation cell set up consists of an electrolyte solution, a reference electrode, a counter-electrode and a working electrode (metal sample). The electrodes are connected to a potentiostat (Quraishi & Jamal, 2002). The working, reference and counter-electrodes are placed in the electrolyte solution. This solution must resemble the actual application environment of the material undergoing testing (Quraishi *et al.,* 2005). Thereafter the electrochemical potential between the various electrodes in the solution is generated. Corrosion potential is measured by the potentiostat as the energy difference between the working and reference electrodes. In potentiometric measurements the current remains constant while the potential is increased. In electrochemical measurements both the potential and the current of the oxidation or reduction reactions are measured (Quraishi & Jamal, 2002; Cano *et al.,* 2005).

Cano *et al.* (2005) used both the electrochemical and potentiometric measurement methods to evaluate the protection of carbon steel with nitrite and carboxylic acid-based VCIs. They

found that there were large inconsistencies in the inhibitive effectiveness values obtained using the electrochemical measurement method. Several other authors obtained uneven results with the potentiometric measurement method as well (Quraishi & Jamal, 2002; Quraishi *et al.*, 2005; Cano *et al.*, 2005). Duprat *et al.* (1981) attributes these discrepancies in the inhibition efficiency values to the differences in the actual principles of the methods and the hydrodynamic conditions involved. The presence of such discrepancies indicates that the electrochemical methods do not provide reliable and/or reproducible results. This is attributed to the fact that the atmospheric conditions are not accurately represented in the electrochemical measurement method (Du Preez, 1998).

2.4.4 Eschke's test method

This corrosion inhibition test method is applicable mainly when the VCI is impregnated in plastic films. It involves polishing known sizes of metal strips, followed by wrapping them with a single layer of VCI-containing plastic film. The wrapped metals are then placed in a climatic test cabinet at a known relative humidity and temperature for the required test period (Quraishi & Jamal, 2002; Rawat & Quraishi, 2003; Quraishi *et al.*, 2005). Similarly to the potentiometric measurements, the Eschke test method also yielded a large spread of results (Quraishi & Jamal, 2002).

2.4.5 Other corrosion inhibition test methods

Other reported corrosion inhibition test methods include: sulphur dioxide and salt inoculation test methods (Quraishi *et al.*, 2005); continuous condensation; impedance measurements; salt spray test; Stevenson chamber; biocide action; and polarisation resistance (Duprat *et al.*, 1981; Submaranian *et al.*, 2002; Rammelt *et al.*, 2011). Among these methods mentioned in this section, the reasonable corrosion rate and inhibitor efficiency were obtained using the sulphur dioxide and salt inoculation test methods (Quraishi *et al.*, 2005).

2.5 Factors affecting the effectiveness of VCIs

Corrosion is usually prevented as long as the chemicals remain active (Dutton, 2004). The effectiveness of VCIs depends mainly on factors such as packaging material and porosity, temperature, humidity, acidity, UV exposure and the method of application (Dutton, 2004). Some of these factors are discussed in Sections 2.5.1 to 2.5.5.

2.5.1 pH of the system

All corrosion inhibitors have a pH range in which they are most effective. Adequate metal protection is only reached when the pH value is in the range 5.5–8.5 (Bastidas *et al.*, 2005). The effective solution pH for adequate corrosion inhibition for mild steel was found to be in a wide pH near-neutral range of 6.5–8.5 for benzoate, acetate and carbonate-based VCIs (Rammelt *et al.*, 2011). Nitrite-based corrosion inhibitors were found to lose their effectiveness below a pH of 5.5–6.0. Polyphosphates were found to be effective only in the range 6.5–7.5, while chromates are generally used at a pH of 8.5 (Shreir *et al.*, 1994). In some instances the effective solution pH was found to be strongly alkaline (pH ≥ 10.4). It was found to be in the range of 9–10.3 for weak carboxylate anions such as benzoate, acetate and carbonate, and in strong carboxylate anions it was found to be ≥ 11.4 (Rammelt *et al.*, 2011). This implies that effective corrosion-prevention pH is only achieved in a basic environment. It also suggests that amine has to be present in excess in the vapour for adequate protection, otherwise the mixtures may be corrosive. The value of the pH on the metallic surface is influenced largely by the volatility of the VCI components (Rammelt *et al.*, 2009).

2.5.2 Concentration of an inhibitor

It is difficult to ascertain the effect of an inhibitor concentration in the absorbed moisture film in atmospheric corrosion. However, the performance of inhibitors used in aqueous media clearly shows that concentration is an important factor. This is discussed further in this section.

The efficiency of a corrosion inhibitor depends largely on the concentration of the inhibitor (Roberge, 2000). To be fully effective, inhibitors are required to be present in a certain minimum concentration in aqueous media. Therefore both the initial concentration and the concentration during application are important (Shreir *et al.*, 1994). Typically, a good inhibitor would give >95% protection at a concentration of 0.008%, and >90% protection at a concentration of 0.004% (Roberge, 2000). It was reported in a study of VCIs in packaging materials that the decrease in nitrite VCI concentration in foil resulted in the corrosion inhibitor failing to provide adequate metal protection (Eibl & Reiner, 2011). The inhibition performance of 1,3-bis-diethylamino-propan-2-ol (DEAP) and 1,3-di-morpholin-4-yl-propan-2-ol (DMP) for carbon steel was found to increase with an increase in concentration of the inhibitor. Submaranian *et al.* (2002) also reported an increase in the inhibitor's efficiency with an increase in concentration of the octylamine-based VCI.

2.5.3 Temperature and humidity

The corrosion rate of metals increases with variations in temperature and humidity during storage and transportation. The effectiveness of some inhibitors decreases with increases in temperature and humidity (Sanyal, 1981). When inhibitors are used at higher temperatures, higher inhibitor concentrations are required for some inhibitors to maintain their effectiveness (Shreir *et al.*, 1994). However, other corrosion inhibitors can lose their effectiveness completely with an increase in temperature. A typical example is polyphosphate, which is effective below 40 °C, but loses its effectiveness at higher temperatures because reversion to orthophosphates is then possible (Shreir *et al.*, 1994).

Bommersbach *et al.* (2005) studied the influence of temperature on the amine and carboxylic acid-based VCIs. The study revealed that at a temperature higher than 60 °C there was low protective efficiency for iron metal, less than 30% efficiency being obtained. This was attributed to the iron-dissolution kinetics, which disturbs the formation of the protective layer at high temperatures. The decreased effectiveness of corrosion inhibition at higher temperatures is reported to be the result of desorption of the adsorbed inhibitors and the depletion of oxygen, in the absence of which some inhibitors such as benzoate have no protective action (Sanyal, 1981). Temperatures below 50 °C were found to conserve the protective film on the metal surface (Bommersbach *et al.*, 2005).

Humidity is another major factor that affects the effectiveness of VCIs. It affects the corrosion rate of metals directly because moisture provides electrolytes, which are required for corrosion reactions to take place. In general, an increase in humidity also results in an increase in the corrosion rate of the metal (McConnel, 2008).

2.5.4 Vapour pressure

Vapour pressure is an important parameter for controlling effective VCI transportation (Pieterse *et al.*, 2006). The vapour pressure of the VCI is determined using a variety of methods, such as the Knudsen effusion, Regnault dynamic, torsion effusion and microbalance methods (Bastidas & Mora, 1998; Bastidas *et al.*, 2005). The available vapour pressure values in literature have some inconsistencies. Therefore the reproducibility of the data depends largely on the experimental parameters and the method used to determine the vapour pressure (Bastidas & Mora, 1998; Bastidas *et al.*, 2005). For effective VCI transportation, the vapour pressure should be in the range of 0.002–1 Pa at 20 °C (Skinner *et al.*, 1999; Vuorinen

& Skinner, 2002; Vuorinen *et al.*, 2004; Bastidas *et al.*, 2005; Vuorinen & Focke, 2006). A vapour pressure that is too low leads to slow establishment of protection, which may result in insufficient corrosion protection. When the vapour pressure is too high, the effectiveness of VCIs may be limited to a short period of action due to high consumption rates (Bastidas *et al.*, 2005; Pieterse *et al.*, 2005). Therefore the volatility of VCIs should be just sufficient to render optimum metal protection (Pieterse *et al.*, 2006).

2.5.5 Other factors

A systems approach should be applied when considering the effectiveness of VCIs. The corrosive environments, the type of metal, the state of the exposed surfaces, and the chemical structure of the inhibitor all play a role. For VCIs the environment includes the presence of water vapour but other corrosive gases, e.g. CO_2 or SO_2, might also be present.

The nature of the metal is important as an inhibitor that is effective for one metal may not be effective for another (Sanyal, 1981; Shreir *et al.*, 1994). For example, cyclohexylamine and dicyclohexylamine corrosion inhibitors were found to be more effective for mild steel and zinc than for copper in an SO_2 environment (Subramanian *et al.*, 1999).

The state of the metal surface has an effect. Clean, smooth metal surfaces require lower inhibitor concentrations and full protection can be easily attained, whereas dirty or rough metal surfaces require higher concentrations of an inhibitor with full metal protection still not being guaranteed.

The chemical structure of the inhibitor clearly is important. Badran *et al.* (1982) claim that the electron density of the nitrogen atom also plays an important role in the efficiency of the inhibitors: an increase in electron density was reported to lead to an increase in the inhibition efficiency. In amine carboxylates, the carboxylic acid chain length is another factor plays a significant role in the effectiveness of VCIs. The effectiveness of ammonium monocarboxylic acids as VCIs was found to decrease in the following order (Vuorinen & Skinner, 2002):

Ammonium caprylate > Ammonium laurate > ammonium oleate ≈ ammonium stearate

The longer the carboxylic acid chain length constituent of ammonium, the less effective the inhibitor was found to be (Vuorinen & Skinner, 2002).

Hassan *et al.* (1990) studied the effect of molecular structure on the efficiency of corrosion inhibition of aluminium metal using a series of aromatic acid derivatives. Their paper claims

that the benzene ring attached to carboxylic acid contributes to the efficiency of corrosion inhibitors. The efficiency of the inhibitors studied was found to decrease in the following order in alkaline and acidic environments:

Benzophenone (100%) > benzoic acid > acetophenone > benzaldehyde > benzamide

The reason for the high corrosion protection efficiency of benzophenone was attributed to its large size which imparts better surface-coverage properties (Hassan *et al.*, 1990). However, due to the inductive effect of the hydrogen atom attached, carbonyl carbon benzamide was found to be less effective than benzaldehyde.

The nature of the VCI carrier material, e.g. polymers, also plays a significant role in the inhibitor's effectiveness. Some VCIs lose their efficiency rapidly, resulting in an increase in the corrosion rate and a change in the colour of some plastic carriers. However, this problem is addressed by using a close packaging to prevent rapid loss of inhibitor (Cano *et al.*, 2005). Paper impregnated with sodium benzoate prevents loss of shine in carbon steel, while paper impregnated with benzotriazole was found to be a good corrosion inhibitor for copper and its alloys (Cano *et al.*, 2005).

2.6 Amine-carboxylic acid interactions

Amines are organic compounds containing a basic nitrogen atom with a lone pair of electrons. They are ammonia derivatives with one hydrogen atom being replaced by a substituent, such as an alkyl group. Amines are divided into primary, secondary and tertiary. They are referred to as *primary* when one of the three hydrogen atoms in ammonia is replaced by an alkyl substituent; *secondary* when two substituents are bound to the nitrogen atom together with one hydrogen atom, and *tertiary* when all three hydrogen atoms are replaced by the alkyl group (MacMurry, 2000).

Carboxylic acids have attracted much attention due to their ability to form two hydrogen bonds with each other (see Scheme I). The existence of these hydrogen bonds has been previously confirmed by spectroscopy (Meyer *et al.*, 1975; Maréchal, 1987). The interactions of carboxylic acids with other organic solvents have been of interest for over 70 years. Carboxylic acids are characterised by their tendency to withdraw electrons from the hydroxyl group and by so doing weakening the OH bond, resulting in an increase in polarity (MacMurry, 2000).

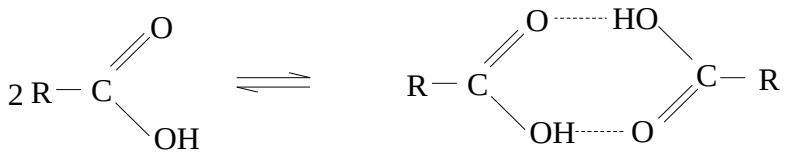

Scheme I: Schematic presentation of acetic acid dimer ring

The interactions between amines (A) and carboxylic acids (C) have been comprehensively studied (Kohler *at al.*, 1972; Kohler & Hyskens, 1976; Hyskens *et al.*, 1980; Kohler *et al.*, 1981a & b; Orzechowski *et al.*, 2000; Karlsson *et al.*, 2001). Mixtures of amines and carboxylic acids interact strongly via hydrogen bonding (Kohler *at al.*, 1972; 1981a & b). In 1:1 mixtures they form either A_1C_1 molecular complexes in the vapour phase (Barrow & Yerger, 1954; Gough & Price, 1968; DeTar & Novak, 1970; Nakanishi *et al.*, 1977; Kubilda & Shreiber, 1978; Wierzejewska-Hnat *et al.*, 1980; Padjowska & Sobczyk , 1982; Friberg *et al.*, 1990; Liljefors & Norby, 1997; Päivärinta *et al.*, 2001; Orzechowski *et al.*, 2003 & 2007) or ionic complexes in the liquid phase via Brønsted-Lowry acid-base reactions, as shown in Scheme II (Karlsson *et al.* 2001; Päivärinta *et al.*, 2001). The A_1C_1 ionic complex requires stabilisation and *ab initio* calculations have shown that, at equimolar mixing ratios, the formation of the A_2C_2 complex is more likely (Karlsson *et al.*, 2001). Friberg *et al.* (1990) also tried stabilising the A_1C_1 complex in a triethylamine-formic acid system by addition of water. They claim that stability was reached in the presence of water. However, in the presence of water it is also that a monomer-water complex may be formed, as previously reported and confirmed by Fourier transform Raman spectroscopy (FT-Raman) for a ternary system of heptanoic acid and heptylamine in water (Karlsson *et al.*, 2001). The A_1C_1 complex is highly polar owing to the polar nature of the carboxylic acid (Pajdowski & Sobczyk, 1982; Päivärinta *et al.*, 2001).

A **B**

Scheme II: Schematic presentation of (A) molecular and (B) ionic amine-carboxylic acid (A_1C_1) complex (Tamada & King, 1990)

The above-mentioned A_1C_1 complex is formed when the basic nitrogen of the amine and the acidic proton interact. The carboxylic acid interacts directly with the nitrogen from the amine in the initial stage (Tamada & King, 1990). At this stage the amine-carboxylic acid interaction results in the formation of an ion pair (Tamada & King, 1990). The ionic nature of this complex was confirmed by:

- heat evolution and slight volume contraction during addition of an amine to the acid (Kohler *et al.*, 1972; Van Klooster & Douglas, 1945)
- FTIR (Orzechowski *et al.*, 2000; Päivärinta *et al.*, 2001; Orzechowski *et al.*, 2003 & 2007)
- ^{1}H-NMR and ^{13}C-NMR (Kohler *et al.*, 1981a; Hafaiedh *et al.*, 2009)
- dielectric spectroscopy and conductivity measurements (Orzechowski *et al.*, 2000 & 2003)
- melting and boiling point measurements (Kohler *et al.*, 1972; 1981a & b)
- ultrasound absorption and relaxation spectroscopy (Bobik, 1977; Orzechowski *et al.*, 2000)
- combinations of different measurement techniques, including density, optical refractive index and shear viscosity (Orzechowski *et al.*, 2003).

The nature of the interaction depends mainly upon the strength of the acid and the type of the solvent used (Tamada & King, 1990).

In the absence of water and in the presence of excess carboxylic acid, the A_1C_1 complex is stabilised by the cyclic dimers of the carboxylic acid, forming the A_1C_3 complex (Kohler *et al.*, 1972; Friberg *et al.*, 1990; Orzechowski *et al.*, 2000; Karlsson *et al.*, 2001; Päivärinta *et al*,. 2001; Orzechowski *et al.*, 2003 & 2007). The formation of the A_1C_3 complex in triethylamine-acetic acid and tri-n-butylamine-propanoic acid mixtures is supported by the sharp viscosity maximum observed at the 1:3 amine to acid mole ratio (Kohler *et al.*, 1981b; Pajdowska & Sobczyk, 1982). The existence of these 1:3 amine-carboxylic acids (see Scheme III) has also been confirmed in triethylamine-formic acid (Hyskens *et al.*,1980), heptylamine-heptanoic acid (Kalsson *et al.* 2001), octylamine-octanoic acid (Friberg *et al.*, 1990), triethylamine-propanoic acid (Bobik, 1977) and propylamine-propanoic acid mixtures (Päivarinta *et al.*, 2001). The 1:3 amine carboxylic acid complex is accompanied by a negative Gibbs free energy and a comparatively small, yet negative, $T\Delta S$ term in the

triethylamine-acetic acid system (Kohler *et al.*, 1972, 1981a & 1b). This is attributed to the indefinite orientation of the constituent molecules and the relative dimer concentration, which is higher in mixtures than in pure carboxylic acids (Miksch *et al.*, 1969; Kohler *et al.*, 1974).

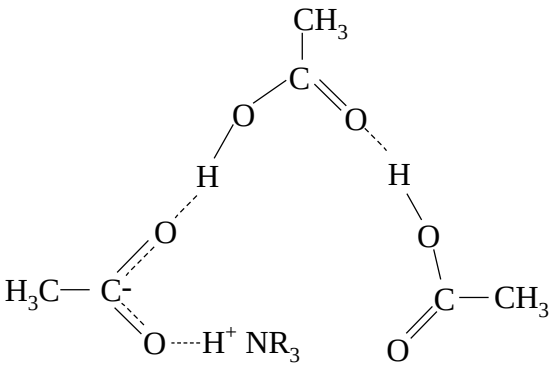

Scheme III: Schematic presentation of the 1:3 amine-carboxylic acid complex (Tamada & King, 1990)

The existence of a A_1C_2 complex has also been reported (see Scheme IV) (Kohler *et al.*, 1972; Orzechowski *et al.*, 2000; 2003 & 2007). There is one oxygen atom in complexes A_2C_2 and A_1C_3 that accepts only a small number of electrons. In the ionised acid this oxygen is not involved in the formation of hydrogen bonding with the ionic amine (Päivärinta *et al.*, 2001). On addition of carboxylic acid, the OH of the carboxyl of the second acid forms a hydrogen bond with the conjugated CO of the carboxylate of the first acid to form a 1:2 amine acid complex (Tamada & King, 1990). The 1:3 amine acid complex is formed when the additional acid is hydrogen bonded to the 1:2 complex. The complexes are formed with either free amine or free acid as the by-products, depending on the initial mole fraction of each component in the mixture (Kohler *et al.*, 1981a; Tamada & King, 1990; Päivärinta *et al.*, 2001).

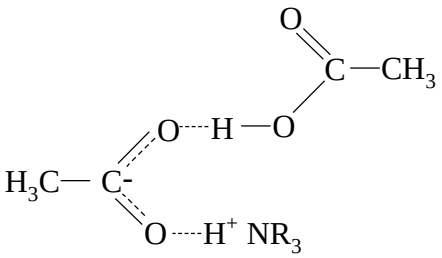

Scheme IV: Schematic presentation of the 1:2 amine-carboxylic acid complex (Tamada & King, 1990)

Kohler *et al.* (1981b) indicated that the methyl protons of triethylamine are not completely attached to the nitrogen, as confirmed by NMR spectroscopy. This finding disagrees with the suggestion by Hyskens *et al.* (1980) that at excess acid almost all amine is in the ammonium form. Kohler *et al.* (1981a) suggest that the orientationally ill-defined aggregate is closely connected to the polarisation of hydrogen bonds, which can be influenced by ions.

When the tertiary amine is replaced with a secondary or a primary amine, the situation changes dramatically. The A_1C_1 complex becomes increasingly important and in the case of primary amines, there is a tendency for these to form large clusters (Kohler *et al.,* 1981a). Similar results were also obtained in a study of the octylamine-octanoic acid (Friberg *et al.*, 1990) and heptylamine-heptanoic acid systems (Karlsson *et al.,* 2000).

Hyskens *et al.* (1980) and Kohler *et al.* (1981a) suggest that in systems containing carboxylic acids with two or more carbon atoms, or containing primary amines, the degree of ionisation of amine in the presence of an excess acid is markedly lower than one. This is contrary to ternary amines and formic acid systems. With FTIR the continuous ionisation of added amine is observed at an excess in the system of octylamine-octanoic acid (Friberg *et al.,* 1990). However, the system precipitates with equimolecular compounds and therefore it was not studied for all proportions. Similar results were obtained by Karlsson *et al.* (2000) in the system of heptanoic acid and heptylamine. In their study the acid and amine mixture was miscible in all proportions. However, the 1:3 complex did not form at excess acid; only 1:1 amine acid stoichiometry was present. The absence of the 1:3 complex is also reported in excess tri-*n*-butylamine in the presence of benzene (Pajdowska & Sobczyk, 1982).

In a static permittivity and dielectric relaxation time study by Orzechowski *et al.* (2007), the questionable 1:9 triethylamine-propanoic acid complex (A_1C_9) was mentioned at a mole fraction 0.1 of the base. However, this complex was not discussed.

Päivärinta *et al.* (2001) explored the possibility of forming an A_xC complex (where $x > 1$) in the presence of excess amine for a binary mixture of propanoic acid and propylamine. The results revealed the non-existence of such a complex, confirmed by ^{13}C-NMR, Raman, FTIR and *ab initio* calculations (Karlsson *et al.,* 2000; Päivärinta *et al.,* 2001). In excess octylamine only, precipitation of the ammonium carboxylate was reported (Friberg *et al.,* 1990).

The possibility of proton transfer via electrostatic interaction when the amine is mixed with the carboxylic acid during A_1C_1 complex formation has been addressed (Pajdowska &

Sobcyzyk, 1982; Friberg *et al.*, 1990; Liljefors & Norby, 1997; Päivärinta *et al.*, 2001). The existence of proton transfer was confirmed in a ternary mixture of octanoic acid and octylamine in formamide (Friberg *et al.*, 1990). Near infrared spectroscopy (near-IR) studies also indicated that there was proton transfer from the carboxylic acid to the amine (Orzechowski *et al.*, 2007). This was also theoretically predicted by *ab initio* calculations for the trimethylamine-formic acid and propylamine-propanoic acid systems (Liljefors & Norby, 1997; Päivärinta *et al.*, 2001). The results indicated that at low base content, the propanoic acid exists mainly as hydrogen-bonded linear and cyclic dimers. Päivärinta *et al.* (2000) claim that proton transfer from an acid to an amine takes place only in strong acids. Orzechowski *et al.* (2003) suggested that the dissociation of proton transfer complexes takes place at a mole fraction of base $z_A > 0.25$ for a triethylamine-propanoic acid binary mixture.

Ternary systems comprising amines and carboxylic acids dissolved in non-ionising or non-dissociating solvents, such as chloroform, carbon tetrachloride and benzene, have been studied as well (Barrow & Yerger, 1954; Gough & Price, 1968; DeTar & Novak, 1970; Pajdowska & Sobczyk, 1982).

Nakanishi *et al.* (1977) studied the charge transfer of hydrogen-bonded ternary mixtures of acetic acid with a series of aliphatic amines in different solvents, such as *n*-heptane and acetonitrile, using vacuum ultraviolet (UV) absorption. In their paper they deny the possibility that acetic acid amines exist as ion pairs ($R_3N^+H\ldots.CH_3COO^-$). This is based on the fact that the absorption bands of (diethyl) ammonium ion and the acetate ion are located in a shorter wavelength region than the new bands of the system. The charge transfer band of the ion pair was expected to shift to lower wavelengths with increasing polarity. However, the reverse tendency was observed. This behaviour was attributed to the transition to the first excited state, which can also be regarded as charge transfer from the amine to the acetic acid band, which is characteristic of the hydrogen bond. The existence of an ion pair was reported for the mixture of triethylamine and benzoic acid in chloroform (DeTar & Novak, 1979).

2.7 The effect of water

The effect of water on mixtures of amines and carboxylic acids has also been studied (Buckland *et al.*, 1997; Karlsson *et al.*, 2001a & b). Raman studies indicated that when water is added to pure carboxylic acid, it breaks the cyclic acid dimers and forms an acid monomer-water complex. However, in amine-carboxylic acid mixtures complexation in the presence of small amount of water molecules proceeds in the same way as without water (Karlsson *et al.*,

2001). On amine addition, the A_1C_1 complex binds predominantly to excess acid instead of to water. The A_1C_3 complex also exists together with the acid monomer-water complex (Karlsson *et al.*, 2001). The study by Buckland *et al*. (1997) revealed no possibility of water hydrogen bonding with an amine. In contrast, Hafaiedh *et al.* (2009) reported the hydrogen-bonded complex between triethylamine and water. This complex breaks down with an increase in temperature, confirmed by the decrease in the volume of contraction in the volumetric measurements (Hafaiedh *et al.*, 2009).

In the VCI corrosion inhibition process, moisture also plays a significant role in the formation of the protective layer on the metal surface. Mixtures of amines with OH ions were found to show protection synergism. This synergism can be used to create effective binary amine based-inhibitors. In these inhibitors one component inhibits corrosion and generates the OH^- ions, while the other one improves the protective effect of the mixture (Andreev & Goncharova, 2004).

2.8 Review of amine-carboxylic acid characterisation methods

Amine carboxylic acid binary mixtures are characterised by a variety of techniques. These include: visible and ultraviolet (UV-Vis) spectroscopy; the ultrasonic relaxation method; FTIR; ^{1}H-NMR; and ^{13}C-NMR.

Other reported methods of characterising the amine-carboxylic acid mixtures include: viscosity, density, thermodynamic, melting and boiling point measurements; ultrasound absorption and relaxation spectroscopy; and conductivity and dielectric relaxation studies (Van Klooster & Douglas, 1945; Kohler *et al.*, 1972, 1974, 1981a & b; Kohler & Hyskens, 1976a; Bobik, 1977; Hyskens *et al.*, 1980; Saeten *et al.*, 1991; Orzechwski *et al.*, 2000, 2003 & 2007). In the viscosity measurements the existence of 1:3 amine-carboxylic acid complex was inferred from the position of the maximum viscosity in binary systems. Of the characterisation techniques listed, dielectric and conductivity measurements are the most frequently used. However, due to the high direct current conductivity of the mixtures, it is difficult to eliminate systematic and experimental errors arising from unnoticed or incompletely considered electrode polarisation. A solution to this problem was devised by combining different methods of measurement, including density, optical refractive index and shear viscosity (Orzechowski *et al.*, 2003).

2.8.1 Ultraviolet visible (UV-Vis) spectroscopy

The analysis of amine carboxylic acid mixtures with the (UV-Vis) technique has also been reported (Nakanishi *et al.,* 1977; DeTar & Novak, 1979). UV-Vis measures the transition in the electronic energy levels of the molecular bonds from the ground to the excited state. The wavelength of the absorption peak can be correlated with the types of bond a molecule has and is also used for determining the functional groups within the molecule. UV-Vis was used to study the amine-carboxylic acid interactions in such a mixture. The existence of hydrogen bonding (Nakanishi *et al.,* 1977) and of proton transfer from acid to amine (DeTar & Novak, 1979) was confirmed using this technique. The polarity of a 1:1 complex was also indicated by the shift in maximum wavelength in UV-Vis (Nakanishi *et al.,* 1977).

2.8.2 Nuclear magnetic resonance (NMR) spectroscopy

^{1}H-NMR and ^{13}C-NMR are structural elucidation techniques that are used to give information about the number and position of hydrogen and carbon atoms respectively in a molecule. Kohler *et al.* (1981b) used ^{1}H-NMR to investigate the existence of amine acid complexes in ratios of 1:1, 1:2 and 1:3. These techniques also revealed, using chemical shift, that the A_1C_1 complex is strongly ionised, with the Et_3NH^+ ion having a lifetime of 10^{-3}s in the magnetically excited state (Kohler *et al.,* 1972). ^{13}C-NMR has also been used to characterise the amine carboxylic acid binary mixtures (Päivärinta *et al.,* 2001; Karlsson *et al.,* 2001).

2.8.3 Fourier transform infrared (FTIR) spectroscopy

Among molecular vibrational spectroscopic techniques, FTIR is one of the most frequently used for the identification of organic functional groups and also for structural elucidation. The infrared band is found in the wavenumber region 1.3 x 10^4 to 3.3 x 10^1 (between microwave and UV visible light) in the electromagnetic spectrum (Socrates, 1980; Skoog *et al.,* 1996). The different functional groups absorb characteristic frequencies of IR radiation. When a material is infrared irradiated, the absorbed IR radiation excites molecules into a higher vibrational state. The wavelength of the light absorbed by a particular molecule is a function of the energy difference between the at-rest and the excited vibrational states. Therefore the wavelengths that are absorbed by a particular molecule or functional group are characteristic of its molecular structure (Günzler & Gremlich, 2002).

The infrared spectrum is produced as a result of the absorption of an electromagnetic radiation at frequencies that correlate to the vibration sets of chemical bonds from within a

molecule (Coates, 2000). The primary requirement for the molecule to absorb infrared radiation is that there must be a net charge in dipole moment during the vibration of the molecules or functional groups under investigation (Socrates, 1980; Coates, 2000). The absorption frequency depends on the vibrational frequency of the molecules, while the absorption intensity depends on how effectively the infrared photon energy can be transferred to the molecule. This depends on the change in the dipole moment which occurs as a result of molecular vibration (Åmand & Tullin, 2012).

The FTIR method of analysis is both a qualitative and a quantitative analytical method. In qualitative analysis the IR spectrum of the material under investigation is collected and compared against that of the standard or reference sample. The specificity of the FTIR absorption bands allows computerised data searches within reference libraries to identify the material (Socrates, 1980; Coates, 2000).

In the quantitative method the concentration of the compound is determined from the area under the FTIR absorption bands for the selected spectrum region (Åmond & Tullin, 2012). The concentration is obtained by establishing a standard curve from the spectra for known concentrations using the Beer-Lambert law. This law states that for a given layer thickness (l), the transmittance, $T(\lambda)$, (i.e. ratio of the transmitted and the incident radiation) is directly proportional to the concentration (c) as given below:

$$A(\lambda) = -\log_{10} T(\lambda) = -\log_{10} \frac{I}{I_0} = \varepsilon(\lambda) l c \qquad (3)$$

where $A(\lambda)$ is the absorbance and $\varepsilon(\lambda)$ is the absorptivity at wavelength λ.

For multi-component mixtures the equation becomes

$$A(\lambda) = \sum_{i=1}^{N} \varepsilon_i(\lambda) l c_i \qquad (4)$$

The important FTIR spectral region for carboxylic acids and amines is between 1800 cm^{-1} and 1500 cm^{-1}, and between 1000 cm^{-1} and 850 cm^{-1} (Karlsson *et al.*, 2000). The ionic nature of the complexes formed between amines and carboxylic acids has been confirmed by both mid-infrared and near-infrared methods (Barrow & Yerger, 1954; Wiezejewska-Hnat *et al.* 1980; Friberg *et al.*, 1990; Orzechowski *et al.*, 2007). The presence of the carboxylic acid dimer form has been confirmed by the presence of the OH out-of-plane deformation mode at 935 cm^{-1}. This peak is a characteristic dimeric acid form (Karlsson *et al.*, 2000). The broad

multiple NH_2 amine wagging and twisting vibrations are found between 850 cm^{-1} and 750 cm^{-1}. Increasing the amine concentration causes the dimeric acid form peak at 935 cm^{-1} to disappear or decrease in intensity, confirming the decrease in acid dimers. This is understood as the amine-acid complexation (Karlsson *et al.*, 2000).

In carboxylic acids the undissociated acid C=O peak is expected at 1700 ± 50 cm^{-1} (Coates, 2000). The absorbance of this peak is high with low amine amounts and it is expected to be reduced or to disappear with high amine content. The proton transfer results in the formation of strong asymmetric COO^- bands at 1650 cm^{-1} and 1550 cm^{-1} (Päivärinta *et al.*, 2001). The protonated amine is expected at approximately 1400 cm^{-1} (Whitehead, 1967). The OH stretching vibration of the acid is observed at 3000 cm^{-1}. In the complex this peak is found in the range from 3257 cm^{-1} to 3315 cm^{-1}. The stretching vibration due to the N-H bond is found at 2895 cm^{-1}. This bond is involved in the hydrogen bond and it is sometimes covered under the broad N-H band (Päivärinta *et al.*, 2000). FT-Raman has also been used to characterise amine-acid mixtures (Karlsson *et al.*, 2000 & 2001; Päivärinta *et al.*, 2001).

2.8.4 Thermo-gravimetric analysis (TGA)

Literature on the analysis of amine-carboxylic acid mixtures using TGA is limited. TGA is a thermal analytical technique in which the change in mass of a substance is measured as a function of temperature while the substance is subjected to a controlled-temperature programme (Heal, 2002). The mass loss may be the result of loss of the volatile components present in the substance (Beverley *et al.*, 1999). TGA is used to study physical processes, such as evaporation of a liquid, sublimation of solids and desorption of gas from the surface of solids, for compositional analysis, and for kinetic and oxidation studies. The derivative TGA (DTG) (*dm/dt or dm.dT*) signal is used for guidance if there are overlapping reactions on TGA (Heal, 2002).

Evaporation rate studies are of interest in assessing the release of volatile active components from commercial products (Beverley *et al.*, 1999). The TGA method has been proposed for estimating the volatility and/or vapour pressure of liquid mixtures (Beverley *et al.*, 1999; Pieterse & Focke, 2003; Pieterse *et al.*, 2006). Beverley *et al.* (1999) described a TGA method in which the sample is held in a partially filled container through which a gas flows in vertically. The evaporation rate is determined as the slope from a linear relationship between mass loss and time (Beverley *et al.*, 1999).

TGA data have also been used to estimate the vapour pressure of low-volatility compounds (Pieterse & Focke, 2003). The revised equation was also reported from isothermal TGA data (Focke, 2003).

Pieterse *et al.* (2006) developed a method for estimating the gas permeability of VCIs at elevated temperatures using TGA. The method involves dynamically scanning a sample in partially filled cylindrical pan, with gas flowing horizontally across the pan. In this study the effects of sample mass, sample holder, gas flow rate and heating rate on evaporation were taken into consideration (Pieterse *et al.*, 2006). The results revealed that at a very low gas flow rate (10 ml/min) the concentration of the volatiles at the top of the cup assumes a finite value. This is attributed to the fact that the released volatiles are not swept away fast enough. The reasonable flow rates were reported to be 20, 50 and 100 ml/min (Pieterse *et al.*, 2006). However, the scan rate was found to have no effect on gas permeability.

2.8.5 Coupling TGA with FTIR

Interpretation of the TGA data does not cause any difficulty if the investigated reaction proceeds only in one or more well-resolved decomposition steps. The interpretation is also simple if the stoichiometry and composition of the reactants, intermediates and products are fully known. However, not all these requirements are always fulfilled. The temperature ranges of the various decomposition steps in multi-component systems overlap and the exact composition of the evolved gaseous products is unknown. This phenomenon has led to thermal analysis being coupled with other techniques, such as mass spectroscopy (MS) and FTIR. These techniques allow the analysis of evolved gases as the temperature is increased (Maciejewski & Baiker, 1997).

The characterisation technique of coupling TGA with FTIR has not yet been explored in the analysis of VCIs. TGA is characterised by high accuracy, reproducibility and sensitivity (Materazzi, 1997). However, TGA alone is a limited technique when it comes to the direct identification of evolved gases and the analysis when two or more volatiles are evolved simultaneously. TGA only provides a net overall weight. Coupling TGA with FTIR offers advantages such as that the decomposition of gaseous products can be identified at all stages during the analysis, and that the evaporation rates and vapour pressure of volatiles can be determined (Focke, 2003; Pieterse & Focke, 2003; Pieterse *et al.*, 2006). TGA weight losses of 10 µg or less may be obscured by noise or drift effects. However, the high sensitivity of FTIR can strongly detect absorbing vapours such as CO_2 and NH_3 at lower levels, and

samples can be introduced into TGA without any chemical or physical modification (Mittleman, 1990; Materazzi, 1997). Both qualitative and quantitative characterisation of the material during thermal decomposition or vaporisation can be performed.

Qualitative TGA analysis is performed by comparing the recorded spectral response with the key fragment ions and their relative intensities for known compounds with those of the reference material (Eigenmann *et al.*, 2006a & b). Compared with other evolved gas analysis methods, FTIR is fast, offers high sensitivity and can detect almost all molecules except the homonuclear diatomic gases (Eigenmann *et al.*, 2006a).

In quantitative measurements the gas flow rate, heating rates and the spectral resolution should be kept constant. The peak area can be calibrated to milligrams of the generated gas, and acceptable linear concentration can be obtained using the Beer-Lambert law (Mittleman, 1990). The calibration requires the preparation of reference mixtures with varying concentrations (Marsanich *et al.*, 2002; Eigenmann *et al.*, 2006a & 2006b).

Eigenmann *et al.* (2006a) described three methods of quantification using TGA-FTIR. The methods are based on calibration by decomposing a sample with a well-known reaction stoichiometry, injection of a known amount of calibration standard into the carrier gas stream flowing through TGA and FTIR, and vaporisation of known amounts of liquids in TGA. These quantification methods are discussed below.

Pulse calibration

In this calibration method, FTIR signal quantification is achieved by injecting (through the installed injection ports) the pulses of a known volume before and after the decomposition of the samples being investigated (Eigenmann *et al.*, 2000; 2006a & 2006b). This is followed by heating of the installed injection ports. The method requires a relatively low gas flow rate. This is because of the short residence time in the transfer line which results in a sharp and narrow FTIR signal (Eigenmann *et al.*, 2006a). The method was recently used by Marsanich *et al.* (2002).

Pinhole calibration

This method involves placing a known amount of liquid in a crucible. The crucible is then closed with a lid with known pinhole diameters. This is followed by placing a sample on TGA and this is then vaporised isothermally or by linear heating ramp (Eigenmann *et al.*,

2006a). The sample leaves the pan through the pinhole by diffusion until the vapour pressure is greater than the atmospheric pressure (Slager & Prozonic, 2005). For highly volatile liquids it is necessary to use lids with smaller pinholes (Eigenmann *et al.*, 2006a). The carrier gas flow is important in this method because it affects the intensity and shape of the FTIR bands (Slager & Prozonic, 2005; Eigenmann *et al.*, 2006a). Low flow rates lead to high maximum intensities but increase the residence time of the evaporated molecules in TGA-FTIR. This might result in back-mixing which leads to significant tailoring of the FTIR signal. This makes it difficult to evaluate the peak intensities of the recorded FTIR signals. The main disadvantage of this method is the uncontrolled evaporation of sample during experimental settling, which means that calibration and decomposition cannot be done in one experimental run (Eigenmann *et al.*, 2006a).

Differential calibration

This method is based on the isothermal or non-isothermal vaporisation of a liquid compound at different temperatures. It entails utilising low heating rates. In the differential time periods, simultaneous monitoring of the corresponding mass losses and intensities of the FTIR signal is required. The method involves plotting a calibration curve of mass lost versus the FTIR integral intensity. The calibration standard and sample under investigation are placed in two separate pans which are weighed continuously during the TGA runs (Eigenmann *et al.*, 2006a). Marsanich *et al.* (2002) used this method and the results revealed that it is only reliable if the liquid solution under investigation has low volatility at ambient temperature.

3 EXPERIMENTAL

3.1 Reagents and suppliers

Table 1 shows all the reagents, the molecular mass, the melting and boiling points, and the suppliers. All the reagents were used without further purification.

Table 1: Reagents, molecular mass, melting and boiling points, and the suppliers

Reagent	M ($g.mol^{-1}$)	ρ ($g.cm^{-3}$) at 20 °C	m.p. (°C)	b.p. (°C)	Supplier
Hexylamine (99%)	101.19	0.77	-22.90	131.00	Merck Chemicals
Morpholine (99.5%)	87.12	1.01	-5.00	129.00	Sigma Aldrich
Triethylamine (99%)	101.19	0.73	-114.70	88.70	Merck Chemicals
Formic acid (85%)	46.03	1.22	8.40	100.80	Associated Chemical Enterprises
Acetic acid (99.8%)	60.05	1.05	16.50	118.10	Merck Chemicals
Propanoic acid (99%)	74.08	0.99	-21.00	141.00	Merck Chemicals
Hexanoic acid (98%)	116.16	0.92	-3.40	205.00	Fluka
Octanoic acid (99.5%)	144.21	0.91	16.70	237.00	Sigma Aldrich
Sodium hydrogen carbonate (99%)	84.01	2.20	50.00	851.00	Merck Chemicals
Sodium sulphate anhydrous (99%)	142.04	2.66	884.00	1429.00	Unilab
Sodium chloride (99.5%)	58.44	2.16	801.00	1413.00	Unilab
Silica gel	-	-	-	-	Merck Chemicals
Drierite 8 mesh	-	-	-	-	Sigma Aldrich
pH strips	-	-	-	-	Merck Chemicals

3.2 Experimental methods

Amine-carboxylic acid binary mixtures were prepared in a dry glove-box under a nitrogen atmosphere to avoid air oxidation or contamination with moisture. The mixtures were prepared by weighing out the predetermined amounts of the constituents. The primary amine used in the present study was hexylamine, the secondary was morpholine and the tertiary was triethylamine. The carboxylic acids used were formic, acetic, propanoic, hexanoic and octanoic acids.

Each binary system consisted of the amine-acid mixture with amine mole fractions of 0.20, 0.25, 0.33, 0.50, 0.67, 0.75 and 0.80. All the experiments were performed at an atmospheric pressure of 91.6 ± 0.3 kPa. Phase-separated amine-carboxylic acid mixtures were individually characterised and labelled top or bottom, depending on the position of the phase-separated layer.

Liquid-liquid phase composition data were determined by titration under reflux at atmospheric pressure. Amine was added to a known amount of carboxylic acid at 50 °C from a burette until the mixture became turbid. The temperature of the mixture was controlled by a heated water bath. Each experiment was repeated at least three times for statistical purposes.

The densities of the neat amines, carboxylic acids and the selected mixtures were determined at atmospheric pressure with a glass pycnometer. The temperature was maintained at 50 ± 1°C using a heated water bath fitted with a temperature controller.

Corrosion tests were performed on mild steel, galvanised steel and copper metal buttons using Skinner's corrosion test method (Skinner, 1993). The method was used as is, without any further modifications. In this test the metal buttons are first exposed to a small quantity of the VCI during a film forming period. This is followed by a corrosion period during which electrolyte produces continuous condensation on the downward-facing exposed metal surface. The test simulates relatively harsh conditions with the actual metal temperature reaching a temperature of approximately 33 °C. In every corrosion experiment performed new glass-wares and or equipment were used.

The full method was as follows. The metal buttons were 16.0 mm in diameter. The thicknesses were 0.49 mm, 0.59 mm and 0.66 mm for the galvanised steel, mild steel and copper metals respectively. The surfaces of the mild steel and copper were first polished and rinsed several times in acetone. The polishing was omitted for the galvanised steel buttons to

avoid removing the zinc layer from the surface. The surface roughness of polished metal buttons was determined with Bruker Dimension Icon® atomic force microscope (AFM). Experiments were carried out in the contact mode with SNL tip (silicon tip on nitride lever). The spring constant was 0.12 Nm^{-1}. For each metal, the surface roughness was determined as an average over fifteen 50 μm image scans (captured at the scan rate of 0.2 Hz or 0.4 Hz) performed on three different samples. The measure root mean square average of the height deviations, from the mean image data place were 0.21 ± 0.07 μm, 0.22 ± 0.12 μm and 0.26 ± 0.14 μm and for the galvanised steel, mild steel and copper metals respectively.

Weight determinations of the individual metal buttons were performed prior to the corrosion tests. A 10 mm hole was punched into a plastic film with an adhesive side back. This film was placed over the metal disc with the hole located in a concentric position. This assembly was then stuck to the inside surface of the lid of a 1 L glass preserving jar. On closing the jar the exposed polished metal surface pointed down towards the bottom of the jar. Thus the adhesive film held the metal buttons in place such that the metal surface area, exposed to water vapour and moisture condensation during the corrosion test was approximately 80.8 mm^2.

Approximately 250 mg of the VCI model compound to be tested was measured into a glass vial (diameter ca. 54 ϕ mm; height ca. 60 mm) and placed inside a 1 L glass jar. The lid was closed and jar was partially submerged in a water bath with temperature set at 40 °C. About one third of the jar protruded above the water level. Following a 72 h film forming period, electrolyte was added to the 1 L jar and it was left for another 72 h at 40 °C. This corrosive electrolyte was prepared by dissolving approximately 148 mg of sodium sulphate, 165 mg of sodium chloride and 138 mg of sodium hydrogen carbonate in 1 L of deionised water.

At the end of this period the metal buttons were removed from the lid. Following an evaluation by visual inspection, the surfaces of the metal buttons were cleaned by rinsing them several times with acetone. They were left to dry before mass loss was determined. Every experiment was repeated at least three times for statistical purposes. Eight blanks were run for each metal to provide a reference corrosion rate under the test conditions used. These test specimens were treated in the same way except that no corrosion inhibitor was added. The corrosion rate (C_R) and inhibitor effectiveness of each sample in μm $year^{-1}$ were estimated from the mass loss determinations using mass loss determinations using Equations (1) and (2) (given in Chapter 2).

In a separate set of experiments, the corrosion tests were repeated up to the end of the film forming period. At this point the vials were removed and weighed to determine how much of the VCI model compound had evaporated. In addition, vials containing 250 mg VCI mixture were placed in a convection oven set at 40 °C. They were removed after 72 h and the mass loss was recorded.

The pH for the selected VCI model compounds was determined using Schott® instruments lab 860 pH meter. The pH meter was calibrated before measurements by using the standard solutions. Solutions containing approximately 5 wt. % VCI model compound in deionised water were prepared. The pH of the VCI solutions was determined by submerging the probe into a VCI solution while stirring and recording the values for each solution. The probe was thoroughly rinsed with deionised water prior to placing in a solution for pH measurement.

The refractive indices of the amines, carboxylic acids and their mixtures at 20 °C were determined using an ATAGO® NAR-liquid instrument (Model DTM-N) with digital thermo-meter supplied by ATAGO Ltd (Japan). One or two drops of the sample were placed on the polished surface of the refracting prism. The incident prism was closed and locked using the knob so that the liquid was evenly distributed on the face of the refracting prism. This was followed by closing the refraction mirror and opening the light shield for the incident prism. The refractive index was measured by viewing the mixture through the eyepiece. The dispersion was adjusted using a correction knob until a clear light/dark boundary was seen. This boundary was lined up exactly in the centre of the cross-hairs and the refractive indices were determined from the scale below the boundary. After each measurement the surface was cleaned and dried to avoid contamination. The accuracy of the refractometer was checked by using the standards with known refractive index values and comparing the reported values with the measured values before and after the measurements.

3.3 Instrumentation

The binary mixtures were characterised using simultaneous TGA-FTIR. Data were collected by means of a Perkin-Elmer TGA 4000 thermogravimetric analyser coupled with a Spectrum RX 100 spectrometer with a 1 m TL800 EGA transfer line. A 180 µl open aluminium pan was partially filled with 85 ± 5 mg of sample. The pan dimensions are shown in Figure 3. The sample was heated from 25 to 50 °C, at a heating rate of 20 °C min^{-1} and kept isothermal at 50 °C for the duration of the test period. The high test temperature of 50 °C was selected to maximise volatility and because it corresponds to the highest temperature at which VCIs are

expected to function during commercial use. The data were collected under nitrogen (N_2) at a flow rate of 50 mL min^{-1} to prevent oxidation. The evolved gases were transferred from the TGA to the FTIR cell at a flow rate of 30 mL min^{-1}. The spectra were recorded every minute at 2 cm^{-1} wavenumber intervals at a resolution of 2 cm^{-1}. The transfer line and FTIR cell temperature were both kept at 230 °C to avoid condensation and to dissociate all complexes.

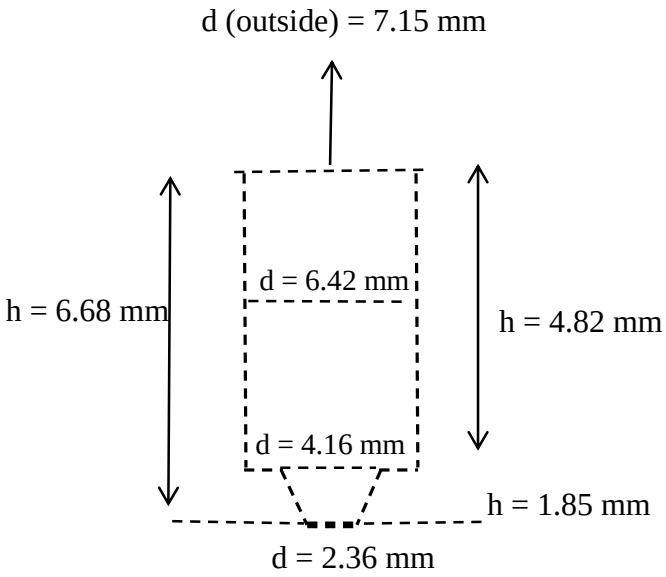

Figure 3: TGA pan dimensions (where d refers to the diameter and h the height)

There is a time lag from the point at which vapours are released and recorded as a TGA mass loss signal and the capture of the corresponding FTIR spectrum. The length of this time delay was determined experimentally by monitoring the thermal decomposition of sodium bicarbonate. This reaction releases carbon dioxide which features a strong IR absorption band at 2349 cm^{-1}. Approximately 30 mg of sodium bicarbonate was placed in an open 180 µl aluminium pan. The sample was heated from 25 to 400 °C at 20 °C min^{-1} under a stream of nitrogen gas at a flow rate of 50 mL min^{-1}. The delay time was determined as the difference between the time that the TGA derivative mass loss signal reached a maximum and the time that the maximum absorption of the CO_2 IR peak was reached. The experiment was repeated at least three times for statistical purposes.

Liquid phase FTIR data were collected using a Perkin-Elmer Spectrum RX 100 spectrometer. Samples were placed between two KBr crystal windows (25 mm diameter and 4 mm thick). Background corrected spectra were recorded at room temperature in the wavenumber range 4000 to 800 cm^{-1} at a resolution of 2 cm^{-1}.

Differential scanning calorimetry (DSC) was performed on a Mettler Toledo DSC1 instrument. Approximately 5–10 mg of each sample was placed in standard a 40 µL aluminium pan with a pinhole and heated from -40 °C to 400 °C at a heating rate of 10 °C min^{-1} in nitrogen flowing at 50 mL min^{-1}.

4 RESULTS

PART 1: METHOD DEVELOPMENT

Figure 4 shows the phase diagram for TEA-acetic acid mixtures at 1 atmosphere using the overall amine mole fraction (z_A) as composition descriptor. It summarises the previously reported liquid-liquid equilibrium (LLE) and vapour-liquid equilibrium (VLE) phase composition data for TEA-acetic acid mixtures (Kohler *et al.*, 1972; Van Klooster & Douglas, 1945). The LLE data of Kohler and co-workers deviate at higher amine concentrations. The LLE data points determined in this study at a temperature of 50 °C (z_A = 0.44 and 0.89) are plotted for comparison. They are in better agreement with the values reported by Van Klooster & Douglas (1945).

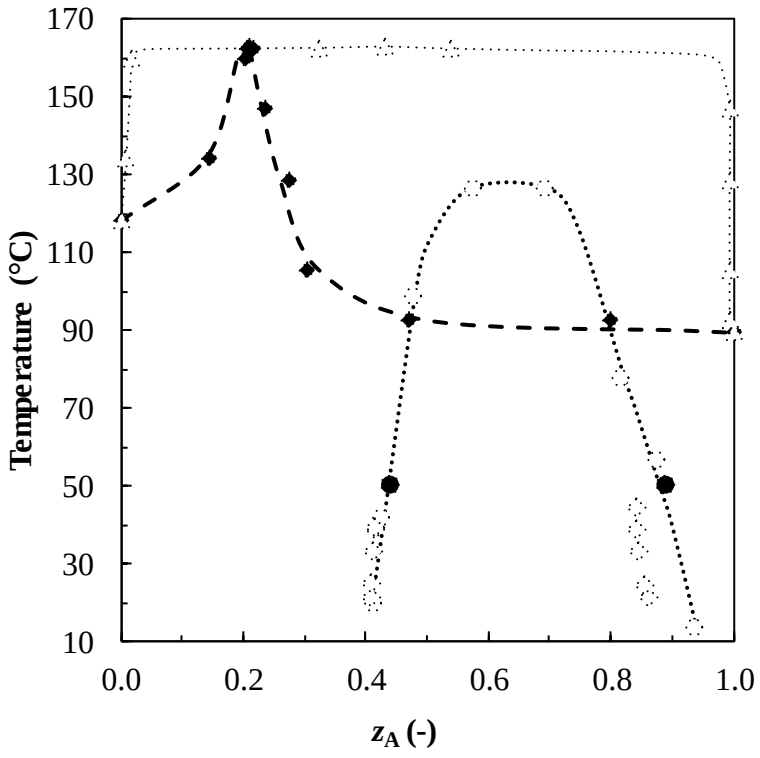

Figure 4: Phase diagram of TEA-acetic acid binary mixtures; ◊ indicates LLE data obtained by Kohler *et al.* (1972), ○ indicates LLE data, ♦ and Δ VLE data obtained by Van Klooster & Douglas (1945) at atmospheric pressure, and ● LLE data obtained in the present study

4.1 Liquid phase FTIR

The liquid phase FTIR spectra of pure acetic acid and pure triethylamine in comparison with their vapour phase spectra are shown in Figures 5(a) and (b). In the liquid phase pure acetic acid shows a broad OH stretching absorption band of the dimer-bonded hydrogen form centred at 3040 cm^{-1} (Marchél, 1987). The contribution due to anti-symmetric and symmetric stretching vibration of the methyl CH_3 group attached to the carbonyl is observed at 2935 cm-^{1}, 2685 cm^{-1} and 2630 cm^{-1} (Päivärinta *et al.,* 2001). A sharp absorption band of strong intensity due to carbonyl C=O dimer form is observed at 1705 cm^{-1}, while the monomer contribution is observed as a very weak band at 1760 cm^{-1} (Coates, 2000). A broad band of weak intensity at 944 cm^{-1} is due to the OH out-of-plane deformation vibration mode of the two hydrogen atoms in the acetic acid dimer ring (Burneau *et al.,* 2000). The presence of the aforementioned band suggests that acetic acid dimers are the dominant species in the liquid phase. The methyl CH_3 asymmetric and symmetric bending vibration bands are observed at 1409 cm^{-1} and 1360 cm^{-1} respectively (Coates, 2000). The position of these methyl bands coincides with that of the COH in-plane bending vibration at 1409 cm^{-1} and a shoulder at 1366 cm^{-1}. The OH deformation vibration is observed at 1051 cm^{-1}, coinciding with the methyl CH_3 rocking mode and the C=O stretching mode calculated to the value of 1021 cm^{-1} (Burneau *et al.,* 2000). The shoulder at 1240 cm^{-1} is due to CO stretching vibration (Coates, 2000).

The position of the OH band in acetic acid shifted to higher wavenumbers of 3580 cm^{-1} in the vapour phase (see Figure 5a). The shape and position of this band indicate that the monomers are dominant in the vapour phase. This is also confirmed by the shift of the C=O absorption band to higher wavenumbers and the absence of the OH out-of-plane deformation vibration mode at 944 cm^{-1} in the vapour phase.

TEA (z_A = 1.00) shows an absorption band at 1477 cm^{-1} due to the CH_3 anti-symmetric deformation mode (see Figure 5b). The CH_3 symmetric umbrella deformation mode is observed at 1385 cm^{-1}. The CN stretching vibration mode is observed at 1212 cm^{-1} and 1057 cm^{-1}(Coates, 2000; Socrates, 1980). The liquid phase and vapour phase FTIR spectra are very similar.

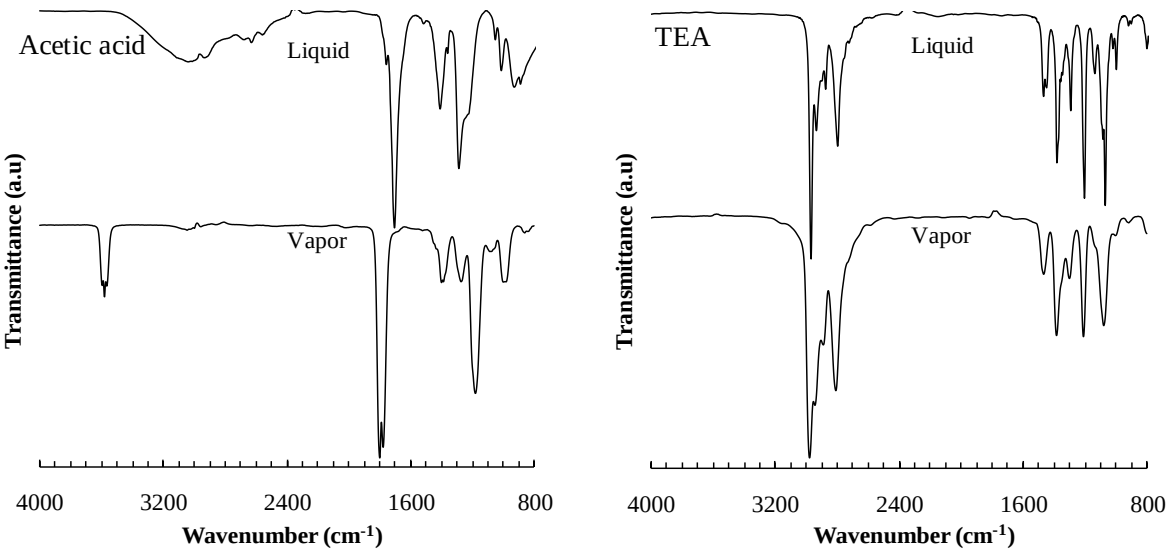

(a) (b)

Figure 5: Liquid phase and vapour phase spectra of (a) pure acetic acid and (b) pure TEA

Figure 6 shows the liquid phase FTIR spectra of the binary TEA-acetic acid mixtures compared with pure TEA and pure acetic acid. Addition of amine results in a shift in the dimer C=O band position to higher frequencies and the disappearance of the dimeric OH out-of-plane deformation band. The lack of the OH out-of-plane dimer form indicates the formation of a complex between TEA and acetic acid (Karlsson *et al.*, 2000). The carbonyl C=O is observed at 1722 cm^{-1} in all TEA-acetic acid mixtures. The contribution due to the C=O monomer form is observed as a shoulder in the mixture with composition z_A = 0.20, but is absent when z_A = 0.33. The new absorption band observed at 1576 cm^{-1} is due to the presence of an ionic carboxylate, COO^- (Wierzejewska-Hnat *et al.*, 1980; Friberg *et al.*, 1990). The COH in-plane bending absorption bands shifted position to a lower frequency of 1378 cm^{-1} due to hydrogen bonding between acetic acid and TEA. This was observed in all the mixtures. The CO stretching absorption band is observed at 1248 cm^{-1}. The intensity of this band is stronger compared with that of acetic acid. This is attributed to the contribution of the CN stretching mode from amine which also occurs at the same position (Socrates, 1980). The bottom phase of the sample prepared as z_A = 0.80 shows absorption bands similar to z_A = 0.20, 0.25 and 0.33.

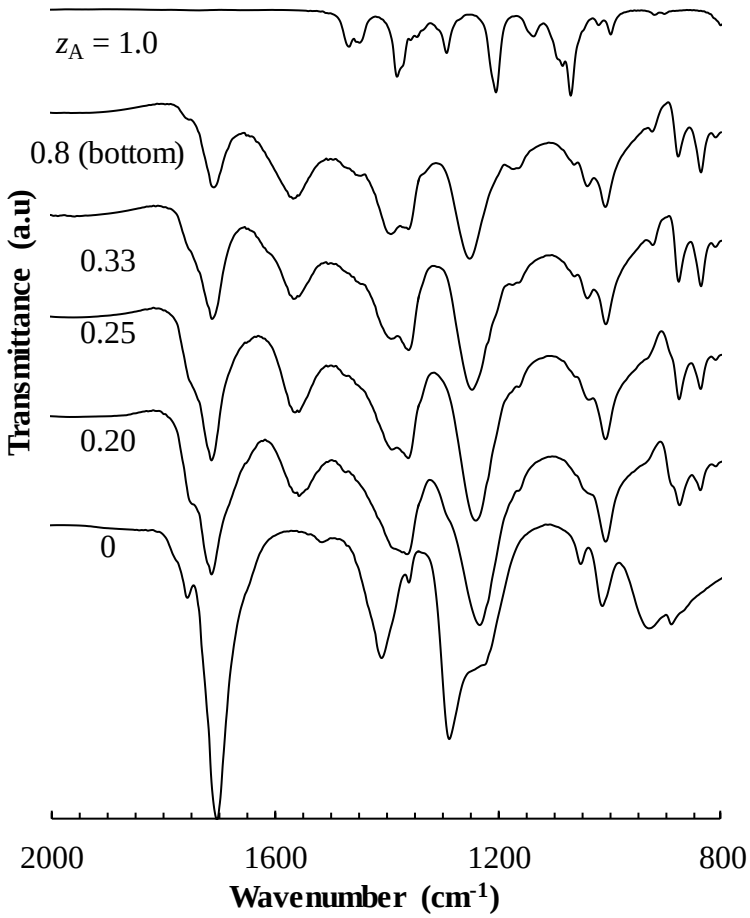

Figure 6: Liquid phase FTIR spectra of binary acetic acid-TEA mixtures in comparison with pure acetic acid and pure TEA

4.2 DSC

The DSC data for acetic acid showed two thermal transitions (see Figure 7). The first was the melting transition and had an onset of 11 °C, while the second was a boiling transition with an onset of 108 °C. TEA melts at -115 °C. Consequently, in the temperature range studied, TEA showed only a single thermal (boiling) transition with an onset temperature of 84 °C. The TEA-acetic acid mixtures featured significantly higher boiling transitions when evaporated into a stream of nitrogen gas. A sample with z_A = 0.39 and a mixture with z_A = 0.33 featured onset temperatures of 156 °C. Mixtures with compositions z_A = 0.20 and z_A = 0.25 showed boiling onsets occurring at 154 and 158 °C respectively. This suggests that the mixtures with the highest apparent boiling points are those that closely match the composition of the A_1C_3 complex, i.e. an amine to acid mole ratio of 1:3.

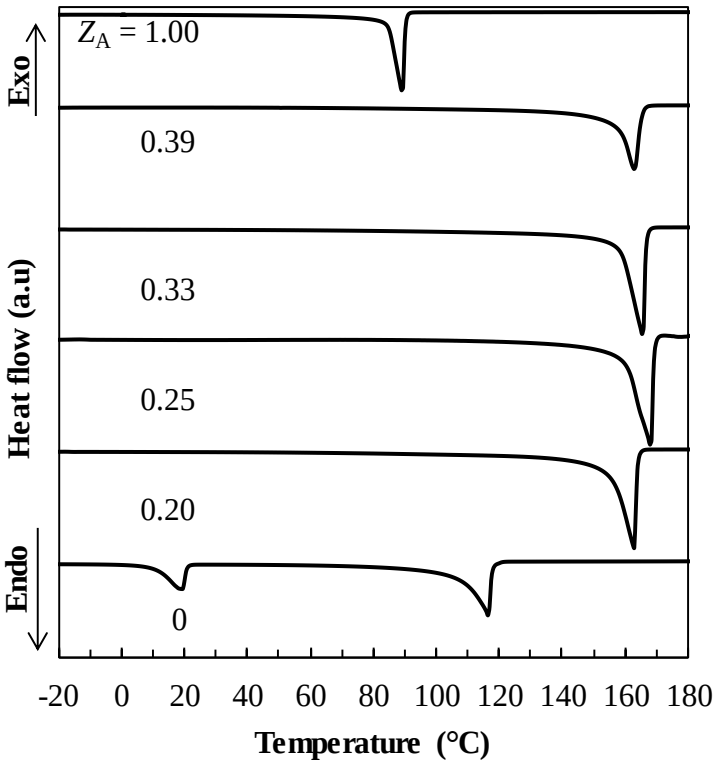

Figure 7: DSC profiles of acetic acid-TEA binary mixtures in comparison with pure acetic acid and pure TEA

4.3 TGA-FTIR

Figure 8 illustrates how the lag time between the mass loss and the FTIR signals was determined. It shows plots of the TGA derivative mass loss signal and the maximum absorbance of the band located near 2300 wavenumbers in the FTIR spectrum. The excellent match of the superimposed signals was obtained by an appropriate time shift of the former signal. The average lag time was determined as 0.56 ± 0.03.

Figure 9 shows the TGA mass loss curves for TEA-acetic acid and selected mixtures. The pure compounds evaporated much more rapidly than the mixtures. Mass loss was most rapid for TEA, reflecting its higher volatility compared with acetic acid. Interestingly, the z_A = 0.24 mixture was the least volatile as it showed the lowest mass loss rate. This composition is close to that of the A_1C_3 complex. The sample of the top layer phase with z_A = 0.89 evaporated at a similar rate to pure triethylamine, suggesting that only the amine was released. The sample with z_A = 0.39, with a composition matching that of the bottom layer obtained following phase separation, evaporated at an intermediate rate.

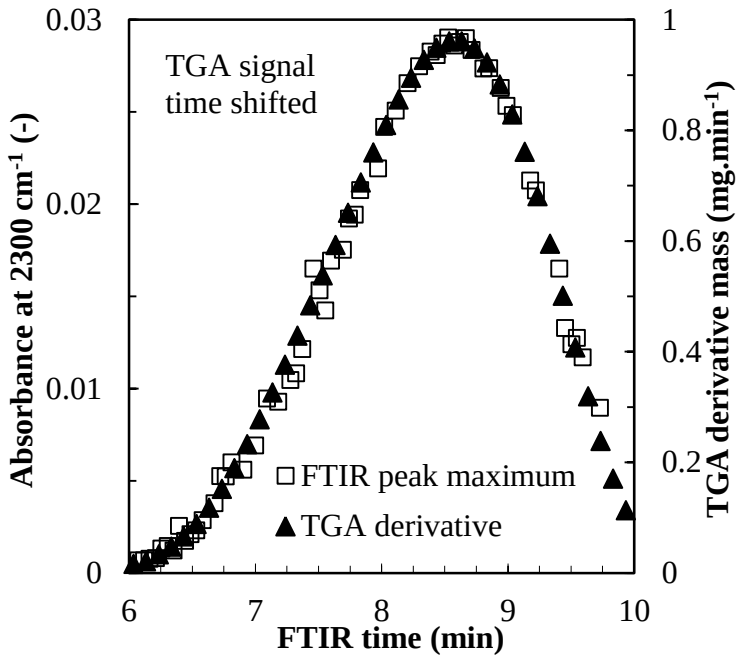

Figure 8: TGA-FTIR data for heating sodium bicarbonate from 25 °C to 400 °C at a scan rate of 20 °C min^{-1} in nitrogen gas flowing at a rate of 50 mL min^{-1}. The maximum absorbance of the band located near 2300 wavenumbers in the FTIR spectrum (□) and the TGA derivative mass signal shifted by a time interval of 0.56 min (▲) are shown

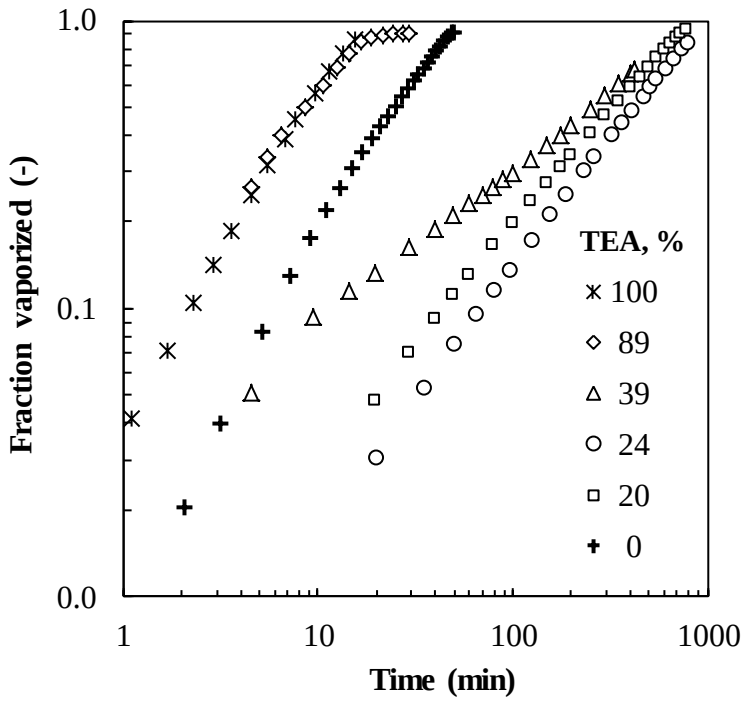

Figure 9: TGA evaporation profiles of selected acetic acid-TEA binary mixtures compared with pure acetic acid and pure TEA

Figures 10(a) and (b) compare the vapour phase FTIR spectra of representative TEA-acetic acid mixtures with the spectra obtained for pure TEA and pure acetic acid vapours. Consider the spectra in Figure 10(a) for the mixture with initial composition $z_A = 0.33$. Now it appears that it is TEA that evaporates initially as the spectra that is recorded when just 3% had evaporated is nearly identical to that of pure TEA. The C=O monomer and OH absorption bands for acetic acid at 1790 cm^{-1}, 1814 cm^{-1} and 3580 cm^{-1} respectively are only noticeable at a much later stage.

In Figure 10(b) (for the mixture with composition $z_A = 0.20$), the spectrum recorded when just 1% had evaporated is nearly identical to that for pure acetic acid. No TEA absorption bands are noticeable at this stage. This implies that the steady-state vapour composition lies between these two compositions.

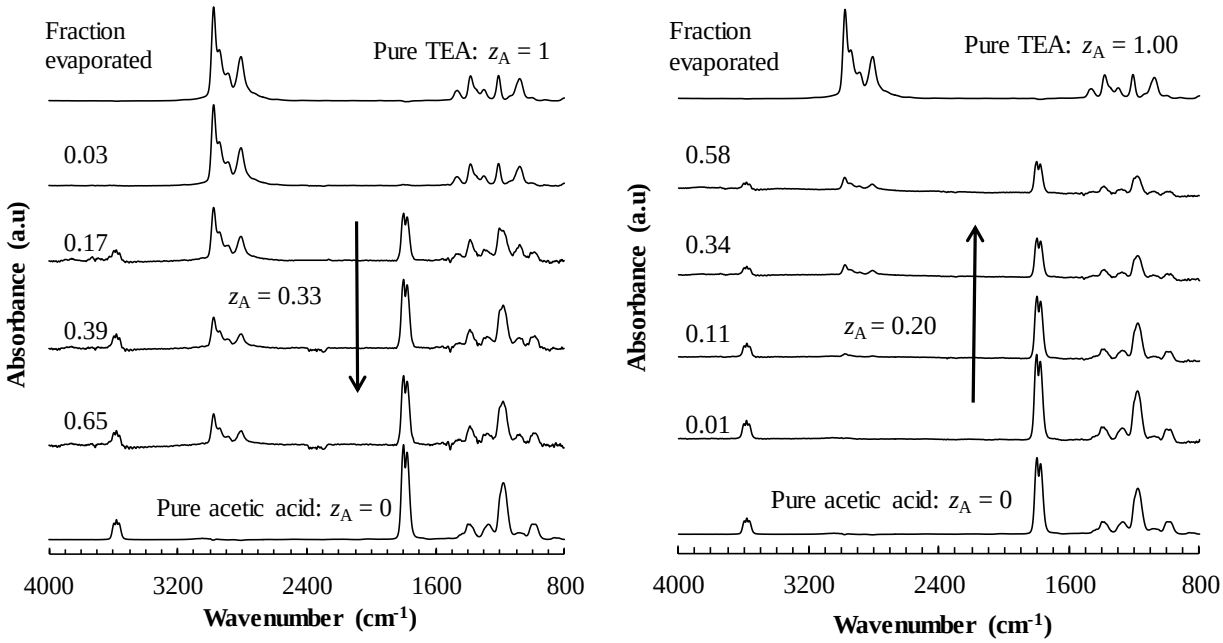

(a) (b)

Figure 10: Time evolution of the gas phase FTIR spectra for a mixture with initial composition $z_A = 0.33$ (a) and $z_A = 0.20$ (b) as a function of mass fraction evaporated. The arrows indicating the time direction and the spectra for pure TEA and pure acetic acid are shown for comparison

The dominant features that distinguish the FTIR spectra for TEA and for acetic acid are the groups of bands between 3300 cm^{-1} and 2450 cm^{-1}, and those between 1950 cm^{-1} and 1600 cm^{-1} respectively. These were used to determine the composition of the vapour streams in the following way. The areas under the absorbance vs. wavenumber plots, from 3300 cm^{-1}

and 1600 cm^{-1}, were determined using fourth-order Newton Cotes integration (Gerald, 1970). However, interfering CO_2 absorption bands are found in the region between 2270 cm^{-1} and 2450 cm^{-1}, and this region was therefore excluded from the integration range. The integrated areas were scaled directly with the TGA mass loss rates according to

$$a_i = k_i \dot{m}_i = \int_{1600}^{2270} A d\sigma + \int_{2450}^{3300} A d\sigma \qquad (5)$$

where a_i is the integrated area under the absorbance curve (in the wavenumber ranges indicated) in cm^{-1}; $\dot{m}_i$ is the TGA mass flux of component i entering the vapour phase in $mg.min^{-1}$; k_i is a characteristic constant for component i with units $min.mg^{-1}.cm^{-1}$; A is the dimensionless absorbance; and σ is the wavenumber measured in cm^{-1}.

The proportionality constants for the instrument combination used in this study were experimentally determined as k_A = 20.0 ± 0.2 and k_C = 18.3 ± 0.4 for triethylamine and acetic acid respectively (see Figure 11).

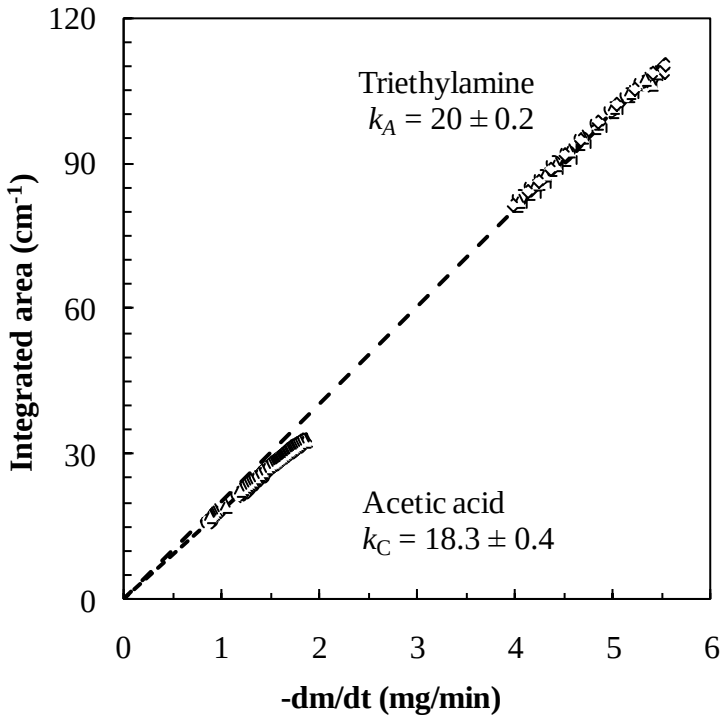

Figure 11: TEA and acetic acid calibration curves used for the determination of the proportionality constants

A characteristic normalised shape function for each of the pure components was defined by the following integral:

$$\alpha_i(\sigma) = \int_{\sigma}^{3300} A d\sigma \Big/ \left(\int_{1600}^{2270} A d\sigma + \int_{2450}^{3300} A d\sigma \right) \quad (6)$$

where the symbols have the same meaning as in Equation (5), with the integral in the numerator excluding the wavenumber range from 2270 cm^{-1} to 2450 cm^{-1}.

This shape function defines the profile of the integrated absorbance as a function of the wavenumber, σ. The shape function profile for pure components is independent of the mass flux and this was confirmed experimentally. The shape function profiles for triethylamine and acetic acid are shown in Figure 12.

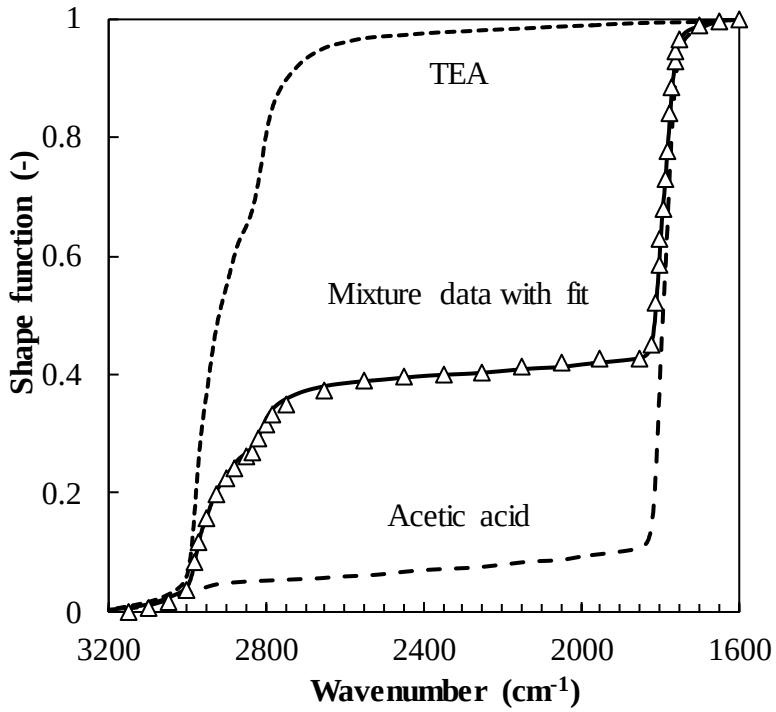

Figure 12: Shape function profiles α for pure acetic acid, pure TEA and experimental data (Δ) for a vapour mixture. The solid line for the mixture was generated using Equation (7) with the β_{mix} = 0.638 value determined via a least squares curve fit. According to calculations using Equations (8) and (9), this indicates that the mixture contained approximately 25 mol % amine

Next consider the (normalised) shape function expected for a mixed vapour composition. Van Klooster and Douglas (1945) previously found that no molecular interactions occur above 162 °C in the TEA-acetic acid system. The present vapour phase spectra were recorded at an even higher temperature and both components should therefore be present in their monomer forms. Indeed, all the FTIR spectra recorded at 230 °C for the mixtures in this study were

consistent with this assumption. The absence of the carbonyl C=O dimer band at 1705 cm^{-1}, the shape and position of the OH band at 3580 cm^{-1}, and the strong C=O absorption band at 1790 cm^{-1} in the spectra recorded for the pure acetic acid vapour confirmed that acetic acid was predominantly present in the monomer form and that the contribution from dimers was insignificant. The ionic carboxylate bands were absent in the vapour spectra obtained for the mixtures. Furthermore, in the mixtures the acetic acid C=O absorption band was observed at almost precisely the same position found for the neat acetic acid (1790 cm^{-1} and 1814 cm^{-1}). This confirmed negligible interaction between acetic acid molecules and TEA molecules in the vapour phase at 230 °C.

The absence of complex-forming interactions in the vapour phase at the measurement temperature that was used means that the recorded spectra are simply a combination of the spectra expected for the pure compounds. Thus the shape function for a mixed vapour is given by a linear combination of the two pure-component shape functions:

$$\alpha_{mix} = \beta_{mix}\alpha_A + (1-\beta_{mix})\alpha_C \qquad (7)$$

where β_{mix} is a characteristic measure of the mixture composition and α_A and α_C are the shape functions for triethylamine and acetic acid respectively.

The β_{mix} values were determined from experimental data using least squares data fits of Equation (7). Once the β_{mix} values were known, the mass fraction of amine in the vapour phase was calculated using the following equation:

$$w_A = \frac{\beta_{mix}}{\beta_{mix} + \frac{k_A}{k_C}(1-\beta_{mix})} \qquad (8)$$

where w_A is the mass fraction of an amine in the vapour.

The mole fraction of amine in the vapour (y_A) was determined as follows:

$$y_A = \frac{w_A/M_A}{w_A/M_A + (1-w_A)/M_C} \qquad (9)$$

where M_A is the molar mass of an amine and M_C is the molar mass of carboxylic acid.

Figure 12 compares the measured shape functions α for pure acetic acid, pure TEA and the vapour released by a specific mixture. As mentioned above, such plots were used to

determine the composition of the vapours. This was done by first extracting the β_{mix} values in Equation (7). Next the amine mole fraction in the released vapour was determined by applying Equations (8) and (9). These were then plotted against time (Figure 13) or against the mass fraction of mixture released (Figure 14).

Figures 13 and 14 show that the mole fraction of an amine in the released vapour (y_A) initially either increases or decreases but then stabilises at a plateau value (see Figure 15). This value is, within experimental error, the same for all mixtures irrespective of their initial concentration. The plateau composition was determined as $y_A = 0.267 \pm 0.017$ by averaging all the vapour compositions measured beyond the point where 50% of the original charge had volatilised for mixtures initially containing 19, 20, 23, 24 and 38 mol % TEA. This value is only slightly higher than the composition of the A_1C_3 complex.

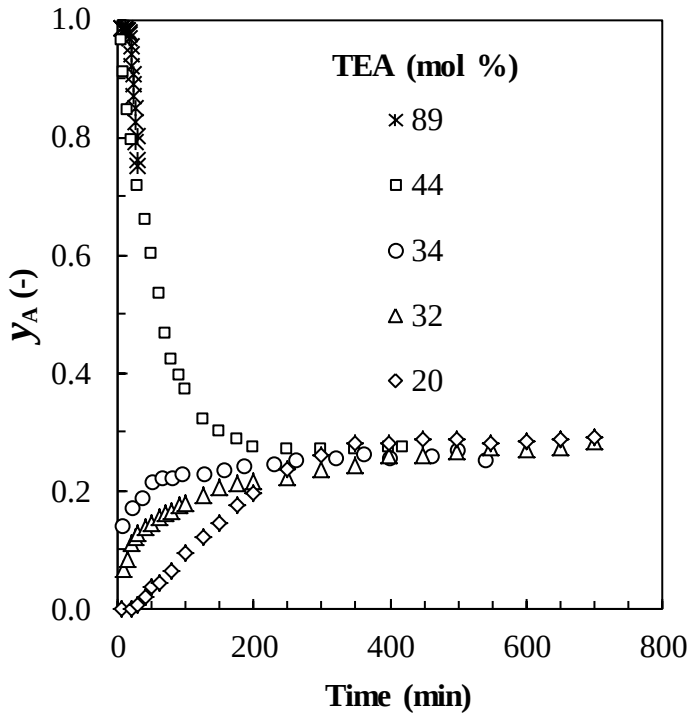

Figure 13: Time dependence of the mole fraction of TEA present in the released vapour. The indicated TEA concentrations refer to the initial TEA content of the liquid phase

When the composition of the emitted vapour stabilises at a plateau value, it must mean that this should also be true for the liquid phase. In fact, the compositions of the vapour and liquid phases should be the same. This can be checked by performing a mass balance. The differential equation is:

$$\frac{dm_A}{dm} = \frac{1}{\dot{m}}\frac{dm_A}{dt} = y_A \tag{10}$$

and

$$\frac{dm_C}{dm} = 1 - y_A \tag{11}$$

where m_i is the mass of component i in the liquid phase.

These two equations can be solved by numerical integration using the TGA mass loss data and the vapour phase composition determined from the FTIR results. The mole fraction of amine in the liquid phase can then be determined from:

$$x_A = \frac{m_A/M_A}{m_A/M_A + (1-m_A)/M_C} \tag{12}$$

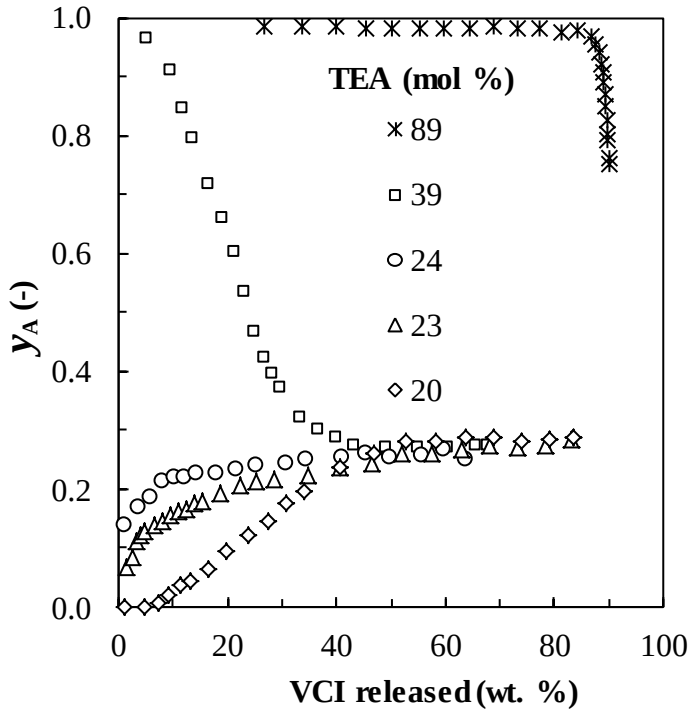

Figure 14: Mole fraction of TEA released into the vapour phase as a function of the fraction of VCI released. The indicated TEA concentrations refer to the initial TEA content of the liquid phase

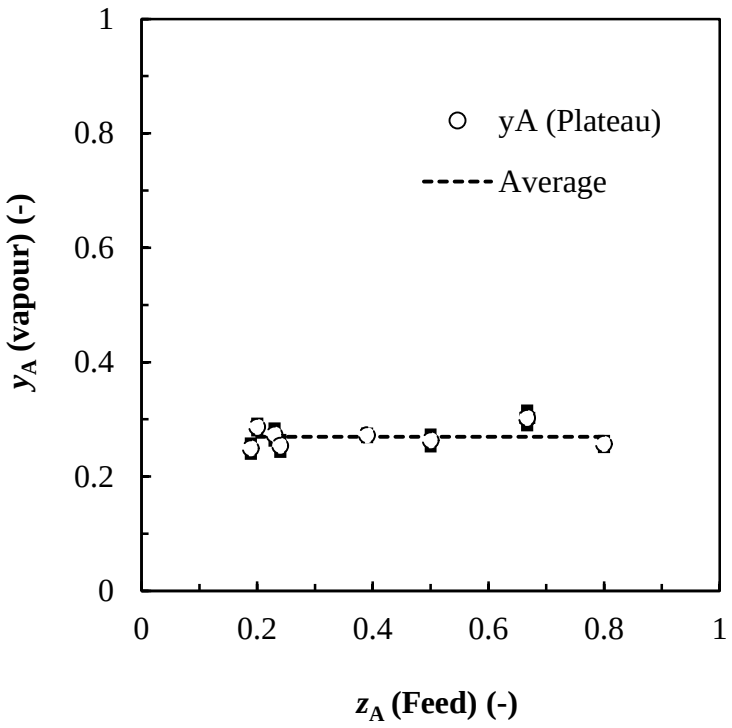

Figure 15: Evaporation trend obtained for TEA-acetic acid binary mixtures

The results of these calculations are presented in Figure 16. They confirm that the liquid compositions also approached the same plateau value as found for the vapour phase. This indicates that, over time, evaporation of an amine-acetic acid mixture will reach an "azeotrope"-like point where the relative concentrations of the vapour and liquid phases become identical.

The present results indicate that the steady-state composition of the vapour released by the TEA-acetic acid binary mixtures contains excess acetic acid. When this vapour comes into contact with the adsorbed moisture on the surface of a metal, the acid dimers in the A_1C_3 complex will dissociate and hydrolyse to form free monomeric acids. This may lower the pH values of the water film, which may then induce corrosion (Bastidas *et al.*, 2005). This may provide an explanation as to why TEA-acetic acid is a poor VCI (Vuorinen & Skinner, 2002). An effective VCI vapour has to contain excess amine and should not result in too low a pH for the liquid water film adsorbed on the metal surface.

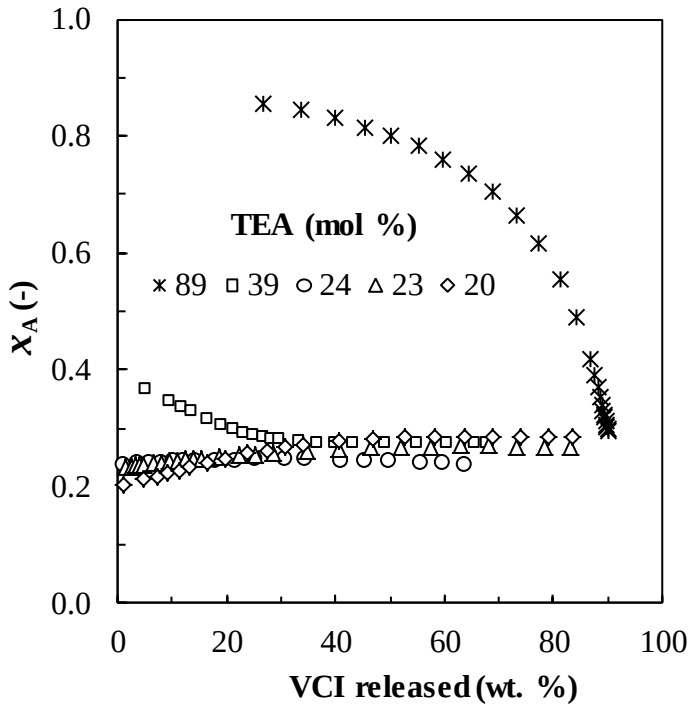

Figure 16: Calculated mole fractions of TEA in the liquid phase as a function of the initial mixture composition and the fraction of VCI released. The indicated TEA concentrations refer to the initial content of the liquid phase

PART 2: METHOD APPLICATION

4.4 Liquid phase FTIR and refractive index

The measured refractive index values are shown in Appendix A. Numerous liquid phase FTIR data were collected and these are shown in Appendix B. The data set in Figure 17 shows the effect of liquid phase composition on the FTIR spectra for triethylamine-hexanoic acid mixtures. The figure only shows the FTIR region of interest (between 1750 and 1350 cm^{-1}). The pure carboxylic acids (z_A = 0) all showed a sharp absorption band of high intensity at approximately 1705 cm^{-1}, which is characteristic of the hydrogen-bonded carbonyl (C=O) functional group in the carboxylic acid dimer (Coates, 2000). The absorbance of this peak decreases rapidly as the amount of amine present in the mixtures increases. It is very high in mixtures with low amine content and low in mixtures with high amine content.

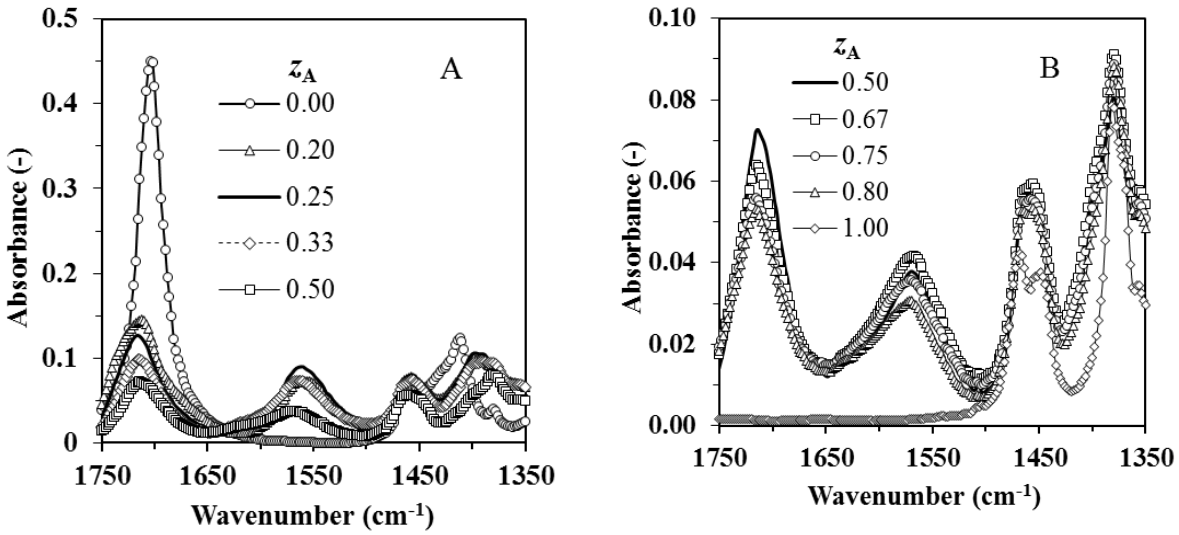

Figure 17: Liquid phase FTIR spectra of binary mixtures of triethylamine and hexanoic acid. The absorption maximum at ca. 1560 cm^{-1} is attained at a composition corresponding to the A_1C_3 complex, i.e. z_A = 0.25

As the intensity of this peak decreases upon amine addition, several new absorption bands develop that are consistent with the formation of an ionic complex (salt formation) between the amine and the acid in the liquid phase. The band observed at approximately 1560 cm^{-1} is due to the ionic carboxylate ion, COO^- (Päivärinta *et al.*, 2001; Coates, 2000), while the band near 1400 cm^{-1} is attributed to the protonated amine (Whitehead, 1969; Coates, 2000).

The effect of amine addition on the position of the carboxylic acid (C=O), carboxylate ion (COO^-) and the protonated amine absorption bands for various amine mixtures with octanoic acid is shown in Figures 18 and 19. No shift is observed in the position of the undissociated carboxylic acid absorption band in the mixtures with low amine content. The shift in the position to slightly higher wavenumbers is only observed from an amine mole fraction of $z_A = 0.50$ for hexylamine and at a later stage, i.e. when the amine mole fraction is $z_A = 0.67$ in mixture containing TEA. The shift in the position of this band is observed at an even higher amine mole fraction, $z_A = 0.80$, in the mixture containing morpholine (see Figure 19). The shift in the position of this band and the reduced intensity in the mixtures are considered to be an indication that amine addition breaks down the acid dimers in favour of salt formation and hydrogen bonding with acid (Päivärinta *et al.*, 2001; Orzechowski *et al.*, 2003).

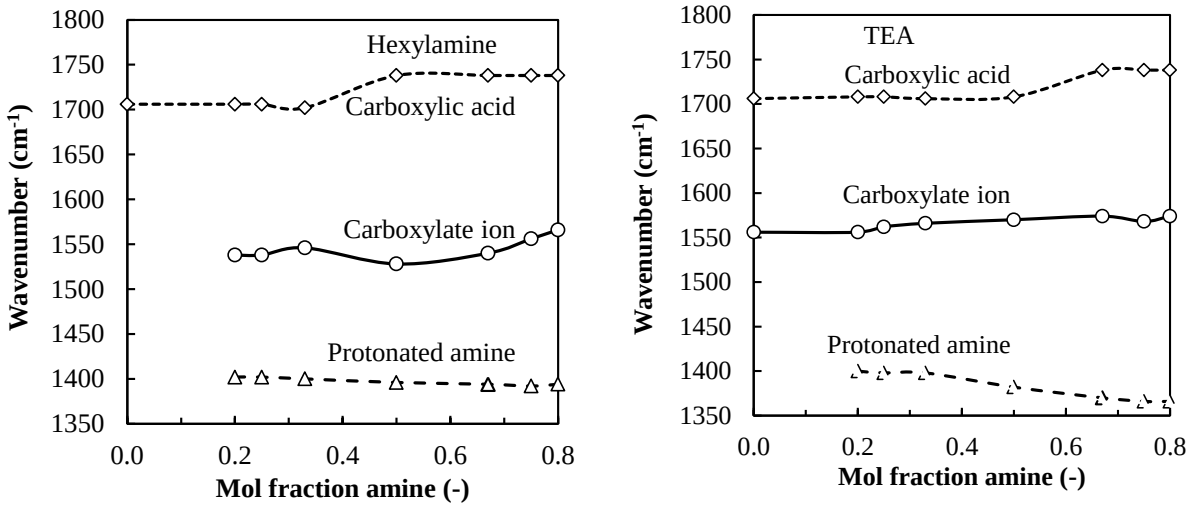

Figure 18: The effect of amine addition on the position of the FTIR absorption bands due to carboxylic acid (C=O), carboxylate ion (COO^-) and the protonated amine in the mixtures with amines (hexylamine and TEA) with octanoic acid

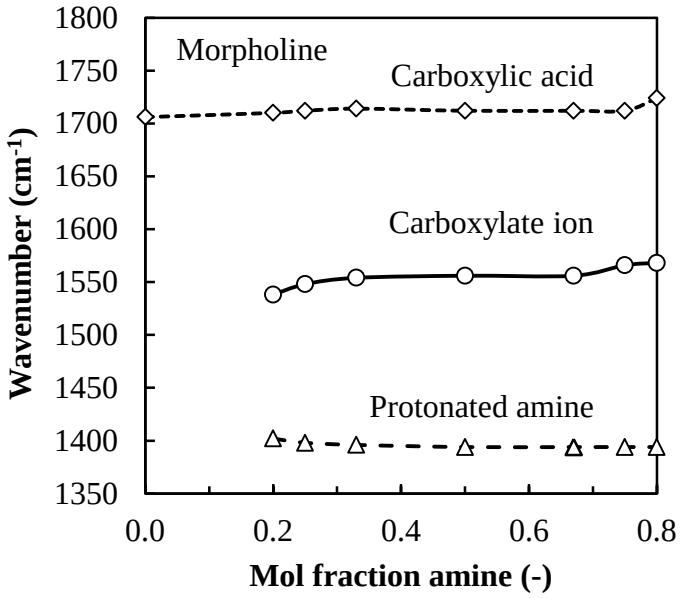

Figure 19: The effect of amine addition on the position of the FTIR absorption bands due to carboxylic acid (C=O), carboxylate ion (COO^-) and the protonated amine in the mixtures of morpholine with octanoic acid

The presence of these two absorption bands (carboxylate ion and protonated amine) confirms that amine addition leads to proton transfer from the acid to an amine during the complex-formation process and thus the ionic nature of the mixtures (Karlsson *et al.*, 2000; Orzechowski *et al.*, 2003). Both these bands (carboxylate ion and protonated amine) grow in intensity as amine is added but start waning again beyond a critical amine concentration. Figure 20 shows the effect of amine content on the intensity of the carboxylate ion band for mixtures containing octanoic acid. It reaches maxima at amine concentrations of $z_A = 0.25$ for the tertiary amine and $z_A = 0.50$ for the primary and secondary amines. The liquid phase FTIR spectra obtained using the other carboxylic acids also showed a similar trend. Thus the liquid phase FTIR spectra suggest that the A_1C_3 complex dominated in mixtures of the alkanoic acids with the tertiary amine (TEA), while the A_1C_1 (or more correctly the A_2C_2 complex) was strongly favoured in the mixtures containing the primary amine (hexylamine) and the secondary amine (morpholine).

The representative data for the variation of the refractive index with composition are shown in Figures 21A and B. These refractive index data also support the aforementioned hypothesis. The refractive index data reached a maximum value at $z_A \approx 0.25$ for the tertiary amine and at $z_A \approx 0.50$ for the primary and secondary amines. This was observed for all the amine-alkanoic acid mixtures.

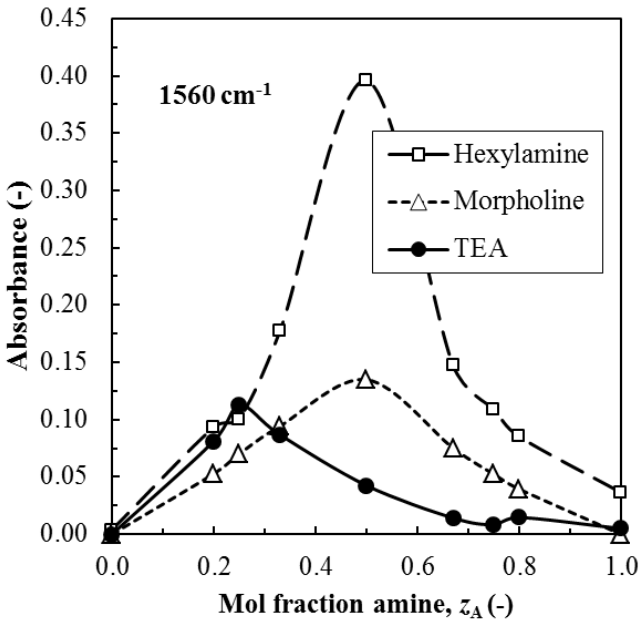

Figure 20: The effect of liquid phase composition on the absorbance maximum near 1560 cm^{-1} in the FTIR spectra of binary mixtures of the various amines with octanoic acid. The absorption maximum at ca. 1560 cm^{-1} is attained at a composition corresponding to the A_1C_3 complex for TEA, but for the other two amines it corresponds to the A_2C_2 complex, i.e. $z_A = 0.50$

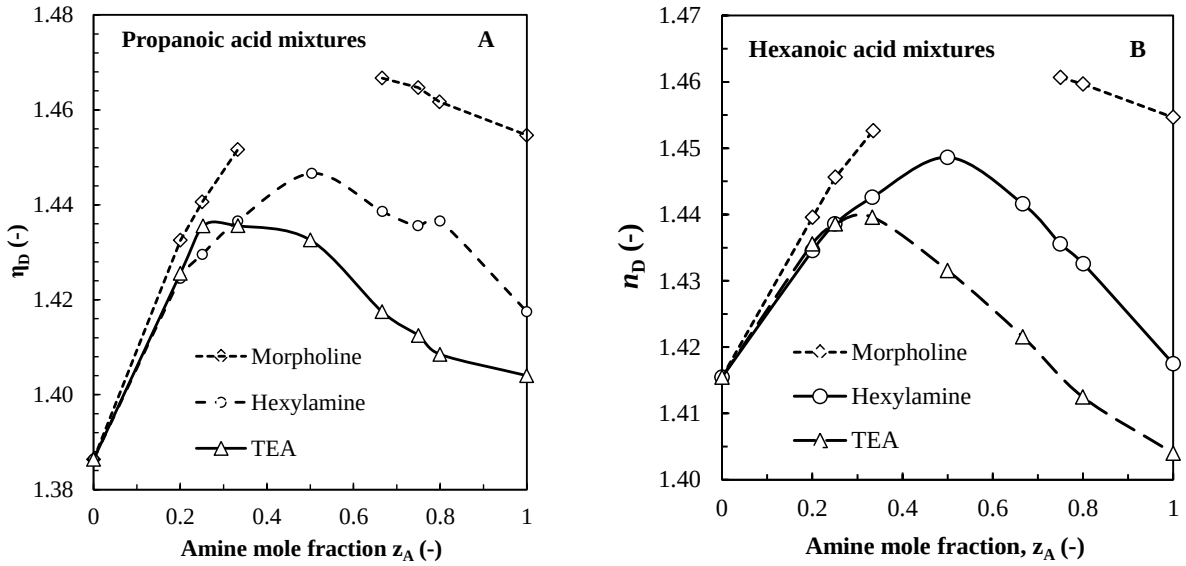

Figure 21: The effect of liquid phase composition on the refractive index of amine-propanoic (A) and amine-hexanoic acid (B) mixtures at 20 °C. The 1:1 and 2:1 (mole basis) mixtures of hexanoic acid and the 1:1 mixture of propanoic acid with morpholine are not reported because they were solids at this temperature

4.5 Liquid phase DSC

DSC scans covering the temperature range -40 °C to 250 °C collected under a flowing nitrogen stream are shown in Figure 22 for the pure amines and pure carboxylic acids. DSC scans for hexylamine and carboxylic acids (acetic, hexanoic and octanoic) featured two endothermic thermal transitions. The first DSC peak, with onset temperatures of -23, 11, -4.97 and 14.73 °C for hexylamine, acetic acid, hexanoic acid, and octanoic acid respectively, corresponds to the melting transition. The second endothermic event corresponds to the onset of boiling. The scans for TEA, morpholine and propanoic acid showed only a single thermal transition due to boiling. The boiling temperature of carboxylic acids used in the present study increases with an increase in chain length. It is lower in acetic acid and high in octanoic acid as seen in Figure 22B.

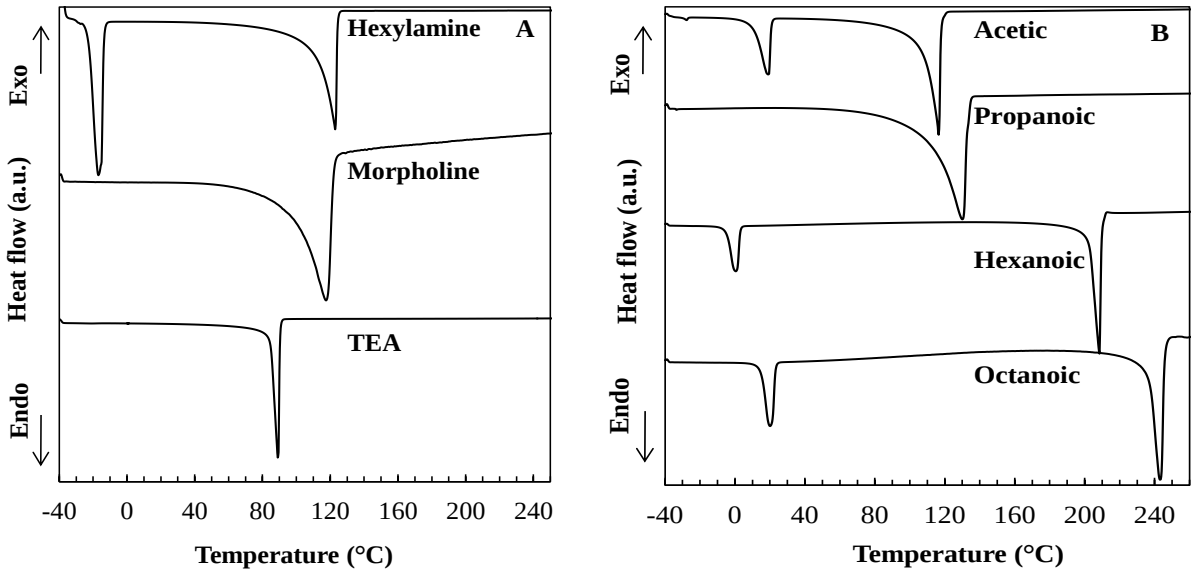

Figure 22: DSC traces of pure amines (A) and pure carboxylic acids (B)

Figure 23 shows the effect of composition on the DSC traces in the system of hexylamine-carboxylic acid mixtures. The position of the melting endotherms shows complex composition dependence. The highest melting temperature was shown by the mixture with a 1:1 composition. This behaviour is observed in the hexylamine-acetic acid (Figure 23A), hexylamine-hexanoic acid (Figure 23C) and hexylamine-octanoic acid (Figure 23D) mixtures. Compositions intermediate to this and the pure amine and carboxylic acids featured melting temperatures that were lower than those of the latter. This melting point trend is consistent with a eutectic comprising the A_2C_2 salt and the neat carboxylic acid. The systems containing morpholine also showed similar behaviour (a representative DSC scan is shown in

Figure 24). These observations provide further support for the prevalence of the A_2C_2 complex for the primary and secondary amines.

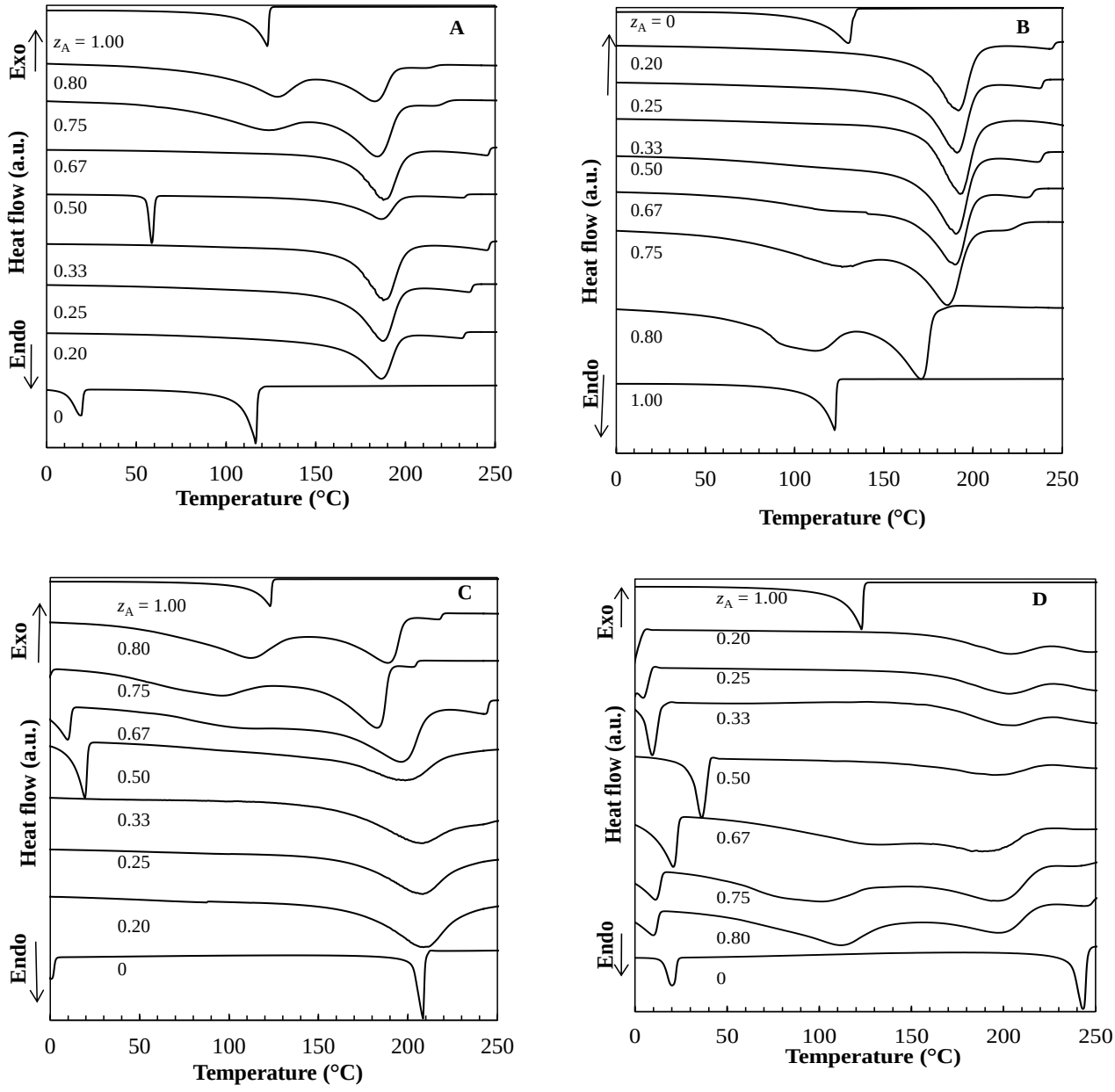

Figure 23: DSC traces of binary hexylamine and (A) acetic, (B) propanoic, (C), hexanoic and (D) octanoic acid mixtures in comparison with pure hexylamine and pure carboxylic acids

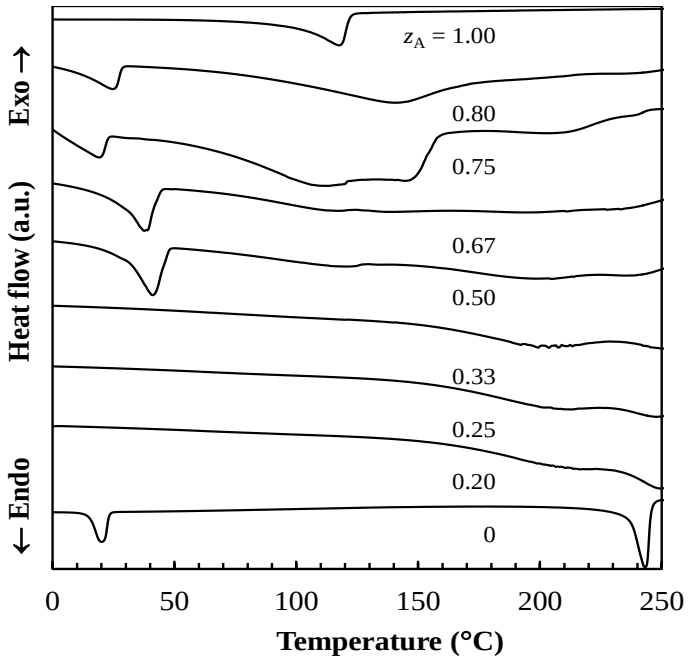

Figure 24: DSC traces of secondary amine, morpholine, with octanoic acid mixtures

Figure 25 shows the representative DSC scans obtained with tertiary amine, TEA. It shows the TEA-hexanoic and TEA-octanoic acid mixtures with different compositions. In this case no melting endotherm transitions were observed above -40 °C. Only the boiling transition is observed. However, the highest boiling transitions showed a smooth variation with composition (see Figure 26). The enthalpy of vaporisation peaked near a composition consistent with the prevalence of the A_1C_3 complex as previously observed for the TEA-acetic acid system in Part 1 of this chapter. The amine-carboxylic acid mixtures based on the shorter chain carboxylic acids in all mixtures featured higher boiling transitions than the parent compounds when evaporating into a stream of nitrogen gas. The highest boiling temperatures were found for the mixtures with compositions close to those of the 1:3 amine-carboxylic acid complexes (z_A = 0.25). When the amine was present in excess beyond this level in the mixtures, an additional endothermic thermal transition was observed. The temperature of the first endothermic transition event matched the boiling transition of the pure parent amine. This suggests that when the mixture is rich in amine, mostly TEA volatilises during the initial stages.

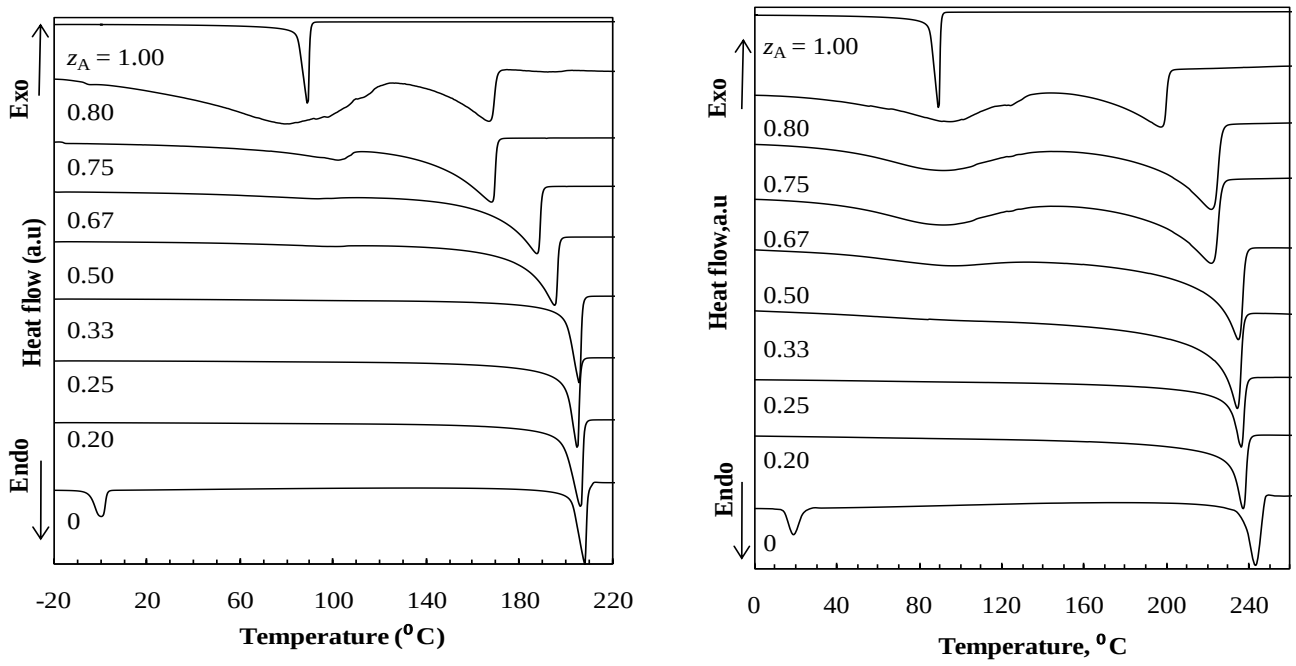

Figure 25: DSC scans of binary TEA systems with (a) hexanoic and (b) octanoic acid mixtures

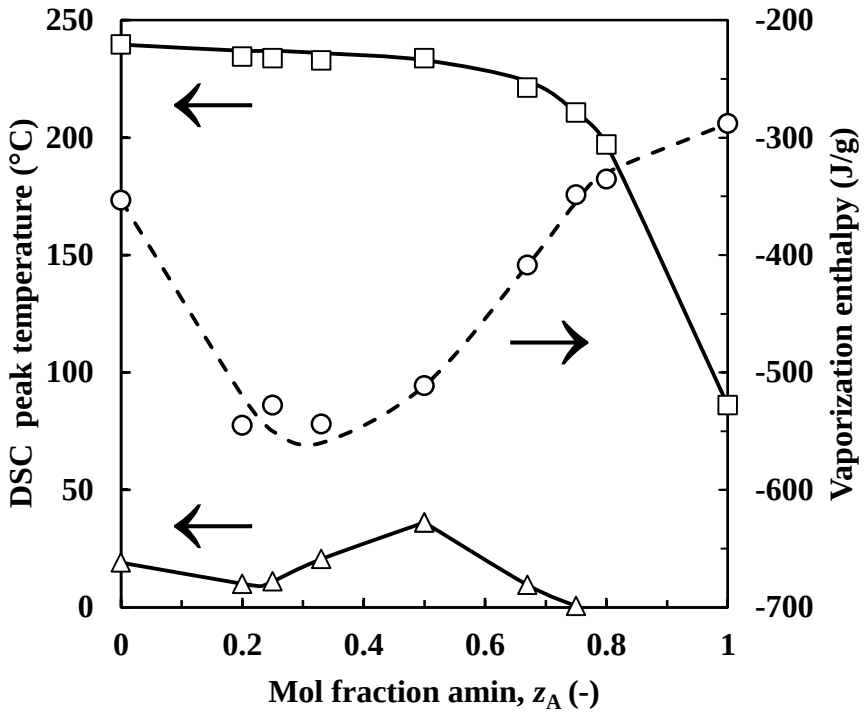

Figure 26: DSC results for liquid mixtures: —Δ— DSC melting peak temperatures for hexylamine-octanoic acid mixtures; – –○ – – vaporisation enthalpies; and — □ — vaporisation peak temperatures for triethylamine-octanoic acid mixtures

4.6 TGA

Figure 27 shows the mass loss rates of the neat carboxylic acids and the neat amines evaporating into nitrogen at 50 °C. At this temperature evaporation was fastest for TEA and slowest for octanoic acid. TEA evaporated completely in less than 20 minutes, whereas only about 0.6% fraction of the octanoic acid had evaporated after 90 minutes. As expected, the rate of evaporation correlated with the ranking of the normal boiling points for the compounds and decreased with the increasing chain length of the carboxylic acid. This indicates that the volatility of the carboxylic acids is dependent on the chain length. The longer the carboxylic acid chain length the less volatile the acid.

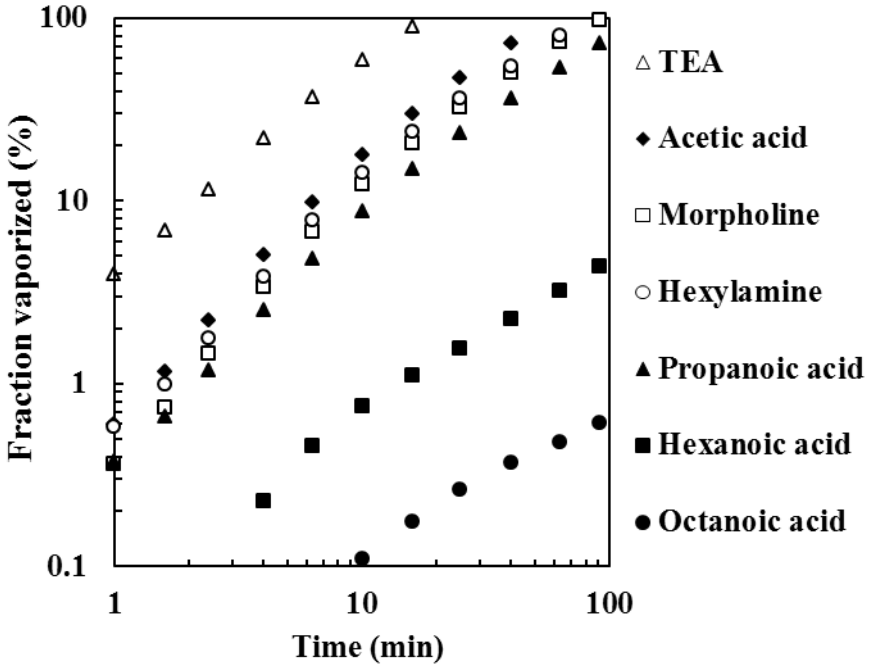

Figure 27: TGA evaporation rates for the neat amines and carboxylic acids measured at 50 °C

Hexylamine systems

Figure 28 shows the evaporative mass loss curves for hexyalmine with (A) acetic, (B) propanoic, (C) hexanoic and (D) octanoic acid binary mixtures. Figure 29 plots the time it takes to reach the selected fractional mass loss values as a function of the initial mixture composition. Pure acetic acid evaporated much more rapidly than the mixtures. Hexylamine also evaporated quicker than the mixtures (see Figures 28A and 29B). The hexylamine-acetic acid binary mixture containing 50 mol % hexylamine was the least volatile (see Figures 28A

and 29B). This is confirmed by the lowest mass loss rate obtained for this mixture. This composition is close to that of the reported A_1C_1 complex.

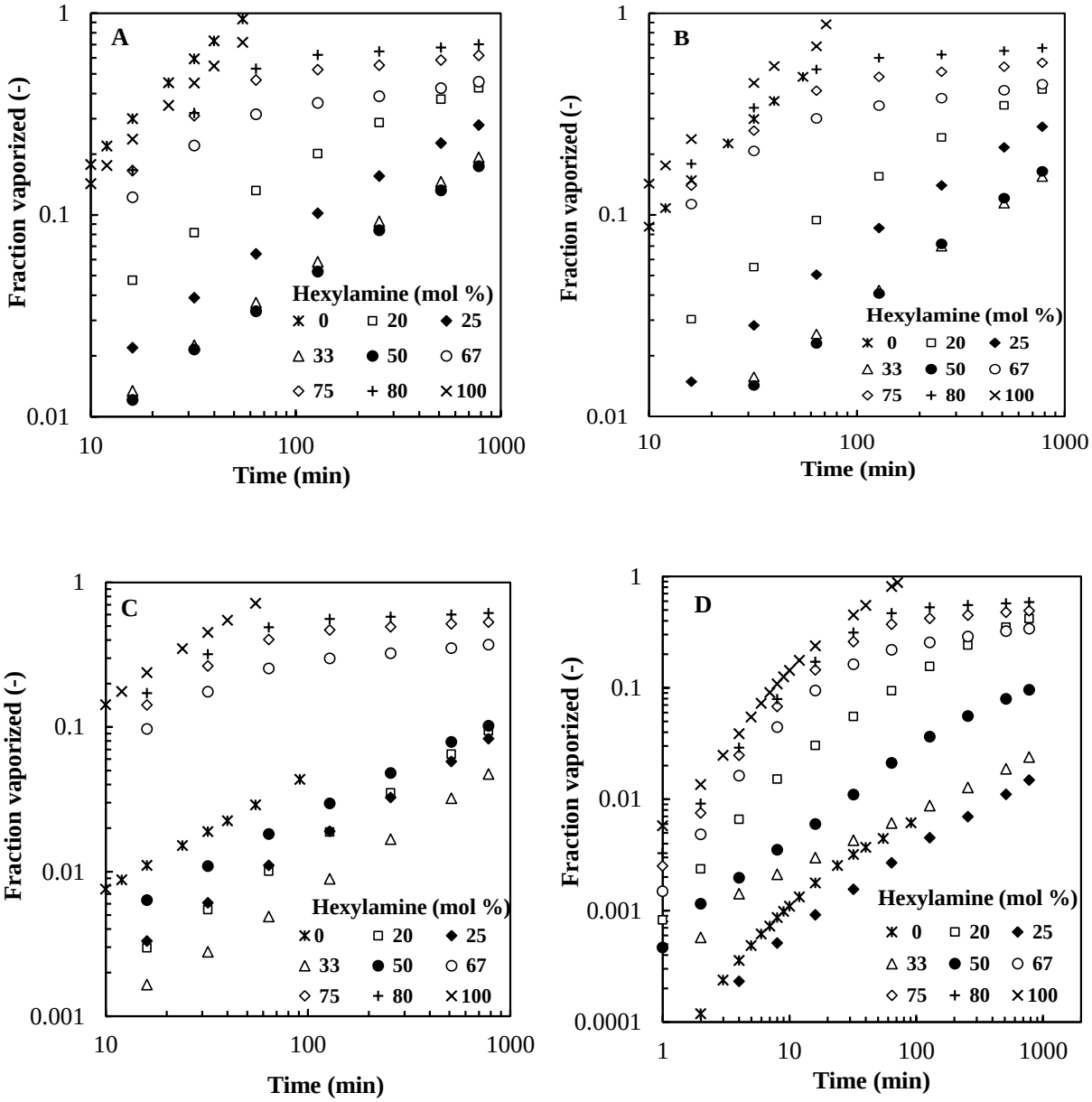

Figure 28: TGA evaporation profiles of hexylamine and (A) acetic, (B) propanoic, (C) hexanoic and (D) octanoic acid binary mixtures compared with those of pure hexylamine and pure carboxylic acids

In the hexylamine-propanoic acid system, propanoic acid evaporates similarly to acetic acid (see Figures 28A and 29(b)). The mixtures also follow a trend similar to that observed for hexylamine-acetic acid. However, in hexylamine-propanoic acid binary mixtures, the mixture with a composition of 33 mol % hexylamine is the least volatile. This composition is close to the reported A_1C_2 complex.

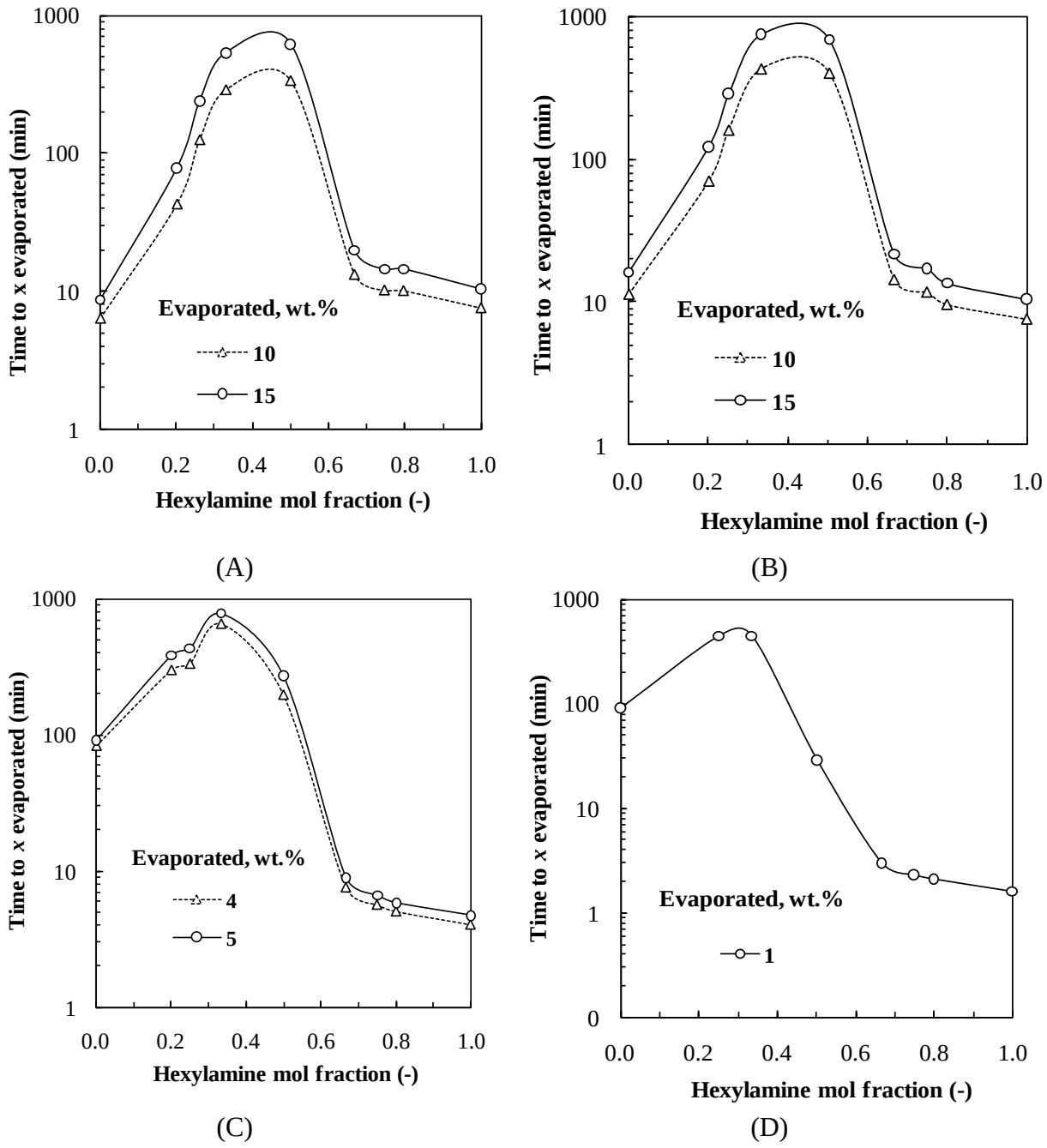

Figure 29: Time it takes to reach the selected fractional mass loss values as a function of composition of the mixtures for (A) hexylamine-acetic, (B) hexylamine-propanoic, (C) hexylamine-hexanoic and (D) hexylamine-octanoic acid

Interestingly, pure hexanoic acid is the least volatile compared with its mixtures with compositions of 67, 75 and 80 mol % hexylamine (see Figures 28C and 29C). However, the mixtures with compositions of 20, 25, 33 and 50 mol % hexylamine show mass loss rates slower than that of the pure hexanoic acid. Again, the mixture with a composition of 33 mol % hexylamine is also the least volatile, as with hexylamine-propanoic acid.

Octanoic acid shows a mass rate slower than that of the hexylamine-octanoic acid binary mixtures with compositions of 20, 33, 50, 67, 75 and 80 mol % hexylamine. This reflects the high volatility of the mixtures when compared with the pure octanoic acid (see Figure 28D and Figure 29D). The binary mixture with a composition of 50 mol % hexylamine is the least volatile even when compared with octanoic acid.

Note that mixtures high in amine content showed rapid rates of evaporation initially but this then levelled out to significantly lower rates at longer times. Again this suggests rapid loss of amine via preferential vaporisation. The slow mass loss rate of the prepared binary mixtures indicates that the interaction between amine and carboxylic acid results in low volatile mixtures. This also reflects the low vapour pressures of these binary mixtures, indicating that their volatility is suppressed.

Morpholine systems

Similarly to the hexylamine-acetic acid system, acetic acid evaporated much more rapidly in the morpholine-acetic acid system, reflecting its high volatility when compared with the pure morpholine (see Figures 30A and 31A). The mixtures showed the slowest rate of mass loss compared with morpholine and pure carboxylic acids. Among the mixtures in the morpholine-acetic acid binary system, the 25 mol % or the 33 mol % morpholine composition were found to be the least volatile (see Figures 30A and 31B).

Pure morpholine evaporated more quickly than propanoic acid in the morpholine-propanoic acid binary mixtures, reflecting its high volatility compared with propanoic acid (see Figures 30B–D and 31B–D). The binary morpholine-propanoic acid mixture with a composition of 33 mol % morpholine was found to be the least volatile among all the binary morpholine-propanoic acid compositions used in the present study. This composition is close to the reported A_1C_2 complex.

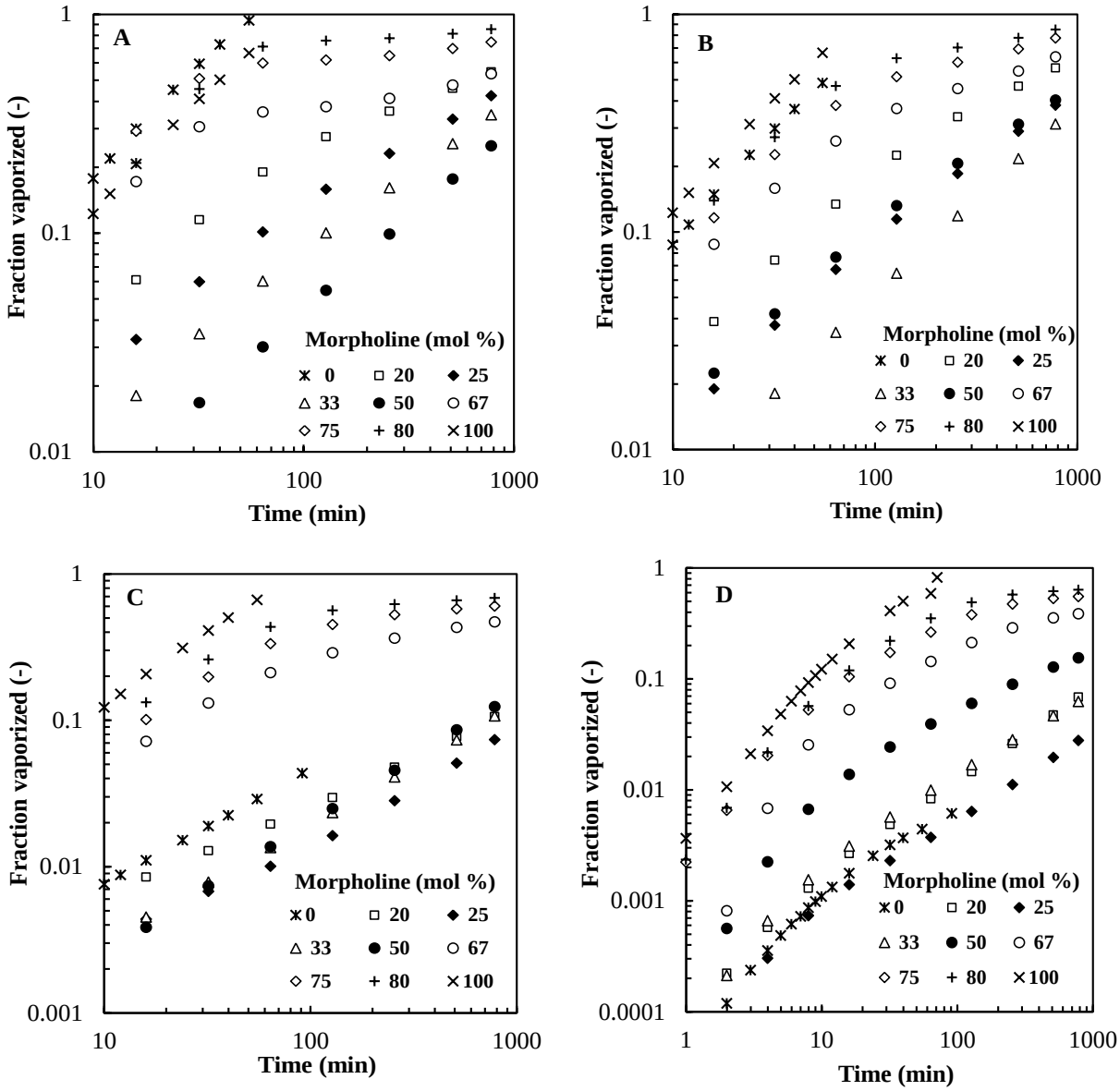

Figure 30: TGA evaporation profiles of morpholine and (A) acetic, (B) propanoic, (C) hexanoic and (D) octanoic acid binary mixture compared to pure morpholine and pure carboxylic acids

Pure hexanoic and pure octanoic acid evaporated more slowly than pure morpholine, and also more slowly than some of their binary mixtures as in hexylamine, reflecting their low volatility (see Figures 30C–D and 31C–D). However, in the morpholine-hexanoic acid system the mixtures with compositions of 20, 25, 33 and 50 mol % morpholine are less volatile than pure hexanoic acid (see Figures 30C and 31C), while in morpholine-octanoic acid only the 25 mol % morpholine composition evaporated more slowly than octanoic acid (see Figures 30D and 31D). The mixture with a composition of 25 mol % morpholine was

found to be the least volatile in both the morpholine-hexanoic and morpholine-octanoic acid binary mixtures. This composition is close to that of the A_1C_3 complex.

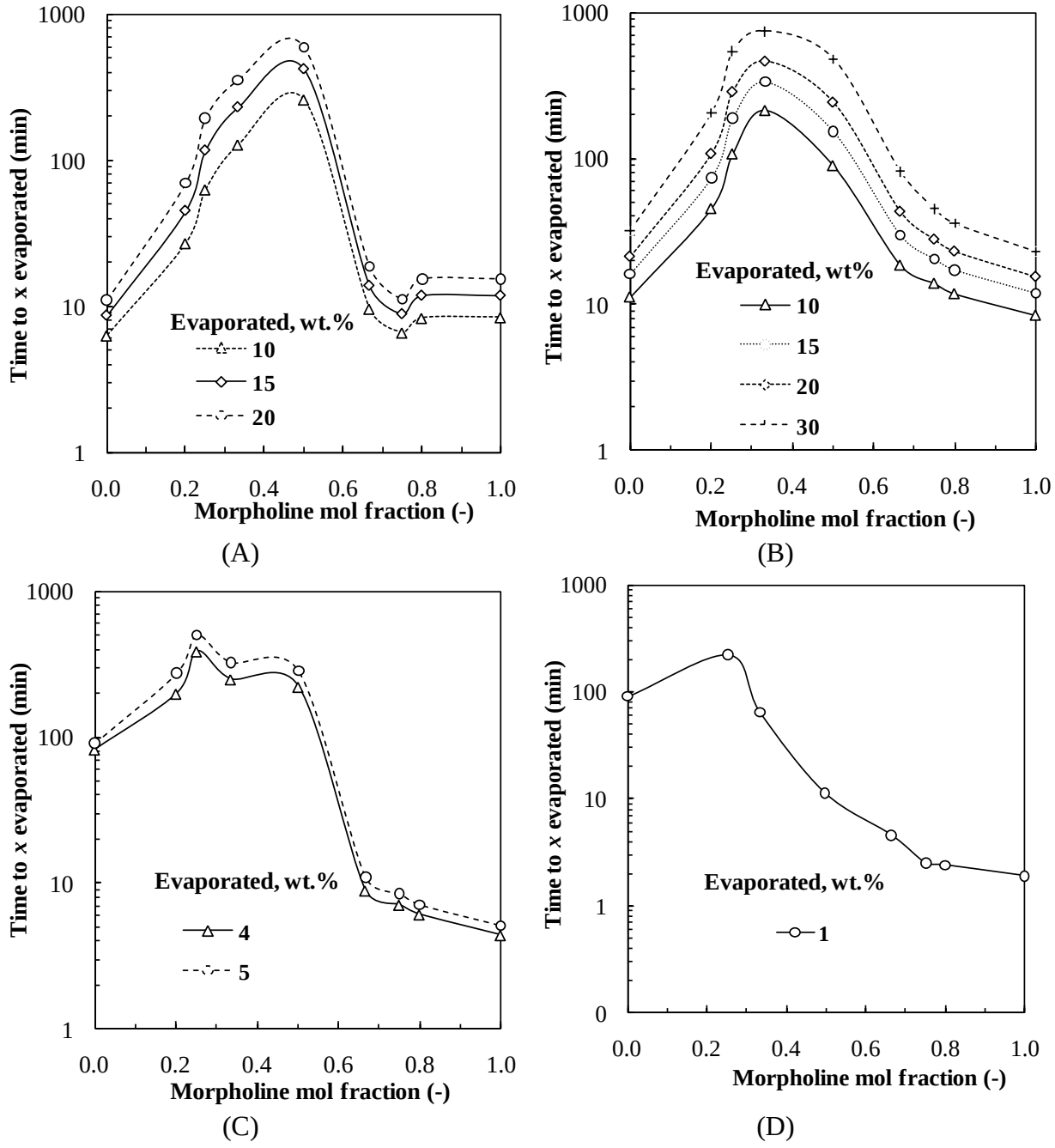

Figure 31: Time it takes to reach the selected fractional mass loss values as a function of composition of the mixture for (A) morpholine-acetic, (B) morpholine-propanoic, (C) morpholine-hexanoic and (D) morpholine-octanoic acid

Triethylamine systems

Figure 32 shows the mass loss profiles for TEA with (A) acetic, (B) propanoic, (C) hexanoic and (D) octanoic acid binary mixtures. Figure 33 plots the time it takes to reach the selected fractional mass loss values as a function of the initial mixture composition. The least volatile mixture in the TEA-acetic acid system was found to be the one with the composition closer to the previously reported A_1C_3 complex. The same composition (25 mol % TEA) was also found to be the least volatile in the binary TEA-propanoic acid and TEA-hexanoic acid systems (see Figures 32B and 33B; 32C and 33D).

Pure propanoic acid was found to evaporate more slowly than TEA, reflecting its low volatility when compared with TEA. The binary mixtures with compositions of 50, 67, 75 and 80 mol % TEA initially show rapid mass loss, and then later reach equilibrium (see Figure 32B). The initial rapid mass loss rate can be attributed to the loss of free TEA.

For the TEA-octanoic acid system, the curves are sandwiched between those for the neat amine and the neat octanoic acid (see Figures 32D and 33D). This was not the case for the mixtures with hexylamine and morpholine. From the present TGA results, it appears that the composition of the least volatile mixture between amine and carboxylic acid occurs at different stoichiometries for every amine-carboxylic acid combination. This least volatile mixture is found to be close to the reported A_1C_1, A_1C_2 or A_1C_3 amine-carboxylic acid complexes. However, it should be kept in mind that this study only considered a limited set of mixtures. It is very unlikely that any of these would correspond exactly to the composition of the least volatile mixture in the respective systems. The reduced volatility of the binary mixtures is attributed to the strong interaction between amines and carboxylic acid, as observed in the liquid phase FTIR results. Free amine and/or free acid were found to evaporate first and then the mixture reaches equilibrium. At this equilibrium point the mixtures behave similarly to an “azeotrope” as described in Part 1 of this chapter.

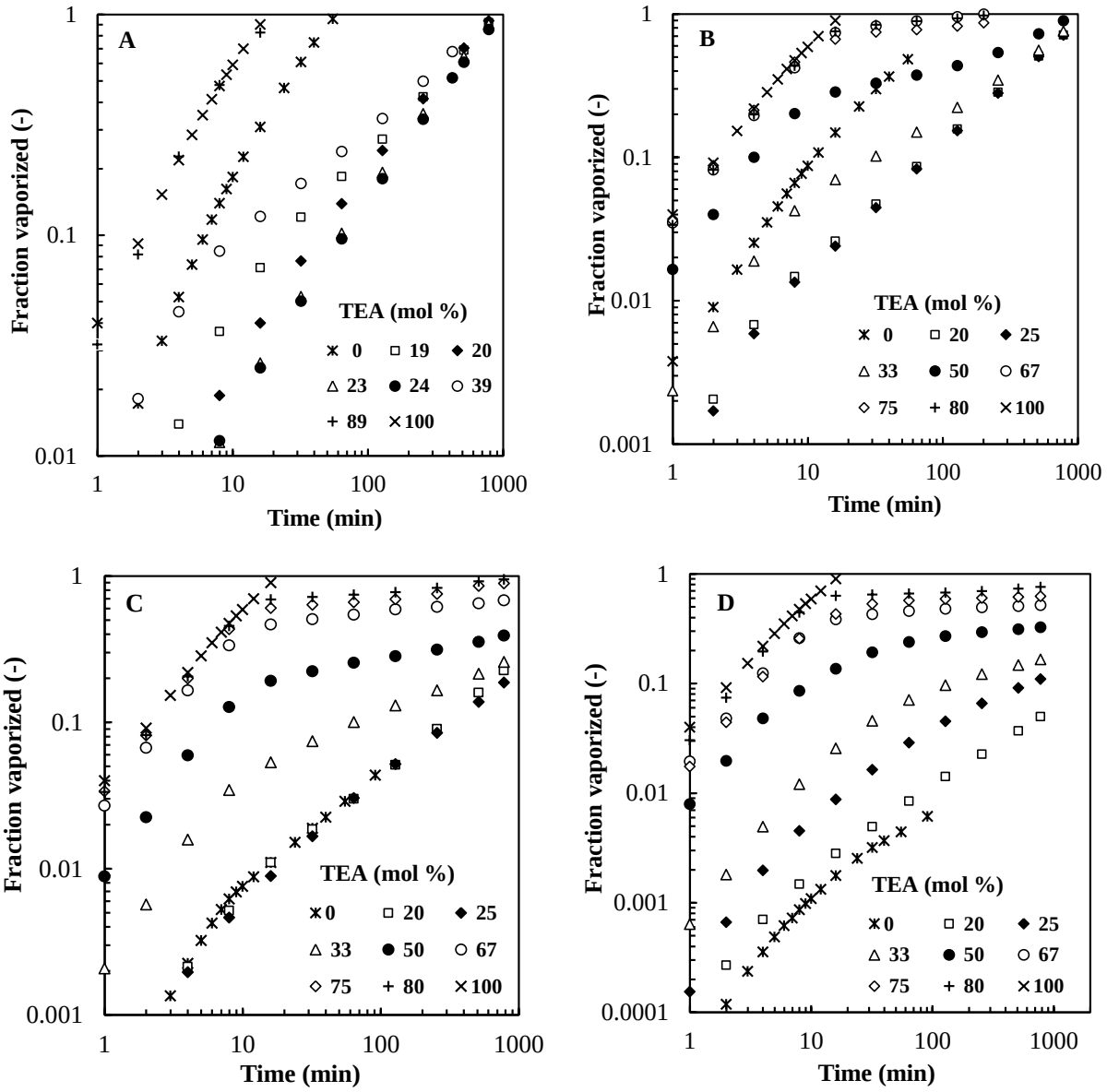

Figure 32: TGA evaporation profiles of TEA and the (A) acetic, (B) propanoic, (C) hexanoic and (D) octanoic acid binary mixtures compared with pure morpholine and pure carboxylic acids

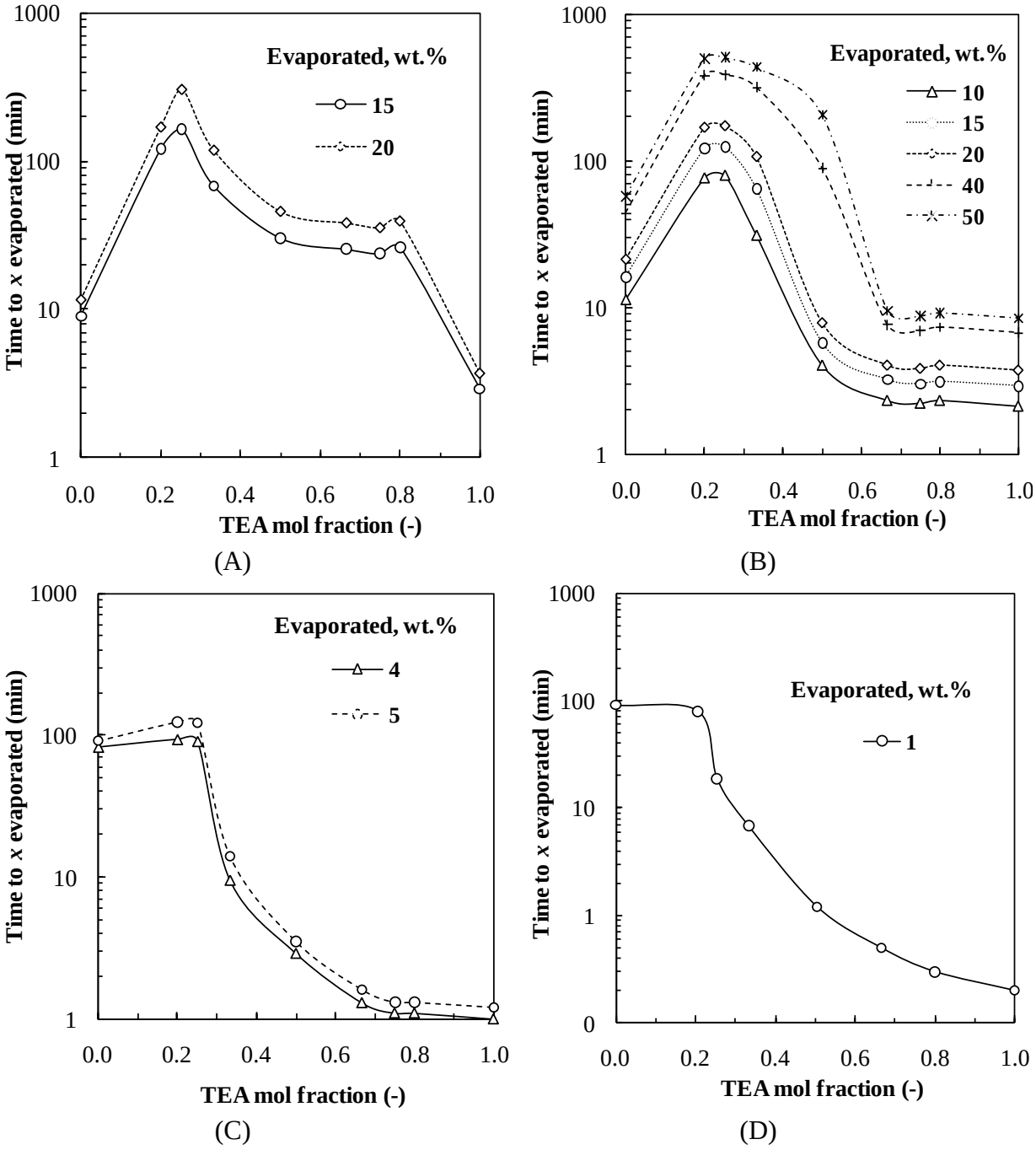

Figure 33: Time it takes to reach the selected fractional mass loss values as a function of the composition of the mixture for (A) TEA-acetic, (B) TEA-propanoic, (C) TEA-hexanoic and (D) TEA-octanoic acid

4.7 Vapour phase FTIR

Numerous vapour phase spectra were collected for all the binary amine-carboxylic acid mixtures. However, systems such as hexylamine-acetic acid, hexylamine-propanoic acid, morpholine-acetic acid and morpholine-propanoic acid showed only the release of amine in mixtures with compositions of 0.67, 0.75 and 0.80 mol %, while the compositions of 0.20, 0.25 and 0.33 mol % showed only the release of carboxylic acid. The mixture with an amine composition of 0.50 mol % showed only the release of amine in the morpholine-propanoic acid system and released both amine and acid in morpholine-acetic acid. No absorption bands were obtained in hexylamine-acetic acid because of the low vapour pressure of the mixture. These collected spectra are shown on Appendix C.

Figure 34A-D compares the vapour phase FTIR spectra of the representative TEA-propanoic acid mixtures with the spectra obtained for pure TEA and pure propanoic acid. The mixture with composition z_A = 0.20 is shown in Figure 34A. The spectrum recorded when just a 1% mass fraction had evaporated to when 23% had evaporated is nearly identical to that of pure propanoic acid. No TEA absorption bands are noticeable at 2980 cm^{-1} and 2818 cm^{-1}. This indicates that the mixture only emits propanoic acid. Therefore all the mass loss observed previously on TGA is due to the evaporation of propanoic acid.

The mixture with composition z_A = 0.25 shows the release of both TEA and propanoic acid throughout (see Figure 34B). This is confirmed by the C=O monomer and OH absorption bands for propanoic acid at 1792 cm^{-1} and 1816 cm^{-1}, and 3600 cm^{-1} respectively. The TEA absorption is confirmed by the bands at 2980 cm^{-1} and 2818 cm^{-1}. The spectra in Figure 32C for the mixture with composition z_A = 0.50 shows that the spectrum recorded when just a 13% fraction had evaporated is nearly identical to that of pure TEA. The mixture with composition z_A = 0.75 also shows the initial evaporation of TEA with a 28% fraction evaporated (see Figure 34D). The C=O monomer and OH absorption bands at 1792 cm^{-1} and 1816 cm^{-1} and 3600 cm^{-1} respectively are only noticeable at a much later stage. The results for this composition are similar to those obtained with compositions z_A = 0.33, 0.67 and 0.80.

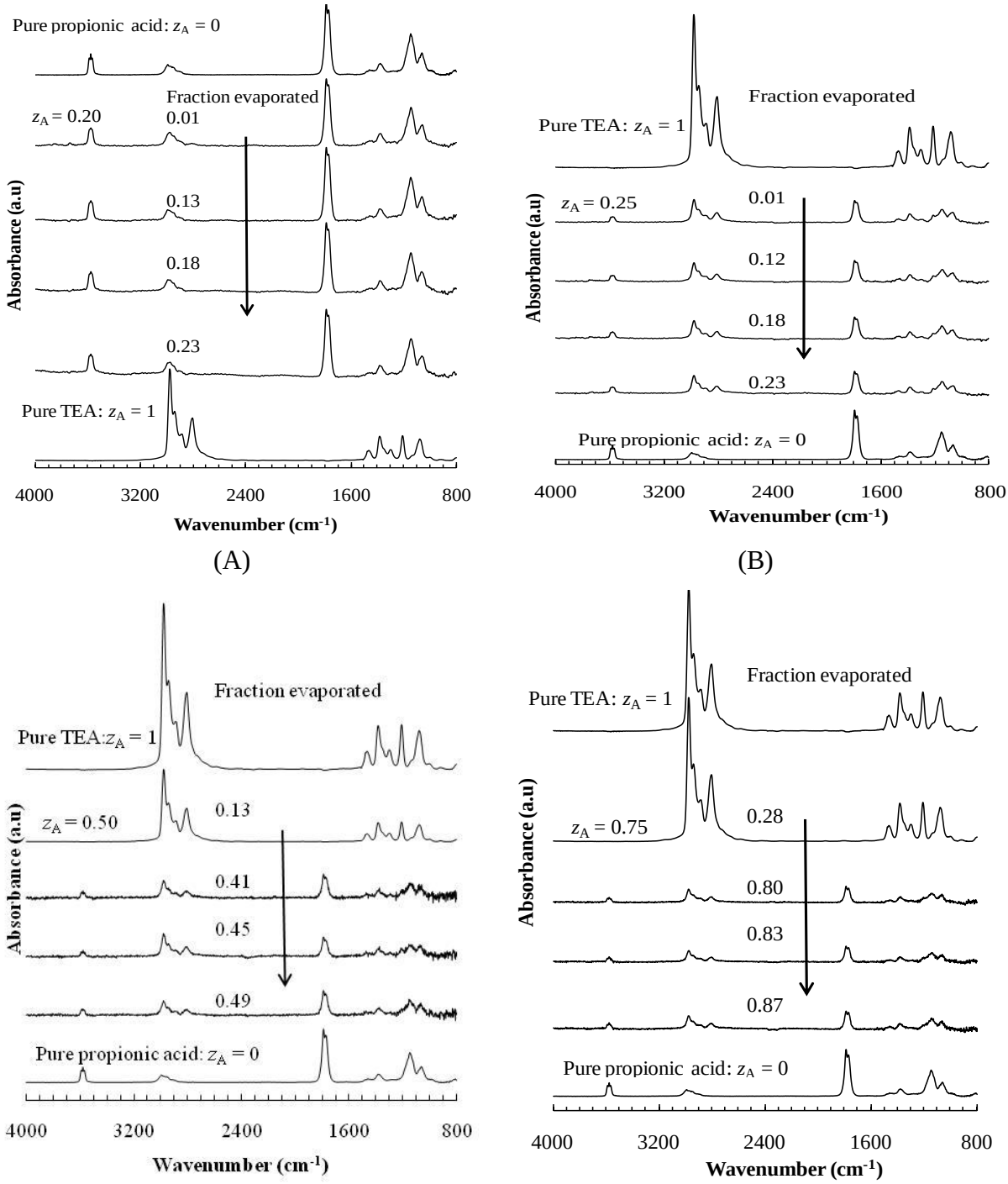

Figure 34: Time evolution of the vapour phase FTIR spectra for binary TEA-propanoic acid mixtures with initial composition (A) z_A = 0.20, (B) 0.25, (C) 0.50 and (D) 0.75 as a function of mass fraction evaporated. The arrows indicate the time direction. The spectra for pure TEA and pure propanoic acid are shown for comparison

The longer chain carboxylic acids (hexanoic and octanoic) used in the present study showed very weak intensity absorption bands on FTIR in the vapour phase. This is attributed to the

fact that the released concentrations were too low for the FTIR instrument to detect. Binary mixtures of amines (hexylamine, morpholine and TEA) with hexanoic and octanoic acid all showed similar behaviour on FTIR in the vapour phase. The selected time evolution vapour phase FTIR spectra of morpholine-hexanoic and morpholine-octanoic acid binary mixtures are shown in Figure 35A and B. Note that the absorption bands were only noticeable for the mixtures with compositions z_A = 0.50, 0.67, 0.75 and 0.80. The results indicate that only morpholine is released by these binary amine-carboxylic acid mixtures. Therefore all the mass loss observed on TGA for the amine-hexanoic and amine-octanoic acid binary mixtures is due to the evaporation of amine.

The present results give a clear understanding as to why octanoic acid-morpholine was reported to be an effective VCI for mild steel (Vuorinen & Skinner, 2002). The synergism between mixtures of amines and the OH ions from moisture on the metallic surface plays a significant role in maintaining the pH at the required values for effective corrosion inhibition. One component in the mixtures is reported to generate the OH ions, while the other one improves the protective effect of the mixture (Andreev & Goncharova, 2004). The present results reveal that the primary role of carboxylic acids (hexanoic and octanoic) in VCIs is to control the release rate of the amine. Similar results were obtained with both primary and tertiary amines. The release of amines is also observed in the mixtures with compositions z_A = 0.75 and 0.80.

The binary amine-hexanoic acid and amine-octanoic acid mixtures with compositions of 0.20, 0.25 and 0.33 mol % showed no absorption bands on FTIR. Only a clear band similar to that obtained for pure hexanoic acid and pure octanoic acid was observed. These spectra are shown in Appendix C. This result implies that the concentration of the released vapours was too low for FTIR to detect. It is also supported by the fact that the mass losses of these compositions observed in TGA for these particular compositions were also very low. This is because the mixture contains more carboxylic acids and hence more stable dimers with low vapour pressures being formed.

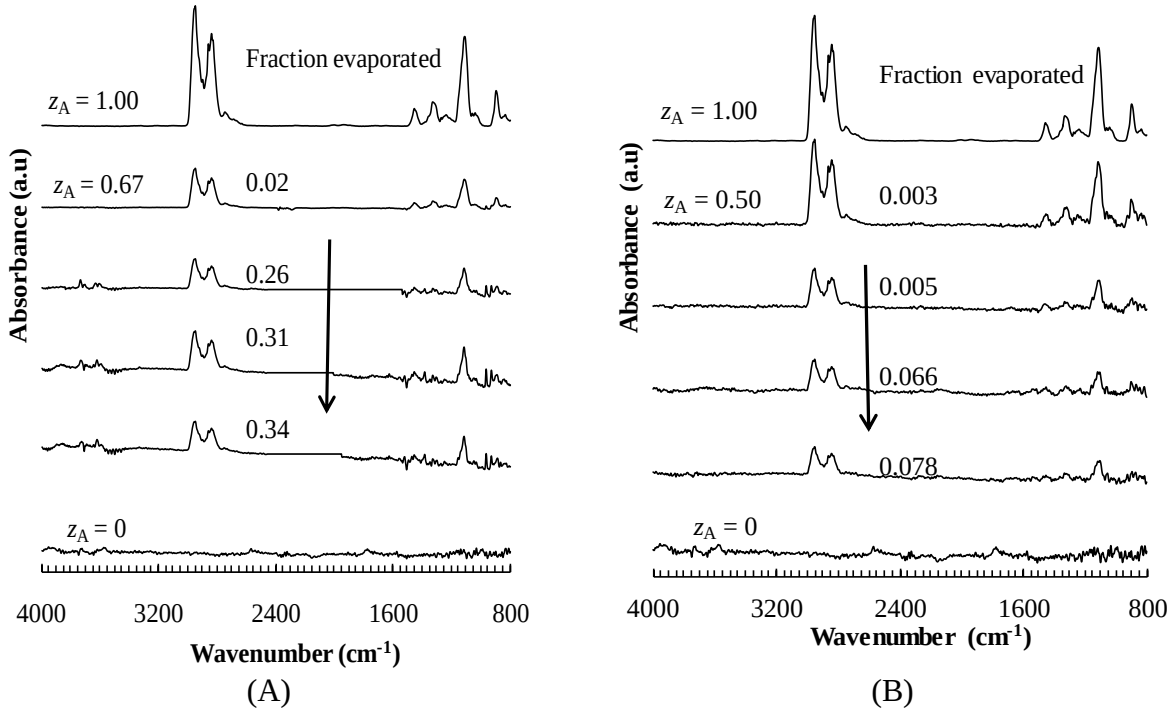

Figure 35: Time evolution of the vapour phase FTIR spectra for (A) binary morpholine-hexanoic acid mixtures with initial composition z_A = 0.67 and (B) binary morpholine-octanoic acid mixtures with initial composition z_A = .0.50 as a function of mass fraction evaporated. The arrows indicate the time direction. The spectra for pure morpholine and pure carboxylic acids are shown for comparison

The dominant feature that distinguishes the vapour phase FTIR spectra for amines (hexylamine, morpholine and TEA) and the spectra for carboxylic acids (formic, acetic, propanoic, hexanoic and octanoic) are the groups of bands between 3300 cm^{-1} and 2450 cm^{-1} and those between 1950 cm^{-1} and 1600 cm^{-1} respectively, as explained for the TEA-acetic acid binary mixtures. The Newton Coates fourth-order integration method was used, followed by scaling the areas directly with the TGA mass loss rates according to Equation (5). The proportionality constants obtained for the TGA-FTIR were experimentally determined and are given in Table 2. The calibration curves are shown in Appendix D. The proportionality constants for hexanoic and octanoic acid were not determined because these carboxylic acids showed no absorption bands on FTIR in the vapour phase, as mentioned.

The shape function profiles of pure amines and pure carboxylic acid and of their respective binary mixtures are shown in Appendix E. These profiles are similar to those obtained for TEA-acetic acid binary mixtures. Mass fractions of the amine in the vapour phase were

calculated, and the mole fraction of amine in the vapour was also determined as described for TEA-acetic acid binary mixtures in Part 1 of this chapter.

Table 2: Experimentally determined proportionality constants for the neat amines and the neat carboxylic acids

Pure component	**k_A or k_C value**
Hexylamine	17.4 ± 0.6
Morpholine	14.8 ± 0.3
TEA	20.0 ± 0.2
Acetic acid	18.3 ± 0.4
Propanoic acid	16.3 ± 0.3

Quantification in the vapour phase was performed using the method described for TEA-acetic acid binary mixtures in Part 1 of this chapter. However, as explained before, most of the binary amine-carboxylic acid mixtures used in the present study showed the release of either acid or amine. Therefore only the mixtures from which both components are released were considered for the calculation of the liquid phase composition, x_A. Figure 36 shows the mole fraction of amine in the released vapours (y_A) and the calculated mole fraction in the liquid phase (x_A) for the TEA-formic acid mixture with an initial TEA composition of 33.3 mol %. The mixture initially emits a vapour that is 90% rich in amine. Later this composition decreases and stabilises at a plateau value, similarly to TEA-acetic acid mixtures. The plateau composition was determined as y_A =0.280 ± 0.002. The value is slightly higher than that obtained in TEA-acetic acid mixtures. However, it is close to the composition of the reported A_1C_3 complex. This composition was also found to be true for the liquid phase.

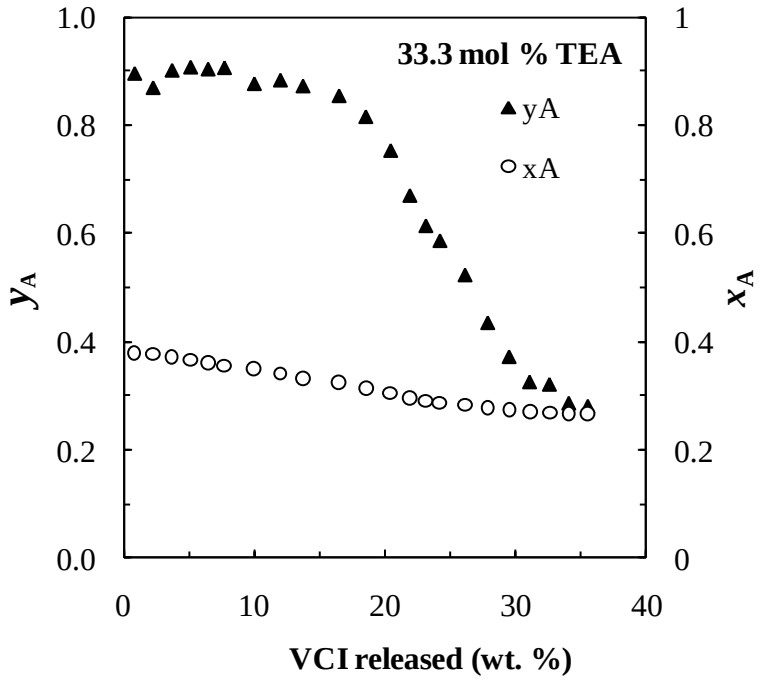

Figure 36: Mole fraction of TEA released into the vapour phase as a function of the percentage weight fraction released by the TEA-formic acid binary mixture with an initial composition of 33.3 mol % TEA

Figure 37 shows the mole fraction of TEA in the vapour phase and in the liquid phase as a function of the percentage weight fraction released by the TEA-propanoic acid binary mixture with composition (a) 33.3 and (b) 50 mol % TEA. These binary mixtures follow the same evaporation trend as that observed in the TEA-acetic acid and TEA-formic acid mixtures. However, the composition of the plateau value for the TEA-propanoic acid binary mixture was found to be approximately 24 mol % TEA on average. This was also found to be true for the liquid phase. This composition is lower than that observed in the TEA-acetic acid and TEA-formic acid binary mixtures. However, it is the closest to the reported 1:3 amine: acid complex. This vapour composition is rich in propanoic acid. The present results suggest that the TEA-propanoic acid system will not be good as a VCI, nor will the TEA-formic acid and TEA-acetic acid systems. The present results also suggest that the amount of each component in the vapour phase is not the same throughout. It can either increase or decrease initially, depending on the amine content, until it reaches a plateau.

The binary TEA-propanoic acid mixture with 80 mol % TEA composition shows the initial release of only TEA (see Figure 38). This result is similar to those obtained for the TEA-acetic acid top layer. No plateau is observed in this mixture.

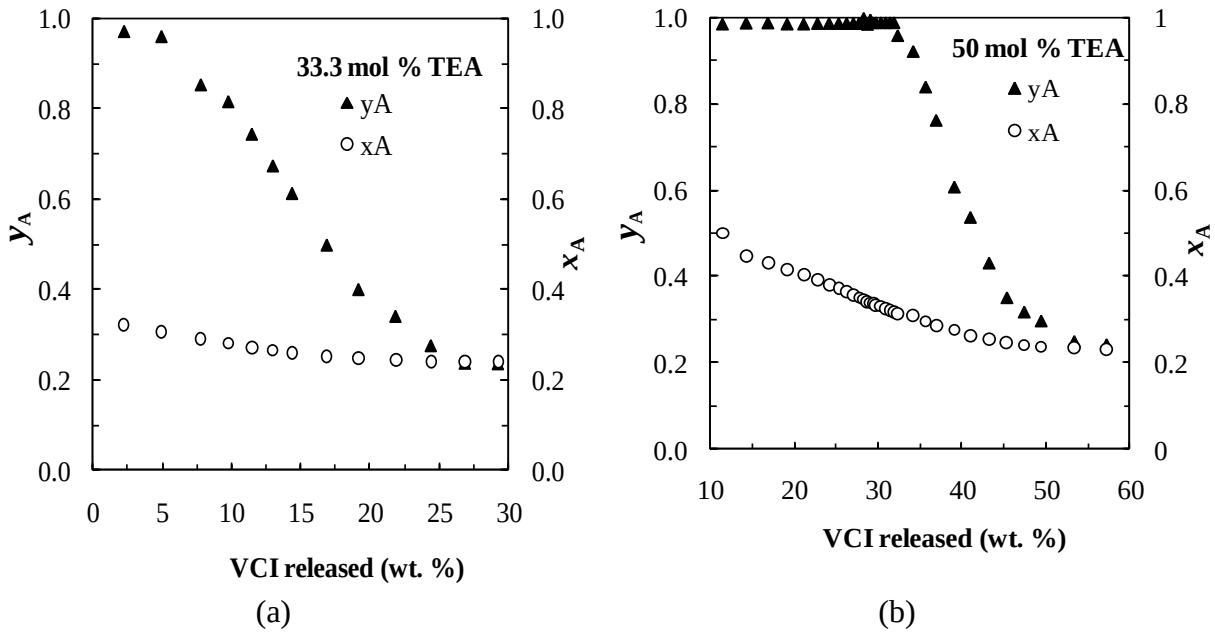

Figure 37: Mole fraction of amine in the released vapour (y_A) and the calculated amine mole fraction in the liquid phase (x_A) for the TEA-propanoic acid mixture with an initial composition (a) 33.3 and (b) 50 mol % TEA

Figure 39 plots the instantaneous composition of the released vapour against the instantaneous (calculated) composition of the remaining liquid. Unfortunately, x_A could not be calculated for the primary amine (hexylamine) systems because they were releasing either an amine or an acid, but not both. Furthermore, in some instances the released concentration was too low for FTIR quantification to be performed. These plots for TEA and morpholine with propanoic acid are reminiscent of lower boiling binary "azeotrope" systems. Stability analysis of batch distillation operations of such systems indicates that the liquid phase composition converges to the "azeotrope" irrespective of the initial composition of the liquid phase. This also explains why the compositions plotted in Figures 36 and 37 approach a constant steady-state value over time as the liquid is allowed to evaporate.

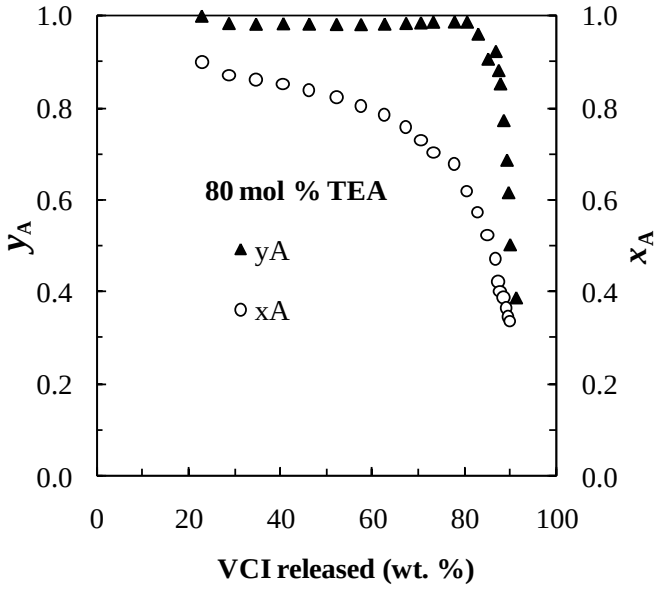

Figure 38: Mole fraction of TEA released into the vapour phase as a function of the percentage weight fraction released by the TEA-propanoic acid binary mixture with an initial composition of 80 mol % TEA

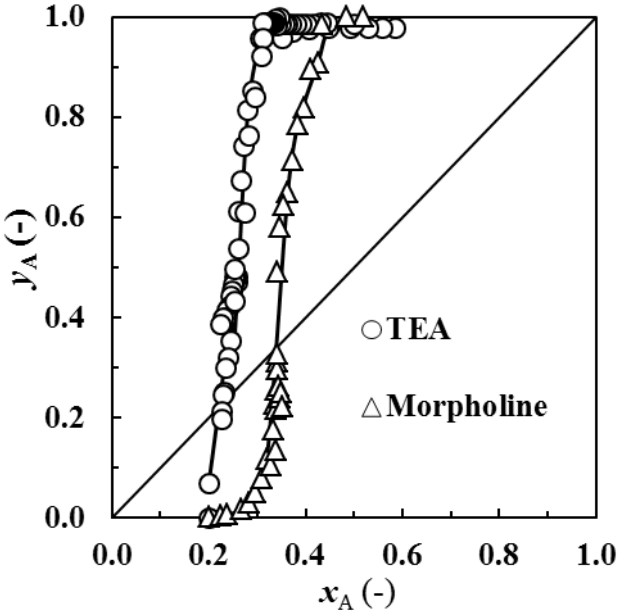

Figure 39: Vapour-liquid "equilibrium" at 50 °C in the TEA-propanoic acid and morpholine-propanoic acid systems

Unfortunately, as mentioned earlier, the volatilities of the mixtures based on hexanoic acid and octanoic acid were too low to allow direct determination of mixed vapour compositions from the IR spectra obtained with the present TGA-FTIR setup. Nonetheless, one can use an indirect approach to infer the likely steady-state composition of such evaporating mixtures.

The steady-state ("azeotrope") composition should correspond to the mixture composition that exhibits the lowest rate of evaporation. This was confirmed within experimental error for the discrete set of compositions that were tested for acetic acid and propanoic acid. Further confirmation is provided by the following observation, which also applied to the hexanoic acid and octanoic acid mixtures. The initial release of the amine was detected for all mixtures higher in amine content. Those with equal moles of amine and acid had the lowest volatility composition (as indicated by the TGA mass loss rate). Thus it may safely be concluded that the composition of the mixtures exhibiting the lowest volatility indicates the steady-state, "azeotrope"-like composition of that particular amine-carboxylic acid VCI system.

4.8 Corrosion tests

The octanoic acid-based VCI model compounds were all found to be corrosive towards galvanised steel. All samples showed white staining after exposure. Therefore, only the corrosion test results for mild steel and copper are presented in Figure 40. None of the mixtures was particularly effective with respect to copper protection, with all of them causing green staining of the copper samples. Surprisingly, the staining was only slight for the 1:1 hexylamine-octanoic acid mixture, even though the inhibition performance was poor.

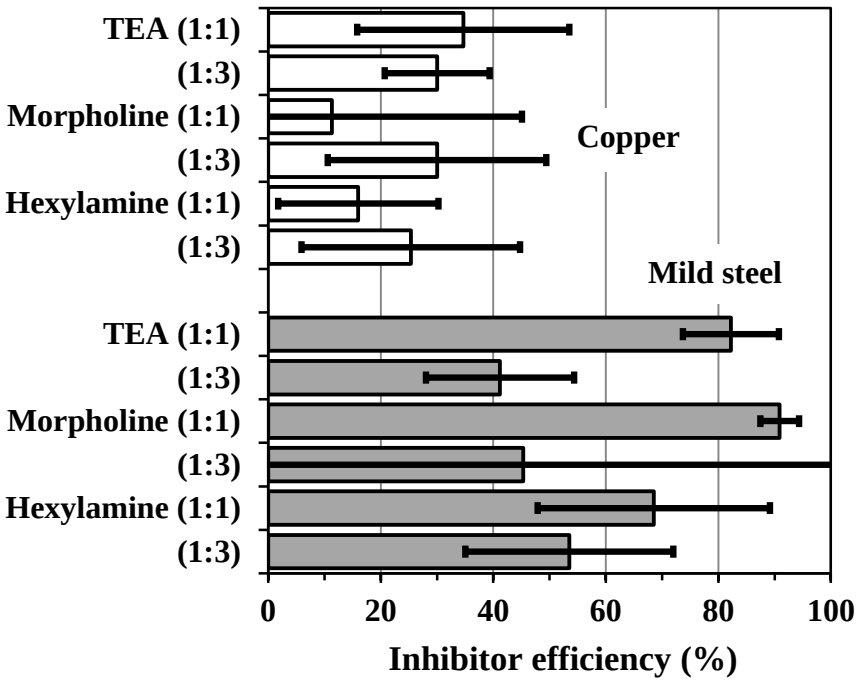

Figure 40: Skinner corrosion test results on copper and mild steel for the amine-octanoic acid mixtures with amine contents of z_A = 0.25 and 0.50

The morpholine-octanoic acid and TEA-octanoic acid mixtures, both with z_A = 0.50, produced the best inhibitor efficiencies for mild steel at ca. 91% (with no staining) and ca. 82% (with slight black staining) respectively. This is in approximate agreement with the findings of the previous study (Vuorinen & Skinner, 2002). The hexylamine-octanoic acid mixture with z_A = 0.50 did not perform as well. In this case the inhibitor efficiency was only about 68%, although the metal surface did not show any staining.

5 DISCUSSION

Volatility is a key property of the VCIs that are used to prevent atmospheric corrosion of metals. Proprietary mixtures of amines and carboxylic acids are suitable for the protection of iron and steel components against atmospheric corrosion during storage and transportation. The interactions between these two types of molecule are well established, but little is known about the nature of the vapours that are emitted. In this study a new method, based on thermogravimetric analysis coupled with evolved gas (TGA-FTIR) was developed in order to shed light on this aspect. The TGA provided information on the rate of VCI release, while the FTIR spectra allowed quantification of the composition of the vapour emitted. The method was applied to study VCI model compounds based on mixtures of triethylamine and acetic acid. The mixtures were kept isothermally at 50 °C and allowed to vaporise into a stream of nitrogen gas. The vapour phase FTIR spectra were recorded at 230 °C as, at this temperature, interactions between the amine molecules and the carboxylic acids are insignificant. At this elevated temperatures the hydrogen-bonded amine-carboxylic acid mixtures dissociate to yield free amine and carboxylic acid molecules. This greatly simplified the task of quantifying the vapour phase compositions as the mixture FTIR spectra were simply composition-weighted linear combinations of the spectra for the pure amine and acid present.

Volatile corrosion inhibitors (VCIs) model compounds, comprising of mixtures of amines and carboxylic acids, were characterised by thermal analysis (DSC and TGA), Fourier transform infrared spectroscopy (FTIR) and also by the TGA-FTIR evolved gas analysis technique. Pure carboxylic acids featured dimers as the dominant species in the liquid phase. However, the dimer concentration decreased significantly on addition of an amine. This was confirmed by the decrease in the intensity of the carboxylic acid dimer (C=O) absorption band and by the absence of the dimer OH out-of-plane bending absorption band at 944 cm^{-1} in the FTIR spectra of the liquid phase mixtures. Therefore, amine addition leads to the dissociation of carboxylic acid dimers in favour of salt formation.

The order of the amines (primary, secondary or tertiary), and the chain length of the aliphatic carboxylic acids, were varied. The carboxylic acid chain length was varied because the shorter chain carboxylic acids are more volatile and it was easier to quantify their vapours in the amine mixtures. Furthermore equimolar mixtures of amines with octanoic acid are known VCIs whereas those with acetic acid may even promote corrosion (Vuorinen & Skinner,

2002). In addition, the interactions between the carboxylic acids and the amines are not significantly affected by the chain length of the former.

It is well known that carboxylic acid monomers form hydrogen-bonded dimers (denoted by C_2) and 1:1 salts with amines via an acid-base reaction (denoted by A_1C_1). The ionic A_1C_1 salt is usually stabilised in organic liquid media by either associating as ion pairs (A_2C_2) or by interactions with acid dimers to form A_1C_3 complexes. The ionic nature of the mixtures was confirmed by the presence of the carboxylate COO^- absorption band at approximately 1560 cm^{-1} and also by the presence of the protonated amine at approximately 1400 cm^{-1} on the FTIR (Figure 17). Liquid phase FTIR spectroscopy, refractive index data and DSC results indicated that the nature of the complexes formed in the liquid phase varied with the composition of the bulk solution (Figure 20, 21 and 26). With the tertiary amine (triethylamine), the maximum ionisation was achieved at a composition corresponding to that of the A_1C_3 complex. It is most likely that steric hindrance effects hampered stabilisation via associated ion pair formation when the salt-forming amine is tertiary. In contrast, the other two lower order amines formed low-melting crystalline 1:1 salts, with the A_2C_2 complex also being favoured in the liquid state.

As expected, the volatility of the pure carboxylic acids decreased as the carboxylic acid chain length increased. This was confirmed by the high boiling temperatures of hexanoic and octanoic acids observed with DSC (Figure 25). It was further confirmed by the low mass loss rates observed in TGA conducted at 50 °C and in consequence the low intensity of the absorption bands in the vapour phase FTIR spectra for the higher acids. Of the pure amines, triethylamine was found to be the most volatile, while morpholine was the least volatile.

VCIs are often present in either a paper sheet or a plastic film and must reach the metal surface by crossing a thin layer of air. In the presence of favourable temperature gradients transport of the VCI will be enhanced by free convection. In the present study, for the duration of the corrosion test the bottom of the jar was kept in a constant water bath set at 40 °C. However, the top of the jar is exposed to the air of the hood. Skinner (1993) estimated that the temperature at the sample could be about 33 °C. Therefore it is expected that the temperature difference will lead to convection currents that could assist the VCI to reach the metal surface. However, if the air is stagnant, the release rate of a pure volatile compound is determined by its gas permeability (Pieterse *et al.*, 2006). It constitutes a lower limit for the isothermal rate at which the VCI will be released. The gas permeability parameter is the

product of the vapour pressure and the diffusion coefficient in air, i.e. $S_i = P_i D_{Ai}$. The former is a measure of the concentration of the compound in air, while the latter is an indication of the mobility of the inhibitor molecules in the gas phase. The gas permeability can be estimated by simple isothermal or dynamic scanning TGA experiments. In essence, the technique is based on the quantification of the vaporisation mass loss rate from a partially filled cylindrical cup (Pieterse & Focke, 2003). The governing equation is

$$\frac{dm_i}{dt} = \left(\frac{M_i A}{zRT}\right) P_i D_{Ai} \qquad (13)$$

where m is the mass of compound i remaining in the pan in kg; t is the time in s; M is the molar mass of the compound in kg mol^{-1}; A is the vaporisation surface area in m^2; R is the universal gas constant in J mol^{-1} K^{-1}; z is the distance from the liquid meniscus to the top edge of the pan in m; T is the temperature in K; P is the vapour pressure of the compound in Pa; and D_{Ai} is the diffusion coefficient of the compound i in air in m^2 s^{-1}.

The calculation of the diffusion length z requires density data and these are reported in Table 3 for the systems of interest here. During the initial period of evaporation the area of diffusion was found to be 3.24 x 10^{-5} m^2.

Table 3: Experimental densities (ρ) of the neat amines, the neat carboxylic acids and the least volatile binary mixtures in the amine-carboxylic acid systems at 50 °C. The number in brackets indicates the concentration of the amine in the mixture in mol %

ρ (kg.m^{-3})	**Neat**	**Triethylamine**	**Hexylamine**	**Morpholine**
Neat		702 ± 2	739 ± 0.4	1 007 ± 2
Acetic acid	1 020 ± 4	991 ± 3 (24)	912 ± 12 (50)	737 ± 0 (50)
Propanoic acid	963 ± 3	960 ± 1 (25)	928 ± 2 (33)	1063 ± 1 (33)
Hexanoic acid	901 ± 1	867 ± 2 (25)	895 ± 0 (25)	959 ± 1 (25)
Octanoic acid	889 ± 1	894 ± 3 (20)	887 ± 1 (25)	935 ± 1 (25)

Equation (13) was used to estimate the gas permeability of the least volatile VCI mixtures. In the present case it was assumed that the molar mass of the active species in these mixtures corresponded to that of the relevant A_1C_n complex. Figure 41 plots the values of the gas permeability for morpholine, propanoic acid, and the mixture containing 33.3 mol % of the amine measured at 50 °C. The $S_i = P_i D_{Ai}$ values in Table 4 are averaged values obtained in

the plateau region of the profiles of the mixtures. Figure 41 provides a representative plot that shows the points at which these values were determined. The calculated S_i values for the least volatile mixtures are independent of the amount of liquid that has evaporated, indicating that such compositions do behave like pseudo-compounds. Numerous P_iD_{Ai} profiles were generated for different amine-carboxylic acid mixtures and they are shown in Appendix F. The values of the gas permeability for other mixtures are presented in Table 4. Among the neat compounds, triethylamine featured the highest and octanoic acid the lowest S_i value. The lowest overall S_i value obtained in this study was 0.009 ± 0.001 Pa $m^2.s^{-1}$ for the hexylamine-octanoic acid binary mixture containing 25 mol % amine.

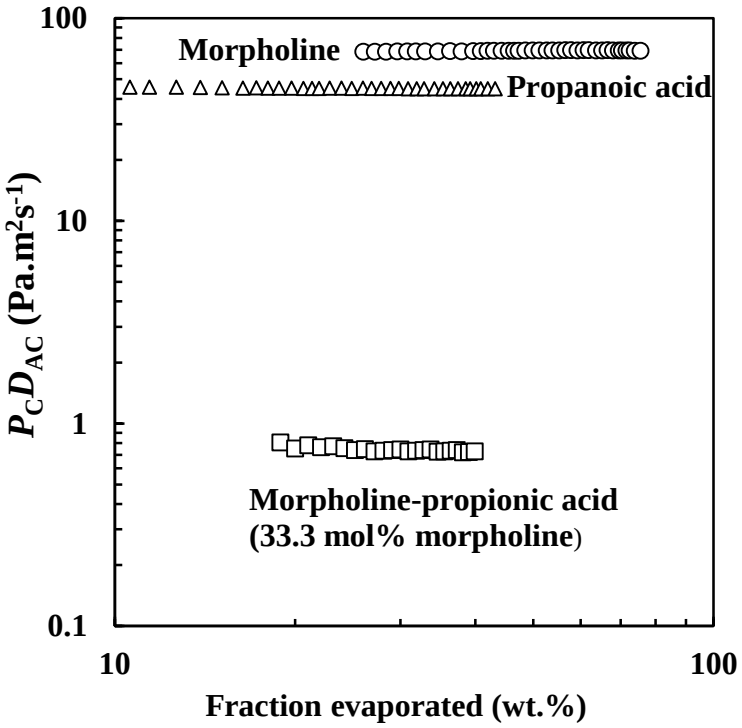

Figure 41: Product of vapour pressure and diffusion coefficient of the morpholine-propanoic acid binary mixture compared with pure morpholine and pure propanoic acid

Irrespective of the initial amine content of a given system, the composition of the liquid remaining and the vapour emitted eventually settled at the same fixed steady-state value as the VCI in the liquid state was depleted. This behaviour is reminiscent of "azeotrope" formation. For triethylamine-based mixtures this steady-state "azeotrope"-like composition was found at approximately 27 mol % TEA. This value is close to the composition of the 1:3 mole ratio amine-acid complex. For the TEA-acetic acid model compound, the steady state ("azeotrope") vapour composition is rich in acetic acid and this may explain why the TEA-

acetic acid mixture is a poor VCI for mild steel. As expected, mixtures close to the "azeotrope" composition featured the lowest volatility.

Table 4: Gas permeability ($S_i = P_i D_{Ai}$) of the neat amines, the neat carboxylic acids and the least volatile binary mixtures in the amine-carboxylic acid systems at 50 °C. The number in brackets indicates the concentration of the amine in the mixture in mol %

$P_i D_{Ai}$ (Pa.m^2.s^{-1})	Neat	Triethylamine	Hexylamine	Morpholine
Neat		-	60 ± 0.2	69 ± 0.3
Acetic acid	164 ± 2	1.89 ± 0.01 (24)	0.41 ± 0.03 (50)	0.67 ± 0.01 (50)
Propanoic acid	45.0 ± 0.2	1.34 ± 0.01 (25)	0.24 ± 0.01(33)	0.74 ± 0.01 (33)
Hexanoic acid	1.28 ± 0.1	0.16 ± 0.01 (25)	0.063 ± 0.002 (25)	0.078 ± 0.02 (25)
Octanoic acid	0.19 ± 0.02	0.048 ± 0.003 (20)	0.009 ± 0.001 (25)	0.022 ± 0.001 (25)

The triethylamine systems all showed "azeotrope" compositions close to the composition of the A_1C_3 complex. The behaviour of the systems based on the primary and secondary amines was different. Here the "azeotrope" composition of the acetic acid systems corresponded approximately to that expected for the 1:1 salt. This was expected as this complex is favoured with these amines in combination with any of the acids tested in this study, as indicated by the FTIR, DSC and refractive index data. However, as the chain length increased, in the series acetic acid to octanoic acid, the amine content of the "azeotrope" decreased, moving closer towards the composition of the A_1C_3 complex. This trend can be attributed to the decreasing volatility of the carboxylic acid dimers as their chain length increased in conjunction with the dissociative evaporation mechanism described in Scheme V.

Important conclusions can be drawn from these results. Firstly, the gas permeabilities of the "azeotrope" compositions tend to be much lower than those of the parent amines or carboxylic acids. The volatility suppression for the present mixtures ranged from one to five orders of magnitude. This implies that the amine-carboxylic acid-based VCIs will emit vapours at a much lower rate than their constituents, permitting prolonged periods of action.

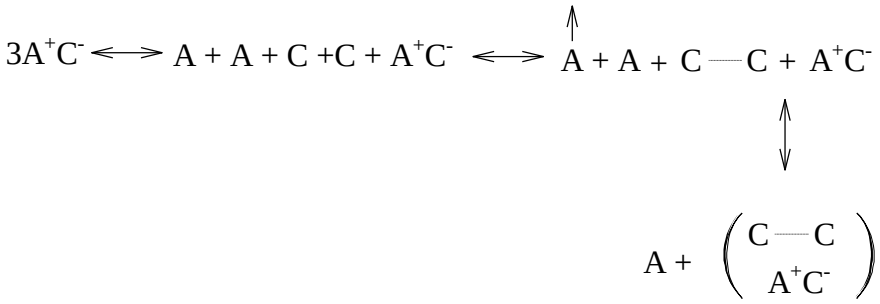

Scheme V: Schematic presentation of an amine-carboxylic acid mixture. A and C represent an amine and a carboxylic acid, while C···C and A^+C^- represent a hydrogen bonded carboxylic acid dimer and an amine-carboxylic acid salt respectively.

The evaporation of the VCI can be explained in terms of the dissociative evaporation mechanism pictured in Scheme V. It represents a modification of the proposal first made by Andreev and Ibatullin (2002). In essence, it is assumed salt and complex formation are dynamic processes and that only neutral molecules evaporate. This means that vaporisation occurs mostly by the release of free amine molecules, acid monomers and possibly acid dimers. In the first step, amine carboxylate salt complexes (A_2C_2) dissociate near the surface to form free amine and carboxylic monomers. The more volatile amine can then be released into the vapour phase. The same is true for the carboxylic monomer. However, its release into the vapour phase is retarded by the dynamic formation of acid dimers (i.e. C_2) and their subsequent complexation with remaining salt species, i.e. forming the A_1C_3 complex. The likelihood of retaining the carboxylic acid molecules increases as the chain length of the alkanoic acid increases because its volatility relative to that of the free amine is suppressed. So, in summary, when ion pair dissociate, the free amine is more easily lost to the vapour phase than the acid monomer. In addition, the volatility of the acid monomer that is left behind is further reduced by dimerisation and the subsequent association of the acid dimer with an amine-acid ion pair.

The application of Equation (13) to the systems tested here in the VCI corrosion test apparatus showed that the 72 h film-forming period used was sufficient to vaporise most of the VCI dosed in the present Skinner's corrosion tests. The 1:3 mixture of hexylamine-octanoic acid was the least volatile system considered in this study. Calculations based on the gas permeability of this composition, and considering the dimensions of the vials used for the VCI liquids, show that about 2.5 h at 50 °C would be sufficient to vaporise 250 mg in the Skinner set-up, provided it formed a uniform layer at the bottom of the vial. Although the

corrosion test was only conducted at 40 °C, it is unlikely that the vaporisation rate would be slower by more than a factor of two at 50 °C. This was confirmed experimentally by the complete mass loss observed for the vials kept for 72 h in the convection oven set at 40 °C. When VCI mixture is allowed to vaporise inside a closed test jar, the rate of vaporization will decrease over time as the air in the jar above the vial becomes saturated with VCI components. However, after 72 h film forming period only minor amounts of the VCI were still present in the vials that were placed inside the test jars. This amount varied from as little as 4.4% for the 1:3 hexylamine-octanoic acid mixture to as much as 18% for the 1:1 morpholine-octanoic acid mixture. Nonetheless, these results do confirm that, for the VCI mixtures tested in the present study, most of the active had indeed evaporated during the film forming period of the corrosion test. As the air in the jar above the vial gets saturated with the VCI components, it is suspected that some VCI will adsorb on the glass and metal surfaces and also condense to form a thin liquid layer at the bottom of the jar.

The inhibitor performance reported in literature pertains to that of equimolar mixture (Skinner, 1993; Vuorinen & Skinner, 2002). The present corrosion tests results (Figure 40) confirmed the previous findings for the 1:1 mixtures containing triethylamine-octanoic acid and morpholine-octanoic acid (Vuorinen & Skinner, 2002). Interestingly, the present TGA-FTIR results indicated that these equimolar mixtures release mostly free amine during the initial stages of evaporation. No carboxylic acid absorption bands were observed on the FTIR spectra in the vapour phase for the octanoic acid and hexanoic acid amine systems. This suggests that on application of these VCIs the primary role of carboxylic acid, at least initially, is to control the release rate of the amine. The equimolar mixtures performed reasonably well as VCIs for mild steel in the Skinners test.

Contrary to the equimolar mixtures, in all three systems a significant drop in inhibitor efficiency was observed when the amine concentration in the VCI mixture was reduced to $z_A = 0.25$ as shown in Figure 40. These samples also showed black staining of the metal surface, although it was only slight for the 1:3 hexylamine systems. Since the major part of the inhibitors vaporized in these tests, the explanation might be found in the excess acid present imparting an adverse pH, outside the passivation range, in the moisture film on the metal surface. To test this hypothesis, the pH of 5 wt.% solutions in deionised water was determined. The results presented in Table 5 confirm that the solutions containing the 1:3

amine-octanoic acid mixtures yielded slightly more acidic solutions than the corresponding 1:1 mixtures.

Table 5: The experimental pH values for 5 wt.% solutions, in deionised water, of 1:1 and 1:3 mixtures of the amines with octanoic acid.

Amine: acid (mol ratio)	Triethylamine	Hexylamine	Morpholine
1:1	6.7	7.6	7.0
1:3	6.1	6.5	6.1

The key finding of the present study is that the amount of amine released initially, by a mixture with carboxylic acids, differs from the ultimate value. Over time the mixtures composition stabilises and reaches an “azeotrope”-like steady state composition. Therefore the main conclusion of this investigation is that the long-term performance of the vapour released from amine-carboxylic acid VCIs may not accord with the results obtained from the short-term inhibitor performance tests. The present observations also suggest that future formulations of amine-carboxylic acid systems should pay closer attention to matching the volatilities of the constituent amines and carboxylic acids.

6 CONCLUSION

A TGA-FTIR method was successfully developed and applied to study the evaporation of amine-carboxylic acid-based VCI model compounds. The method is simple to use and allowed the quantification of both liquid and vapour phase compositions. It is hoped that this method will find utility in the characterisation of other VCIs and thereby aid in understanding their mechanism of action.

Mixtures of amines and carboxylic acid were studied using this new TGA-FTIR technique. Evaporation was followed by TGA and the nature and composition of the released vapours was determined by FTIR. It is well known that carboxylic acids form dimers (C_2) while the amines and acids can undergo Brønsted-Lowry acid-base interactions to form a salt. The salt is stabilized by forming an ion pair (A_2C_2) or by complexing with an acid dimer (A_1C_3). It was found that the A_1C_3 complex dominated in the mixtures containing tertiary amine, while the A_1C_1 complex was favoured in liquid mixtures containing the primary and secondary amines. This was confirmed by the liquid phase FTIR, DSC and the refractive index results. Volatility was quantified by the gas permeability values measured using TGA measurements. The amine-carboxylic acid mixtures were generally found to be much less volatile than the corresponding pure components.

Amine carboxylic acid-based VCIs are traditionally employed as equimolar mixtures in commercial practice. The present study investigated the performance of mixtures of octanoic acid with hexylamine, morpholine and triethylamine. The equimolar mixtures proved to be effective as VCIs for mild steel in the Skinner's test. However, it was found that the composition of the mixtures released by such systems varied over time. Initially the vapours are amine rich implying that it is progressively depleted in the liquid phase. Eventually an "azeotrope"-like steady state is reached where the vapour and the liquid compositions converge to the same value. This composition was close to that expected for the A_1C_3 complex. It consists of a strongly associated ion pair formed by the 1:1 salt of the amine with one carboxylic acid that is stabilized by association with a carboxylic acid dimer. This behaviour can be explained by the dissociative evaporation model. It assumes that complex formation is a dynamic process and that only free amines and carboxylic acids can enter the vapour phase from the liquid. Note that this chemical model does not preclude the subsequent formation of similar complexes in the vapour phase.

The present study was performed at 50 °C. However the compositions of the vapours released by such systems can also be understood by studying the (atmospheric pressure) phase diagram. Figure 4 shows the VLE data obtained by van Klooster and Douglas for TEA-acetic acid binary mixtures. As expected the highest boiling temperature (i.e. lowest volatility) is found for the "azeotrope" composition. This was confirmed by the boiling onset temperatures observed in the DSC data for the TEA-acetic acid mixtures. The reason for this is attributed to volatility suppression caused by the ionic nature of the mixtures, confirmed by the FTIR results. TEA and acetic acid molecules are held together by strong electrostatic forces. Therefore high temperatures are necessary to overcome the strong ionic bonds between TEA and acetic acid and this leads to a higher-boiling "azeotrope".

When the amine is initially present beyond the azeotrope value, the phase diagram reveals that almost pure amine will be released by the mixture. As the excess amine evaporates, the liquid is depleted and the acetic acid concentration in the liquid increases until the mixture reaches the steady state "azeotrope"-like composition. For this system (TEA-acetic acid) this stage is rich in acid and hence mixtures featuring this composition could result in the creation of a corrosive environment. When the initial amine concentration is below the "azeotrope" composition, the phase diagram shows that almost pure acid will vaporize. In this case the vapours could be corrosive right from the start and may cause metal discoloration before the actual corrosion protection sets in.

The inhibitor efficiencies of 1:3 amine-octanoic acid mixtures were tested and compared to those of the traditional 1:1 mixtures for mild steel. The former had compositions close to that of the azeotrope". However, they provided poor corrosion protection when compared to the corresponding equimolar mixtures. Thus the main conclusion of this investigation is that the long term performance of amine-carboxylic acid VCI vapours released from reservoirs may not accord with the results obtained by short term inhibitor performance tests. The present observations also suggest that the future formulations of amine-carboxylic acid systems should pay closer attention to matching the volatilities of the constituent amines and carboxylic acids.

REFERENCES

Ahmad, Z. (2006).Corrosion control by inhibition. In: Amad, Z. (Ed.), *Principles of Corrosion Engineering and Corrosion Control*, Boston, US: Butterworth-Heinemann, pp 352–381.

Åmond, L.-R. and Tullin, C.T. (2012). The theory behind FTIR analysis. Application examples from measurements at the 12 MW circulating fluidized bed. Department of Energy Conversion, Chalmers University of Technology, Sweden. Available at: http://www.fysik.lu.se./cecost [Accessed on 12 January 2012).

Andreev, N. N. and Goncharova, O. A. (2004). The effect of OH^- ions on the inhibition of steel corrosion with amines. *Prot. Met.*, 40 (3): 280–287.

Andreev, N. N. and Ibatullin, K.A. (2002). On the prediction of the vapour's pressure of salt type volatile inhibitors, Prot. Met. 38: 13-16s

Andreev, N. N. and Kuznetsov, Y. I. (2005). Physicochemical aspects of the action of volatile metal corrosion inhibitors *Rus. Chem. Rev.*, 74: 685–695.

Badran, B.M., Abdel-Fattah, A. A. and Abdul A. A. (1982). New corrosion inhibitors based on fatty materials-II. Epoxidized fatty materials modified with aromatic amines. *Corros. Sci.*, 22(6): 525–536.

Barrow, G. M. and Yerger, E. A. (1954). Acid-base reactions in non-dissociating solvents. Acetic acid and triethylamine in carbon tetrachloride and chloroform. *J. Am. Chem. Soc.*, 76: 5211–5216.

Bastidas, D.M., Cano, E. and Mora, E.M. (2005). Volatile corrosion inhibitors: a review *Anti-Corros. Methods Mater.*, 52(2): 71–77.

Bastidas, J.M. and Mora, E.M. (1998). A laboratory study of mild steel vapour phase corrosion and its inhibition by dicyclohexylamine *Can. Metall. Q.*, 37(1): 57–65.

Beverley, K.J., Clint, J.H. and Fletcher, P.D.I. (1999). Evaporation rates of pure liquids measured using a gravimetric technique. *Phys. Chem., Chem. Phys.*, 1: 149–153.

Bobik, M. (1977). Ultrasound absorption in mixtures of triethylamine with carboxylic acids. *Adv. Mol. Rel. Int. Pro.*,11: 191–209.

Bommersbach, P., Alemany-Dumont, C., Millet, J.P. and Normand, B. (2005). Formation and behaviour study of an environment-friendly corrosion inhibitor by electrochemical methods. *Electrochim. Acta,* 51: 1076–1084.

Boyle, B. (2004). A look at the developments in vapour phase corrosion inhibitors. *Met. Finish.*, 102(5): 37–41.

Buckland, S., Friman, R. and Karlsson, S. (1997). Aggregation studies in alkanoic acid-alkyl amine-water systems. *Colloids Surf., A, 123–124:* 125–133.

Burneau, A., Génin, F. and Quilès, F. (2000). Ab initio study of the vibrational properties of acetic acid monomers and dimers. *Phys. Chem. Chem. Phys.*, 2: 5020–5029.

Cano, E., Bastidas, D.M., Simancas, J. and Bastidas, J.M. (2005). Dicyclohexylamine nitrite as volatile corrosion inhibitor for steel in polluted environments. *Corrosion,* 61(5): 473–479.

Choi, H., Song, Y.K., Kim, K.Y. and Park, J.M. (2012). Encapsulation of triethanolamine as organic corrosion inhibitor into nanoparticles and its active corrosion protection for steel sheets. *Surf. Coat. Technol.*, 206: 2354–2362.

Coates, J. (2000). Interpretation of infrared spectra, a practical approach. In: Meyers, R.A. (Ed.), *Encyclopedia of Analytical Chemistry*, Chichester: Wiley, pp. 10815–10837.

DeTar, D. F. and Novak, R. W. (1970). Carboxylic acid-amine equilibria in nonaqueous solvents. *J. Am. Chem. Soc.*, 92: 1361–1365.

Du Preez, P.F. (1998). The development and evaluation of new vapour phase corrosion inhibitors. M Eng thesis, Department of Chemical Engineering, University of Pretoria, Pretoria, South Africa.

Duprat, M., Dabosi, F., Moran, F. and Rocher, S. (1981). Inhibition of corrosion of carbon steel by the aliphatic fatty polyamines in association with organic phosphorous compounds in 3% sodium chloride solution. *Corrosion,* 37: 262–266.

Dutton, R. (2004). Problems with volatile corrosion in the metal finishing industry. *Pollution Control*, 12–15.

Eibl, S. and Reiner, D. (2011). Correlation of content and corrosion protection of volatile corrosion inhibitors in packaging material-regaining trust. VCI *Mater. Corros.*, 62(8): 745–752.

Eigenmann, F., Maciejewski, M. and Baiker, A. (2000). Gas adsorption studied by pulse thermal analysis. *Thermochim. Acta*, 359: 131–141.

Eigenmann, F., Maciejewski, M. and Baiker, A. (2006a). Influece of measuring conditions on the quantification of spectroscopic signals in TA-FTIR-MS system. *J. Therm. Anal. Calorim.*, 83(2): 321–330.

Eigenmann, F., Maciejewski, M. and Baiker, A. (2006b). Quantitative calibration of spectroscopic signals in combined TG-FTIR system. *Thermochim. Acta*, 440: 81–92.

Estevão, L.R.M. and Nascimento, R.S.V. (2001). Modifications in volatilization rate of volatile corrosion inhibitors by means of host-guest systems. *Corros. Sci.*, 43: 1133–1153.

Fiaud, C. (1994). Theory and practice of vapour phase inhibitors, in corrosion inhibitors, European Federation of Corrosion Publications, No. 11, Institute of Materials, London, 1994, pp. 1-11.

Focke, W.W. (2003). A revised equation for estimating the vapour pressure of low volatility substances from isothermal TG data. *J. Therm. Anal. Cal.*, 74: 1107–1118.

Friberg, S.E., Sun, W.M., Yang, Y. and Ward, A.J.I. (1990). Molecular interactions in nonaqueous cationic system. *J. Colloid Interface Sci.*, 11: 503–517.

Gao, G., Liang, C.H. and Wang, H. (2007). Synthesis of tertiary amines and their inhibitive performance on carbon steel corrosion. *Corros. Sci.*, 49: 1833–1846.

Gerald, C. F. (1970). *Applied Numerical Analysis*. Reading, US: Addison-Wesley Publishing Co.

Goldade, V.A., Pinhuk, L.S., Makarevich, A.V. and Kestelman, V.N. (2005). In: Hull R., Osgood Jr, R.M., Parisi, J. and Walimont, H. (Eds), *Plastics for Corrosion Inhibition* Berlin-Heidelberg: Springer-Verlag.

Gough, S.R. and Price, A.H. (1968). Dielectric study of the molecular complexes formed between triethylamine and acetic acid and monochloroacetic acid. *J. Phys. Chem.*, 72: 3347–3349.

Gűnzler, H. and Grelich, H.-U. (2002). *IR Spectroscopy – An Introduction*. Weinheim: Wiley-VCH.

Hafaiedh, N., Toumi, A. and Bouanz, M. (2009). Dynamic viscosity study of binary mixtures triethylamine + water at temperatures ranging from (283.15 to 291.35) K. *J. Chem. Eng. Data*, 5*:* 2195–2199.

Hassan, S.M., Moussa, M.N., El-Tagoury, M.M. and Radi, A.A. (1990). Aromatic acid derivatives as corrosion inhibitors for aluminium in acidic and alkaline solutions. *Anti-Corros. Methods Mater.*, 8–11.

Hays, G.F. (2010). Now is the time. In: Elizer, A. (Ed.), *Corrosion Processes and Advanced Materials in Industry*, Switzerland: Trans Tech Publications Ltd.

Heal, G.R. (2002). Thermogravimetry and derivative thermogravimetry. In: Haines, P.J. (Ed.), *Principles of Thermal Analysis and Calorimetry*, London: Royal Society of Chemistry.

Hœrlé, F., Mazaudier, F., Dillmann, P.H. and Santarini, G. (2004). Advances in understanding atmospheric corrosion of iron. II. Mechanistic modeling of wet and dry cycles. *Corros. Sci.*, 46: 1431–1465.

Hyskens, P., Felix, N., Janssens, A.,, Van den Broeck, F. and Kapuku, F. (1980). Influence of the dielectric constant on the viscosity and on the formation of conducting ions in binary carboxylic acids-triethylamine mixtures *J. Phys. Chem.*, 84: 1387–1393.

Karlsson, S., Backlund, S. and Friman, R. (2000). Complexation in the heptanoic acid-heptylamine system *Colloid Polym. Sci.* 278: 8–14.

Karlsson, S., Päivärinta, J., Friman, R., Poso, A., Hotokka, M. and Backlund, S. (2001). Characterization of the phase behaviour and complexation in heptanoic acid-heptylamime-water system. *J. Phys. Chem. B,* 105: 7944–7949.

Kohler, F. and Hyskens, P. (1976). Some aspects of the structure and interaction potential of hydrogen bonded complexes. *Adv. Mol. Rel. Pro.,* 8: 125–154.

Kohler, F., Atrops, H., Kalal, H., Liebermann, E., Wilhem, E., Ratkovics, F. and Salamon, T. (1981a). Molecular interactions in mixtures of carboxylic acids with amines. 1. Melting curves and viscocities *J. Phys. Chem.,* 85: 2520–2524.

Kohler, F., Gopal, R., Gõtze, G., Atrops, H., Demiriz, M.A., Liebermann, E., Wilhem, E., Ratkovics, F. and Palagyl, B. (1981b). Molecular interactions in mixtures of carboxylic acids with amines. 2. Volumetric, conductimetric, and NMR properties. *J. Phys. Chem.,* 85: 2524–2549.

Kohler, F., Findenegg, G.H. and Bobik, M. (1974). Mixtures of trifuoroacetic acid with acetic acid and carbon tetrachloride *J. Phys. Chem.*, 78(17): 1709–1714.

Kohler, F., Liebermann, E., Miksch, G. and Kainz, C. (1972). On the thermodynamics of the acetic acid-triethylamine system. J. *Phys. Chem.,* 76: 2764–2768.

Kondo, H. (2008). Protic ionic liquids with ammonium salts as lubricants for magnetic thin film media *Tribol. Lett.*, 31: 211–218.

Kubilda, A.I. and Schreiber, V.M. (1978). Infrared study of some complexes with a strong hydrogen bond at high and low temperatures *J. Mol. Struct.*, 47: 323-328.

Kui, X., Chao-Fang, D., Xiao-Gang, L., and Fu-Ming, W. (2008). Corrosion products and formation mechanism during intial stage of atmospheric corrosion of carbon steel. *J. Iron. Steel Res. Int.*, 15: 42–48.

Kuznetsov, Y.I., Frolove, L. and Toming, E.V. (2007). On the protection of carbon steels from hydrogen sulfide corrosion with volatile and contact inhibitors *Prot. Met.*, 43(2): 149–154.

Liljefors, T. and Norby, P.O. (1997). An ab initio study of the trimethylamine-formic acid and trimethylammonium ion-formate anion complexes, their monohydrates, and continuum solvation *J. Am. Chem. Soc.*. 119: 1052–1058.

Maciejewski, M. and Baiker, A. (1977). Quantitative calibration of mass spectroscopic signals measured in coupled TA-MS system. *Thermochim. Acta*, 295: 95–105

MacMurry, J. (2000). *Organic Chemistry*, 5th edition. USA: Brooks/Cole.

Maréchal, Y. (1987). IR spectra of carboxylic acids in gas phase: A quantitative reinvenstigation *J. Chem. Phys*., 87(11): 6344–6353.

Marsanich, A., Barontini, F., Cozzani, V. and Petarce, L. (2002). Advanced pulse calibration technique for quantitative analysis of TG-FTIR data. *Thermochim. Acta*, 390: 153–168.

Materazzi, S. (1997). Thermogravimetry-infrared spectroscopy (TG-FTIR) coupled analysis. *Appl. Spectrosc. Rev.*. 32(4): 385–404.

McConnel, R. (2008). Volatile corrosion inhibitors offer effective protection for processing and shipment of metal-based products. *Met. Finish.*, 23–27.

Meyer, R., Ha, T. K., Frei, H. and Günthard, H. H. (1975). Acetic acid monomer: Ab inito study, barrier to proton tunneling, and infrared assignment *Chem. Phys.* 9, 393–403.

Miksch, G., Ratkovics, F. and Kohler, F. (1969). The system acetic acid + carbon tetrachloride: excess Gibbs energy of mixing. *J. Chem. Thermodyn.*, 1, 257–265.

Miksic, B.A. (1975). Some aspects of metal protection by vapour phase inhibitors. Cortec Corporation. Available at: http://www.cortecvci.com/Publications/Papers/VCIProducts/CTP-10).

Mittleman M. (1990). Quantitative TG/IR. *Thermochim. Acta*, 166, 301–308.

Myles, K. and Associates (1995). *Corrosion Control: Principles and Practice*. Randburg, South Africa: Myles Publications.

Nakanishi, N., Morita, H. and Nagakura, S. (1977). Charge-transfer bands observed with the intermolecular hydrogen-bonded systems between acetic acid and some aliphatic amines *J. Mol. Spectrosc.*, 65: 295–305.

Orzechowski, K., Pajdowska, M., Czarnecki, M. and Kaatze, U. (2007). Complexation and proton transfer in the binary system propanoic acid-triethylamine, evidence from the composition dependencies of mixture properties. *J. Mol. Liq.*, 133: 11–16.

Orzechowski, K., Pajdowska, M., Fuchs, K. and Kaatze, U. (2003). Complex formation in binary propanoic acid-triethylamine mixtures: A dielectric relaxation and titration study. *J. Chem. Phys.*, 119: 8558–8566.

Orzechowski, K., Pajdowska, M., Przybylski, J., Gliński, J. and Kolodziej, H.A. (2000). Dielectric, acaustic, desimetric and viscosimetric investigations of the tributylamine + propanoic acid system. *Phys. Chem. Chem. Phys.*. 2: 4676–4681.

Padjowska, M. and Sobczyk, L. (1982). Dielectric relaxation in propanoic acid-tri-n-butylamine system. *Adv. Mol. Relax. Interact. Proc.*, 22: 159–165.

Päivärinta, J. Karlsson, S. Hotkka, M. and Poso, A. (2000). Calculated and measured vibrational frequencies in an alkanoic acid-alkylamine complex. *Chem. Phys. Lett*. 327: 420–424.

Päivärinta, J., Karlsson, S., Poso, A. and Hotokka, M. (2001). Calculated molecular properties for different alkanoic acid-alkylamine complexes: A comparison with measured FTIR and Raman spectra. *Chem. Phys.*, 263: 127–138.

Pereira, E. A. and Tavares, M.F.M. (2004). Determination of volatile corrosion inhibitors by capillary electrophoresis. *J. Chromatogr. A*, 1051: 303–308.

Pieterse, N. and Focke, W.W. (2003). Diffusion controlled evaporation through a stagnant gas: Estimating low vapour pressures from thermogravimetric data. *Thermochim. Acta*, 406: 191–198.

Pieterse, N., Focke, W.W., Vuorinen, E. and Rácz, I. (2006). Estimating the gas permeability of commercial volatile corrosion inhibitors at elevated temperatures with thermo-gravimetry. *Corros. Sci.*, 48: 1986–1995.

Quraishi, M.A. and Jamal, D. (2002). Development and testing of all organic volatile corrosion inhibitors. *Corrosion*, 58(5): 387-391.

Quraishi, M.A., Bhardwaj, V. and Jamal, D. (2005). Prevention of metallic corrosion by some salts of benzoic hydrazide under vapour phase conditions. *Indian J. Chem. Technol.*, 12: 93–97.

Ramachandran, S., Tsai, B.L., Blanco, M., Chen, H.J., Tang, Y. and Goddard, W.A. (1996). The self-assembled monolayer mechanism of corrosion inhibition for iron surfaces. In:

Jones, R.H. and Baer, D.R. (Eds), *New Techniques for Characterizing Corrosion and Stress Corrosion*. Warrendale, US: The Minerals, Metals & Material Society, pp 177–182.

Rammelt, U., Koehler, S. and Reinhard, G. (2009). Use of vapour phase corrosion inhibitors in packages for protecting mild steel against corrosion *Corros. Sci*,. 51: 921–925.

Rammelt, U., Koehler, S. and Reinhard, G. (2011). Electrochemical characterisation of the ability of dicarboxylic acid salts to the corrosion inhibition of mild steel in aqueous solutions. *Corros. Sci.,* 53: 3515–3520.

Rawat, J. and Quraishi, M. A. (2003). Influence of some 6-methoxy-aminobenzothiazole derivatives on corrosion of ferrous and non-nonferrous metals under vapour-phase conditions. *Corrosion,* 59(3): 238.

Roberge, P. R. (2000). *Handbook of Corrosion Engineering.* New York: McGraw-Hill.

Roberge, P.R., Klassen, R.D. and Haberecht, P.W. (2002). Atmospheric corrosivity modeling – A review. *Mater. Des.,* 23: 321–330.

Rozenfeld, I.L. (1981). *Corrosion Inhibitors*. New York: McGraw-Hill.

Saeten, O. J., Sjöblom, J. and Gestbom, B. (1991). A dielectric spectroscopic study of fatty acid/amine complexes in solution. *J. Phys. Chem.,* 95: 1449–1453.

Sanyal, B. (1981). Organic compounds as corrosion inhibitors in different environments – A review. *Prog. Org. Coat.,* 9: 165–236.

Sastri, V.S. (1998). *Corrosion Inhibitors: Principles and Applications*. New York: Wiley.

Shreir, L.L., Jarman, R.A. and Burstein, G.T. (1994). *Corrosion Control*, 3rd edition, Volume 2. Oxford: Butterworth-Heinemann.

Skinner, W. (1993). A new method for quantitative evaluation of volatile corrosion inhibitors. *Corros. Sci.,* 35: 1494–1501.

Skinner, W., Du Preez, F. and Vuorinen, E. (1999). Evaluation of vapour phase corrosion inhibitors. *Br. Corros. J.,* 34: 151–152.

Skoog, D.A., West, D.M. and Holler, F.A. (1996). *Fundamentals of Analytical Chemistry*, 7th edition. Fort Worth, Texas: Saunders College Publishing.

Slager, T.L. and Prozonic, F.M. (2005). Simple methods for calibrating IR in TGA/IR analyses. *Thermochim. Acta*, 426: 93–99.

Socrates, G. (1980). *Infrared Characteristic Group Frequencies*. Chichester: Wiley.

Subramanian, A., Kumar, R.R., Natesan, M. and Vasudevan, T. (2002). The performance of VPI-coated paper for temporary corrosion prevention of metals. *Anti-Corros. Meth. Mater.*, 49(5): 354–363.

Syed, S. (2006). Atmospheric corrosion of materials. *Emirates J. Eng. Res.*, 11: 1–24.

Tamada, J.A. and King, C.J. (1990). Extraction of carboxylic acids with amine extractants. 2. Chemical interactions and interpretation of data. *Ind. Eng. Chem. Res.*, 29: 1327–1333.

Tamura, H. (2008). The role of rust in corrosion and corrosion protection of iron and steel. *Corros. Sci.*, 50: 1872–1883.

Van Klooster, H.S. and Douglas, W.A. (1945). The system of acetic acid-triethylamine. *J. Phys. Chem.*, 49: 67–70.

VCI-2000. Available at: http://www.vci2000.com/html/technical.html [Accessed on 12 January 2012].

Vuorinen, E. and Focke, W. (2006). A new technique to evaluate the volatility of vapour phase corrosion inhibitors (VCIs) and potential VCIs. *Chemical Technology*, 26.

Vuorinen, E. and Skinner, W. (2002). Amine carboxylates as vapour phase corrosion inhibitors. *Br. Corros. J.*, 37: 159–160.

Vuorinen, E., Kálmán, E. and Focke, W. (2004). Introduction to vapour phase corrosion inhibitors in metal packaging. *Surf. Eng.*, 20: 281–284.

Vuorinen, E., Kálmán, E. and Focke, W. (2004). Introduction to vapour phase corrosion inhibitors in metal packaging. *Surf. Eng.*, 20: 281–284.

Whitehead, E.S. (1969). Quantitative infrared determination of ammonium ion in hydroxylamine sulfate. *Anal. Chem.*, 41: 829.

Wierzejewska-Hnat, M., Mielke, Z. and Ratajczak, H. (1980). Infrared studies of complexes between carboxylic acids and tertiary amines in argon matrices. *J.C.S. Faraday II.* 76: 834–843.

PUBLICATIONS

1. Nhlapo, N.S., Focke, W.W. and Vuorinen, E. (2012). TGA-FTIR study of the vapours released by the triethylamine-acetic acid mixtures. *Thermochimica Acta*, 546: 113–119.

2. Focke, W.W., Nhlapo, N.S. and Vuorinen, E. (2012). Thermal and thermal analysis and FTIR studies of volatile corrosion inhibitor model systems. *Corrosion Science* (Manuscript submitted).

APPENDICES

Appendix A: The refractive index values of the pure components and the mixtures determined at 20 °C

Table A-1: The refractive index data for pure amines, pure carboxylic acids and their respective mixtures (the letter in brackets indicates the top and bottom layers respectively

	Refractive index								
Sample (amine mol %)	**0**	**20**	**25**	**33**	**50**	**67**	**75**	**80**	**100**
Hexylamine-acetic	1.3725	1.4195	1.4275	1.4346	-	1.4386	1.4336	1.4305	1.4175
Hexylamine-propanoic	1.3863	1.4245	1.4295	1.4366	1.4466	1.4386	1.4356	1.4366	1.4175
Hexylamine-hexanoic	1.4155	1.4346	1.43860	1.4426	1.4486	1.4416	1.4356	1.4326	1.4175
Hexylamine-octanoic	1.4276	1.4426	1.4436	1.4436	-	1.4436	1.4376	1.4346	1.4175
Morpholine-acetic	1.3725	1.4295	1.4386	1.4446	-	-	-	-	1.4547
Morpholine-propanoic	1.3863	1.4325	1.4406	1.4516	-	1.4667	1.4647	1.4617	1.4547
Morpholine-hexanoic	1.4155	1.4396	1.4456	1.4526	-	-	1.4607	1.4597	1.4547
Morpholine-octanoic	1.4276	1.4446	1.4486	1.4616	-	-	1.4606	1.4597	1.4547
TEA-formic	1.3692	1.4125	1.4215	1.4346	1.4042 (t) 1.4406 (b)	1.4041 (t) 1.4436 (b)	1.4040 (t) 1.4436 (b)	1.4042 (t) 1.4426 (b)	1.4040
TEA-acetic	1.3725	1.4845	1.4255	1.4335	1.4040 (t) 1.4345 (b)	1.4040 (t) 1.4346 (b)	1.4041 (t) 1.4345 (b)	1.4042 (t) 1.4346 (b)	1.4040
TEA-propanoic	1.3863	1.4255	1.4356	1.4356	1.4326	1.4175	1.4125	1.4085	1.4040
TEA-hexanoic	1.4155	1.4356	1.4386	1.4396	1.4316	1.4216	1.4215	1.4125	1.4040
TEA-octanoic	1.4276	1.4416	1.4436	1.4426	1.4376	1.4286	1.4225	1.4155	1.4040

Appendix B: Liquid phase FTIR spectra

B-1: Hexylamine-acetic acid and hexylamine-propanoic acid binary mixtures

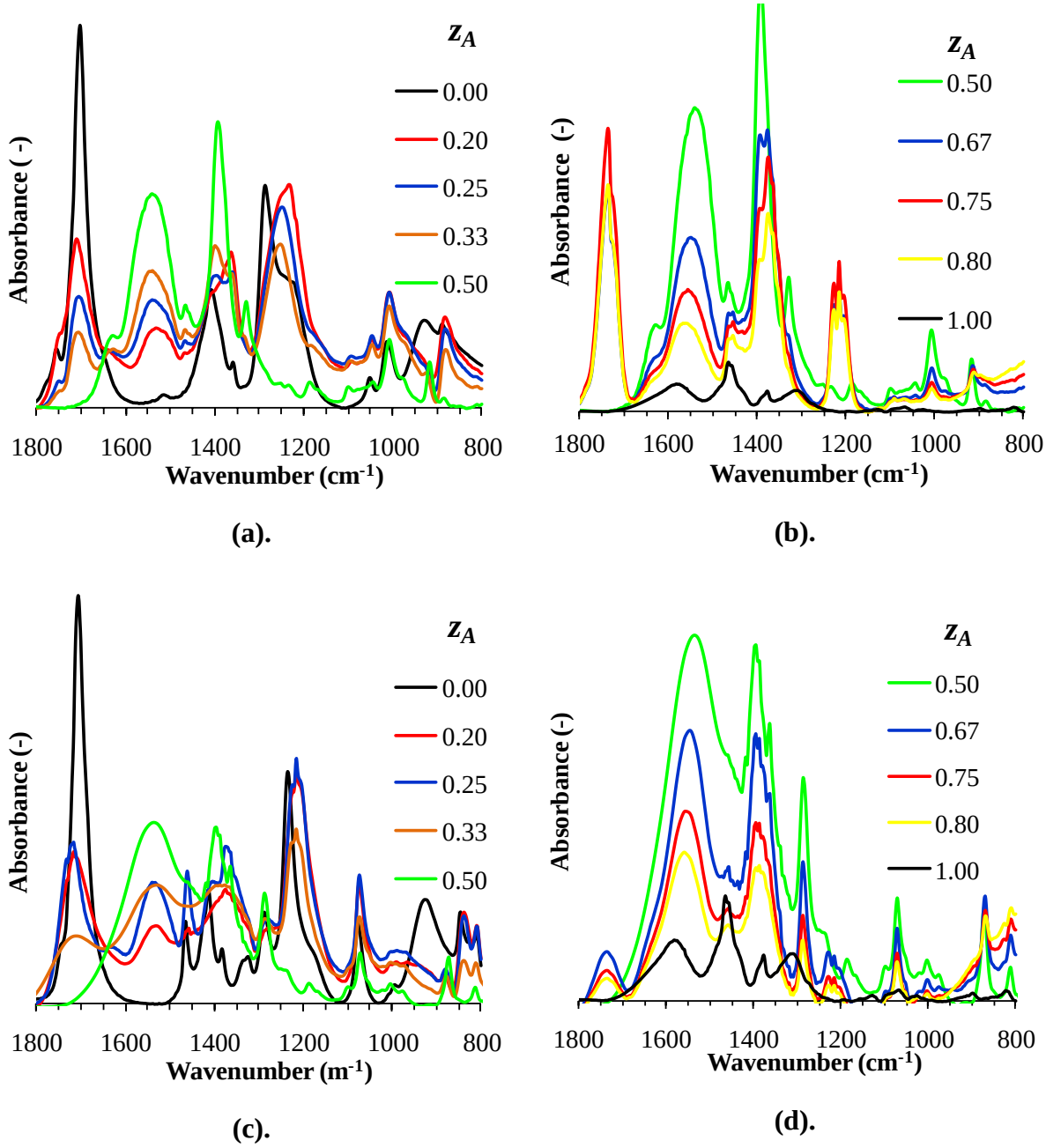

Figure B-1: Liquid phase FTIR spectra of (a-b) hexylamine-acetic acid and (c-d) hexylamine-propanoic acid binary mixtures

B-2: Hexylamine-octanoic acid and morpholine-acetic acid binary mixtures

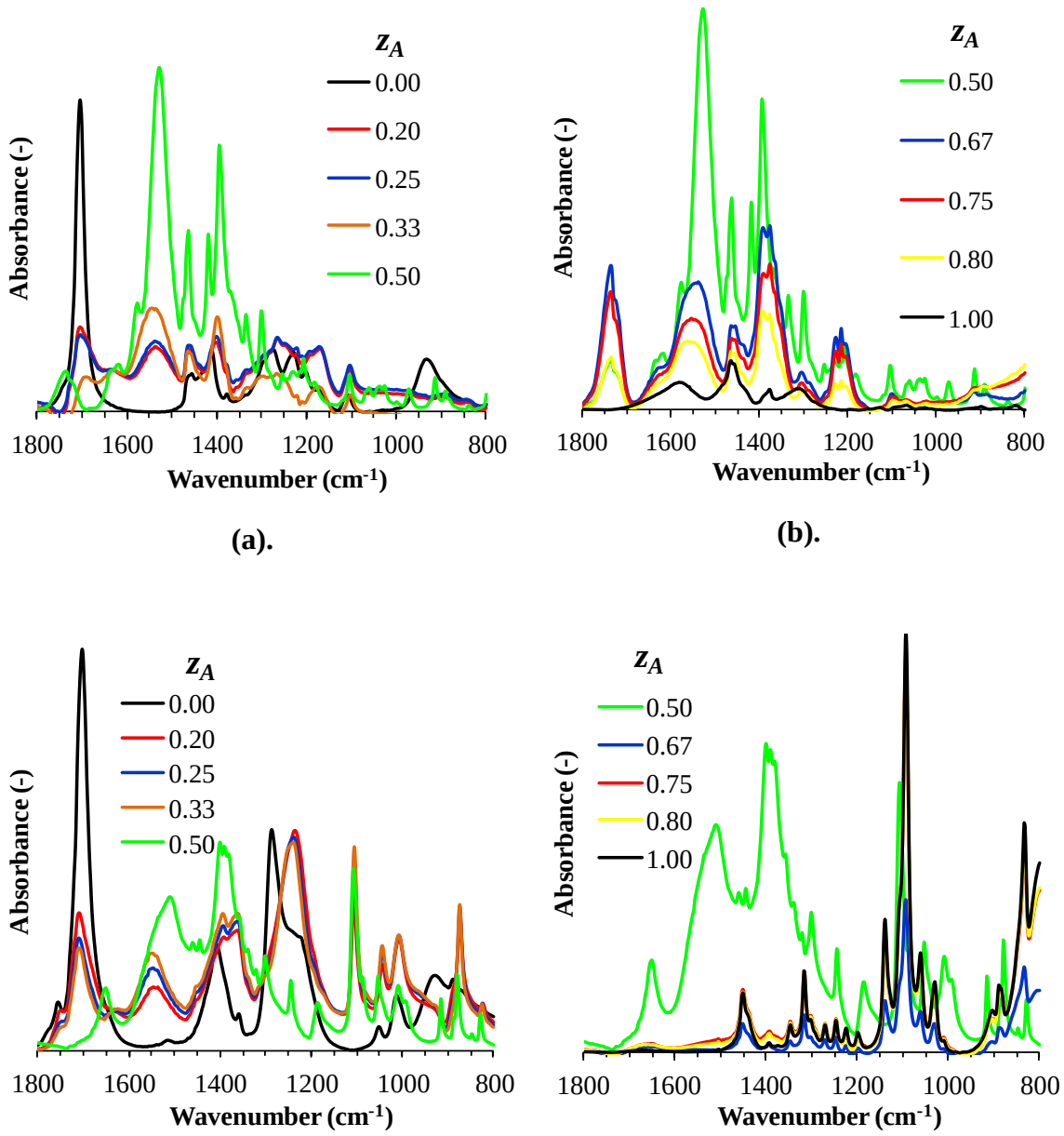

Figure B-2: Liquid phase FTIR spectra of (a-b) hexylamine-octanoic acid and (c-d) morpholine-acetic acid binary mixtures

B-3: Morpholine-propanoic acid and TEA-octanoic binary mixtures

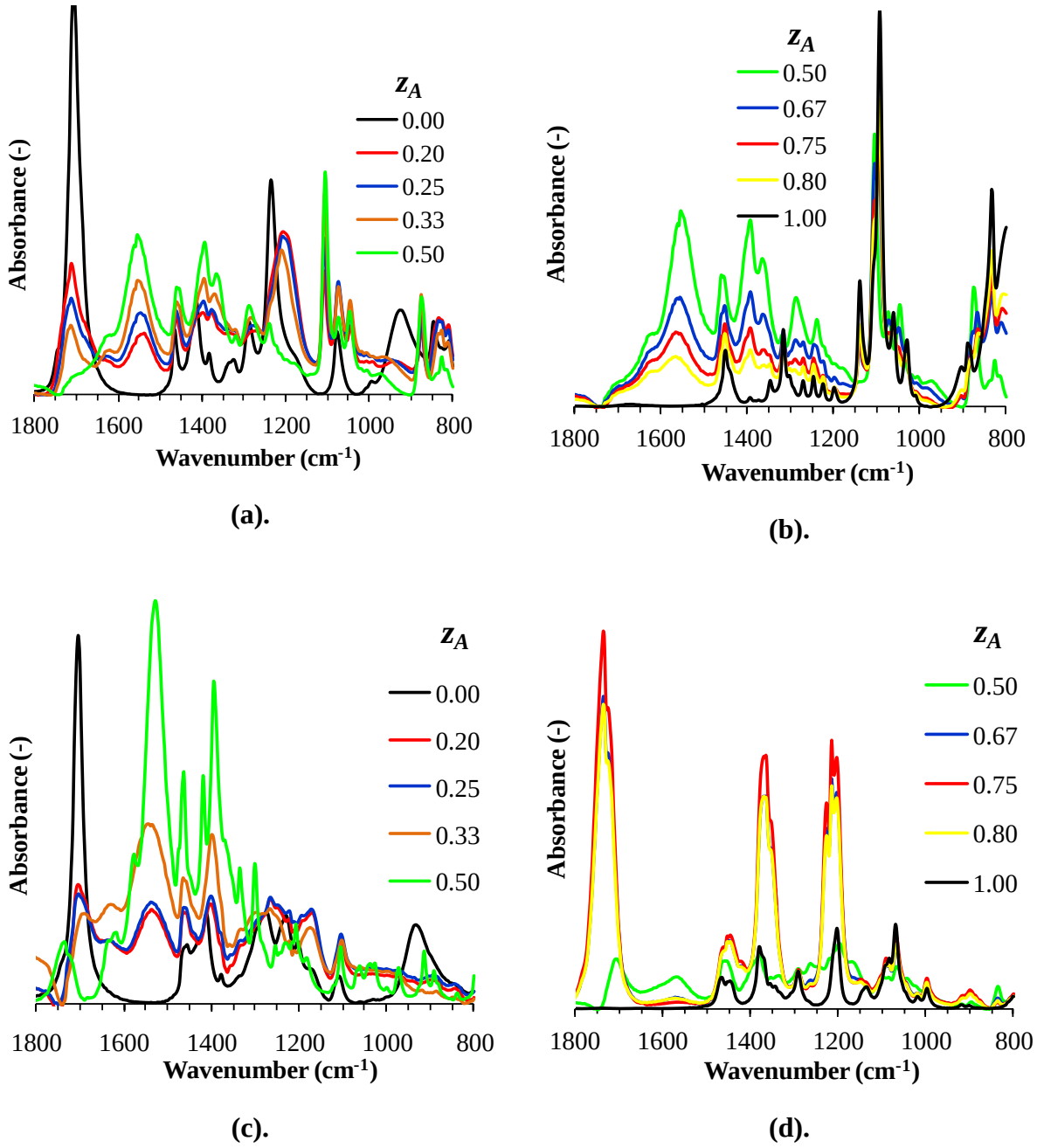

Figure B-3: Liquid phase FTIR spectra of (a-b) morpholine-propanoic acid and (c-d)TEA-octanoic acid binary mixtures

B-4: The effect of liquid phase composition on the absorbance of the FTIR peaks near 1700 cm^{-1}, 1550 cm^{-1} and 1400 cm^{-1}

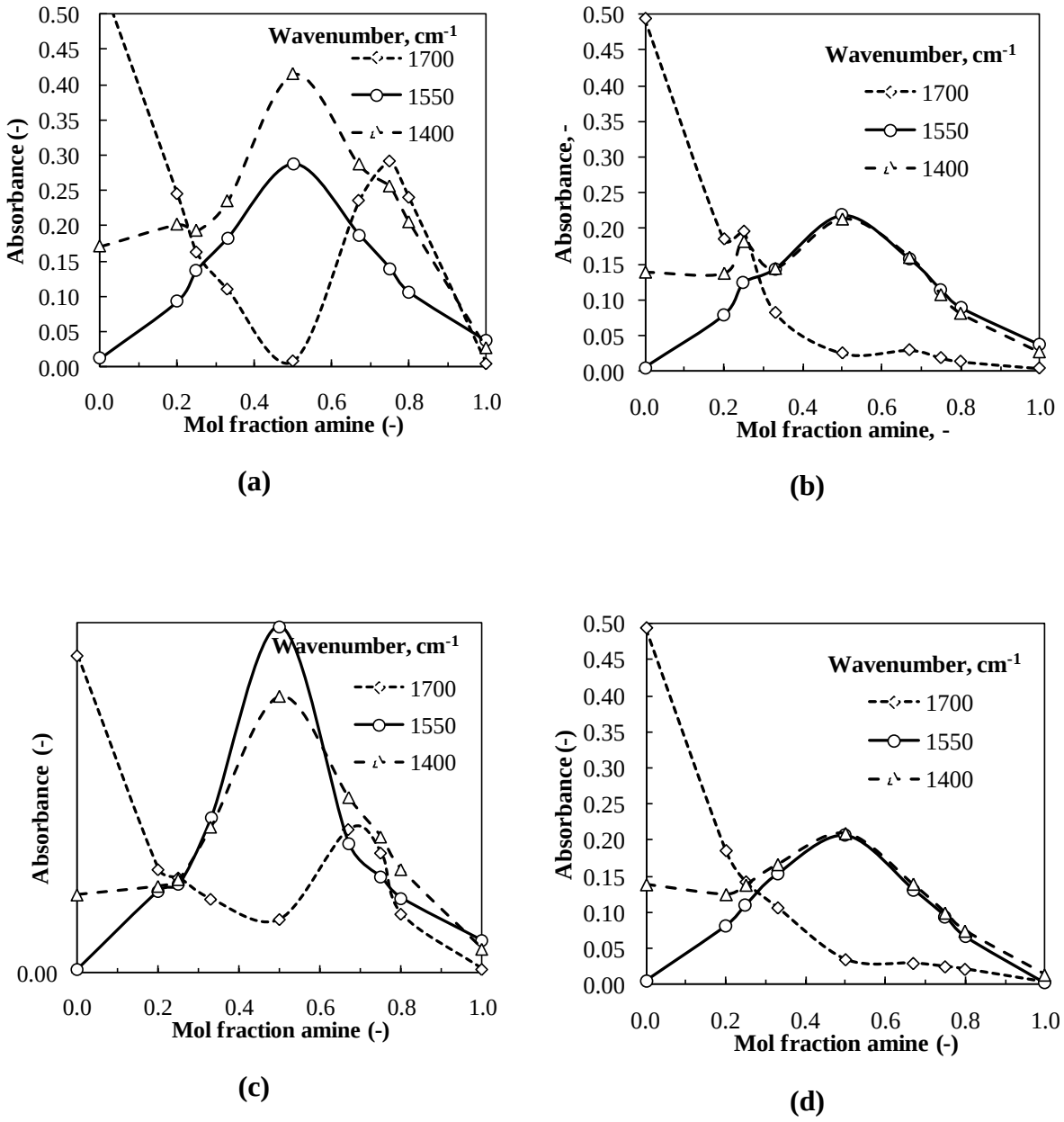

Figure B-4: The effect of liquid phase composition on the absorbance near 1700 cm^{-1}, 1550 cm^{-1} and 1400 cm^{-1} in the FTIR spectra of (a) hexylamine-acetic, (b) hexylamine-propanoic (c) morpholine-acetic and (d) morpholine-propanoic acid

B-5: The effect of liquid phase composition on the absorbance of the FTIR peaks near 1700 cm^{-1}, 1550 cm^{-1} and 1400 cm^{-1}

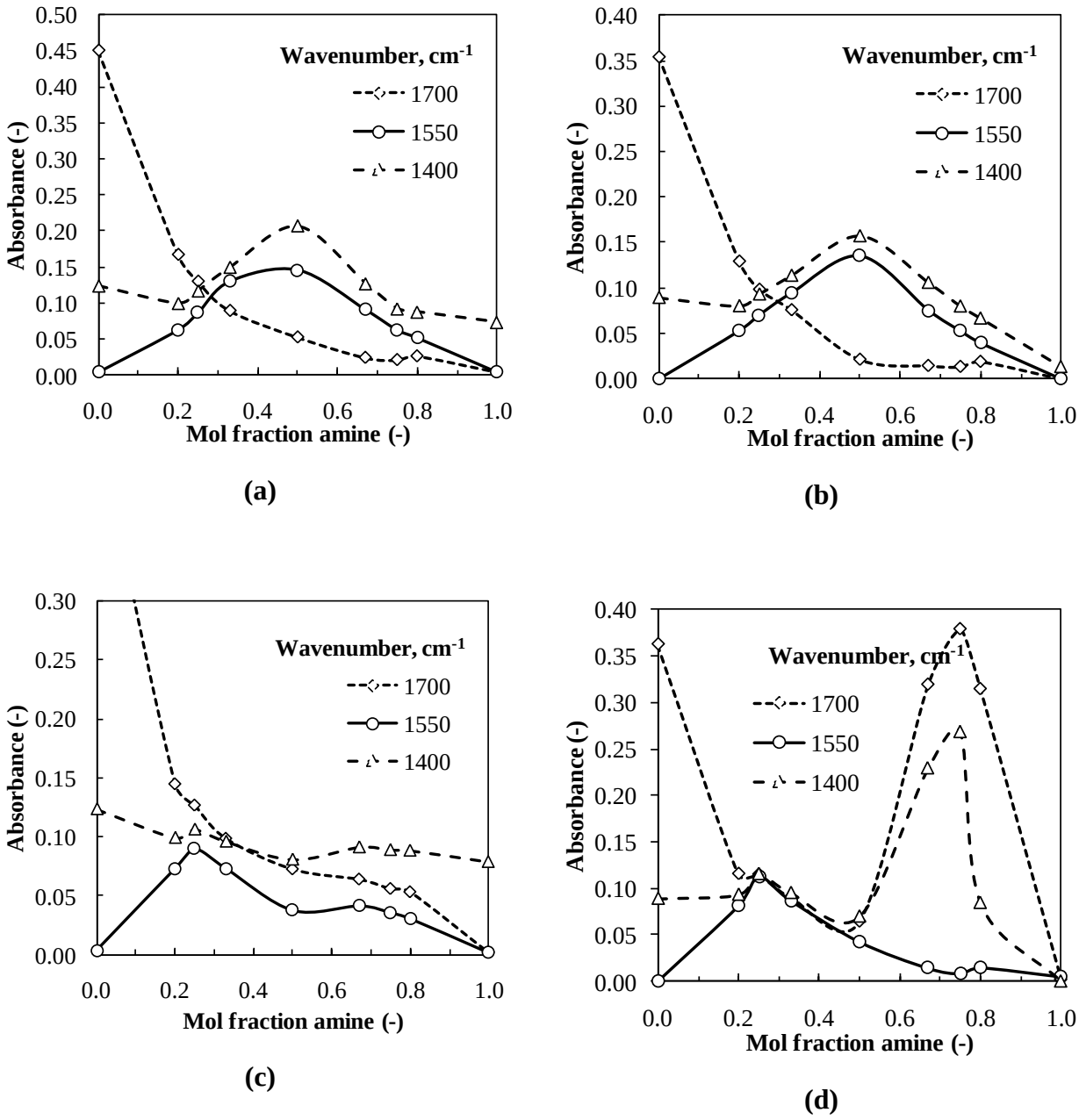

Figure B-4: The effect of liquid phase composition on the absorbance near 1700 cm^{-1}, 1550 cm^{-1} and 1400 cm^{-1} in the FTIR spectra of (a) morpholine-hexanoic, (b) morpholine-octanoic and (c) TEA-hexanoic and (d) TEA-octanoic acid

Appendix C: Time evolution FTIR spectra of binary amine-carboxylic acids

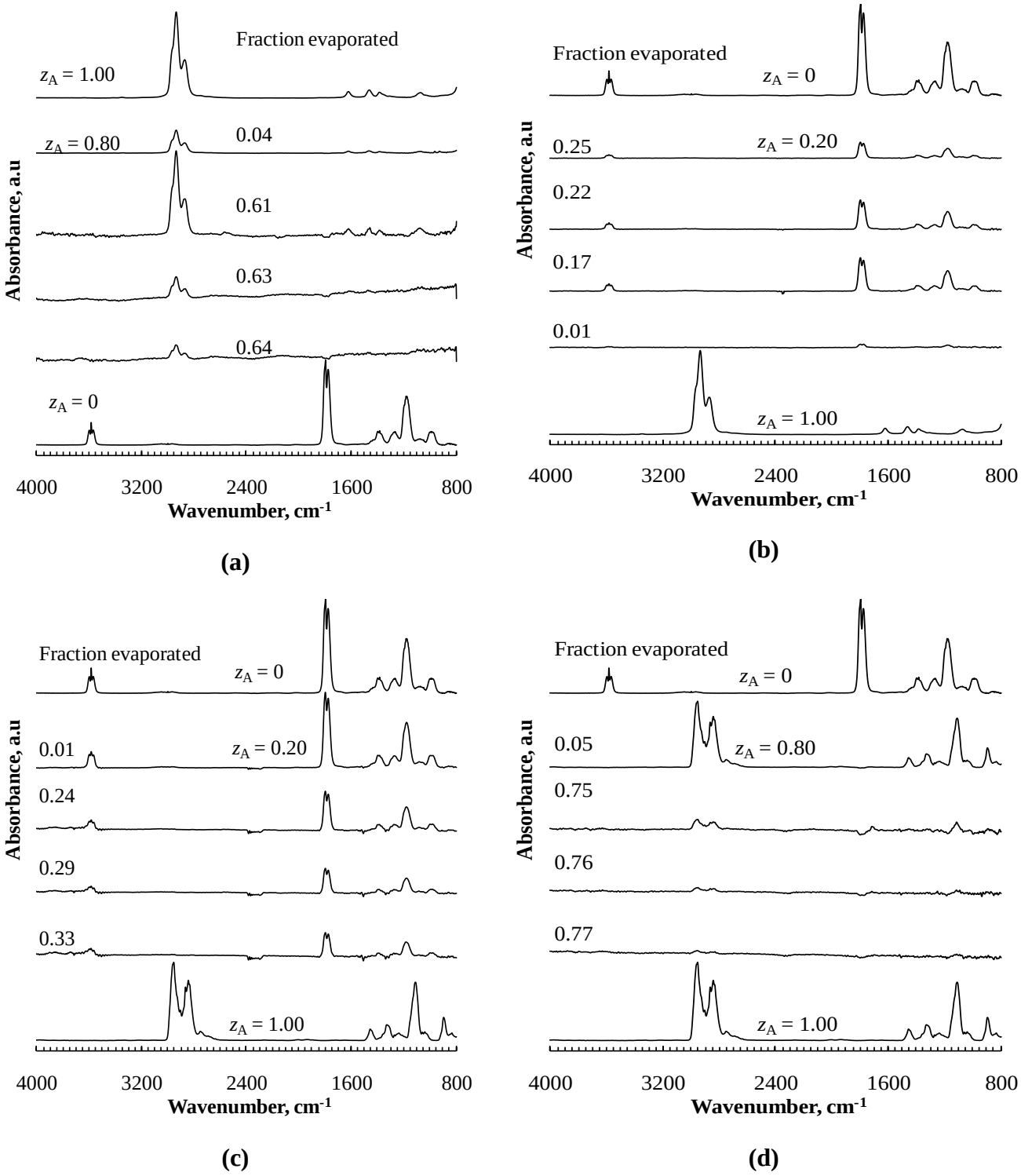

Figure C-1: Time evolution FTIR spectra of (a) and (b) acetic acid-hexylamine; (c) and (d) acetic acid morpholine binary mixtures

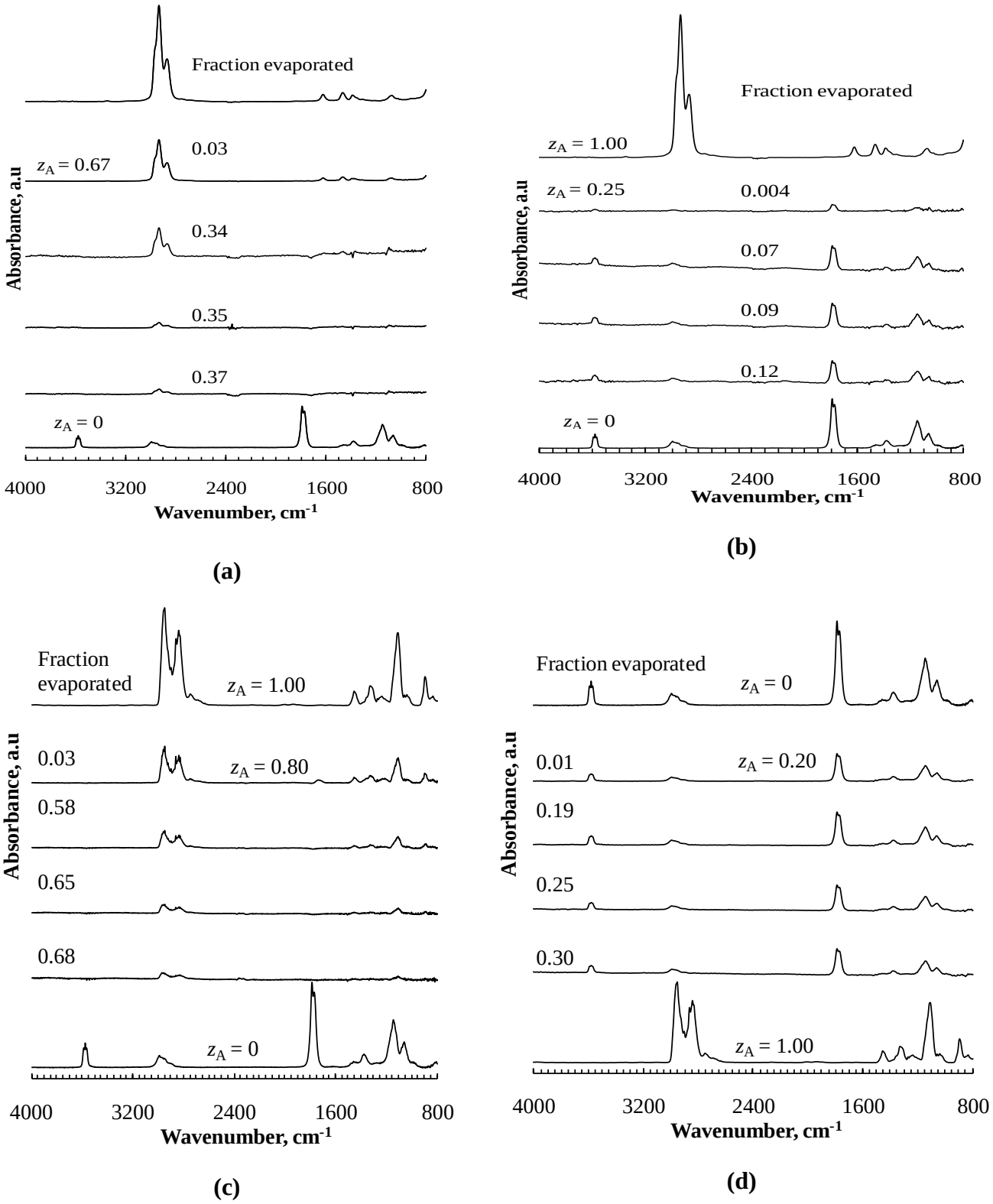

Figure C-2: Time evolution FTIR spectra of (a) and (b) propanoic acid-hexylamine, (c) and (d) propanoic acid-morpholine binary mixtures

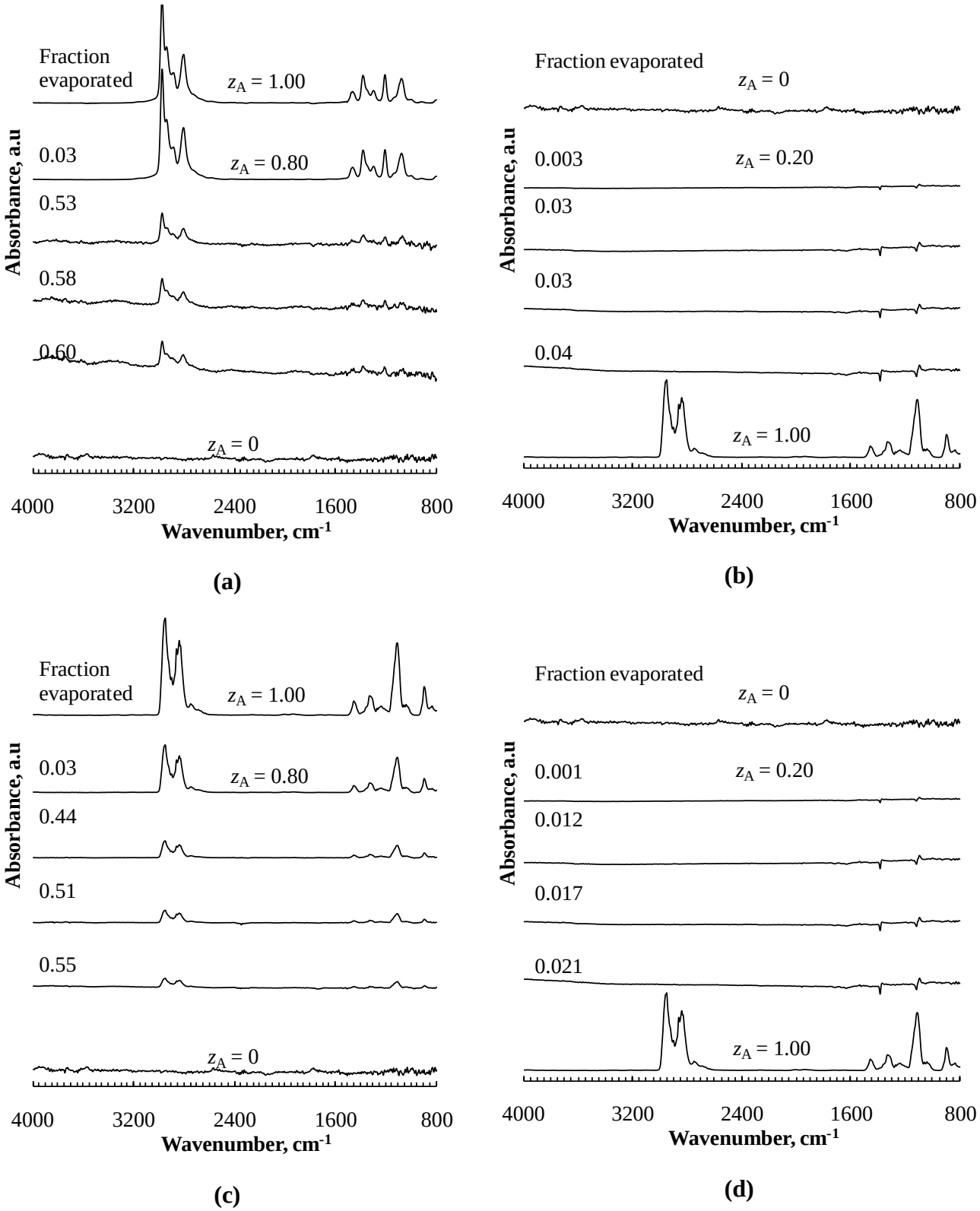

Figure C-3: Time evolution FTIR spectra of (a) TEA-hexanoic acid, (b) morpholine-hexanoic acid, (c) and (d) morpholine-octanoic acid binary mixtures

Appendix D: Calibration curves

D-1: Calibrations curves of pure hexylamine, pure morpholine, pure TEA, and pure formic acid

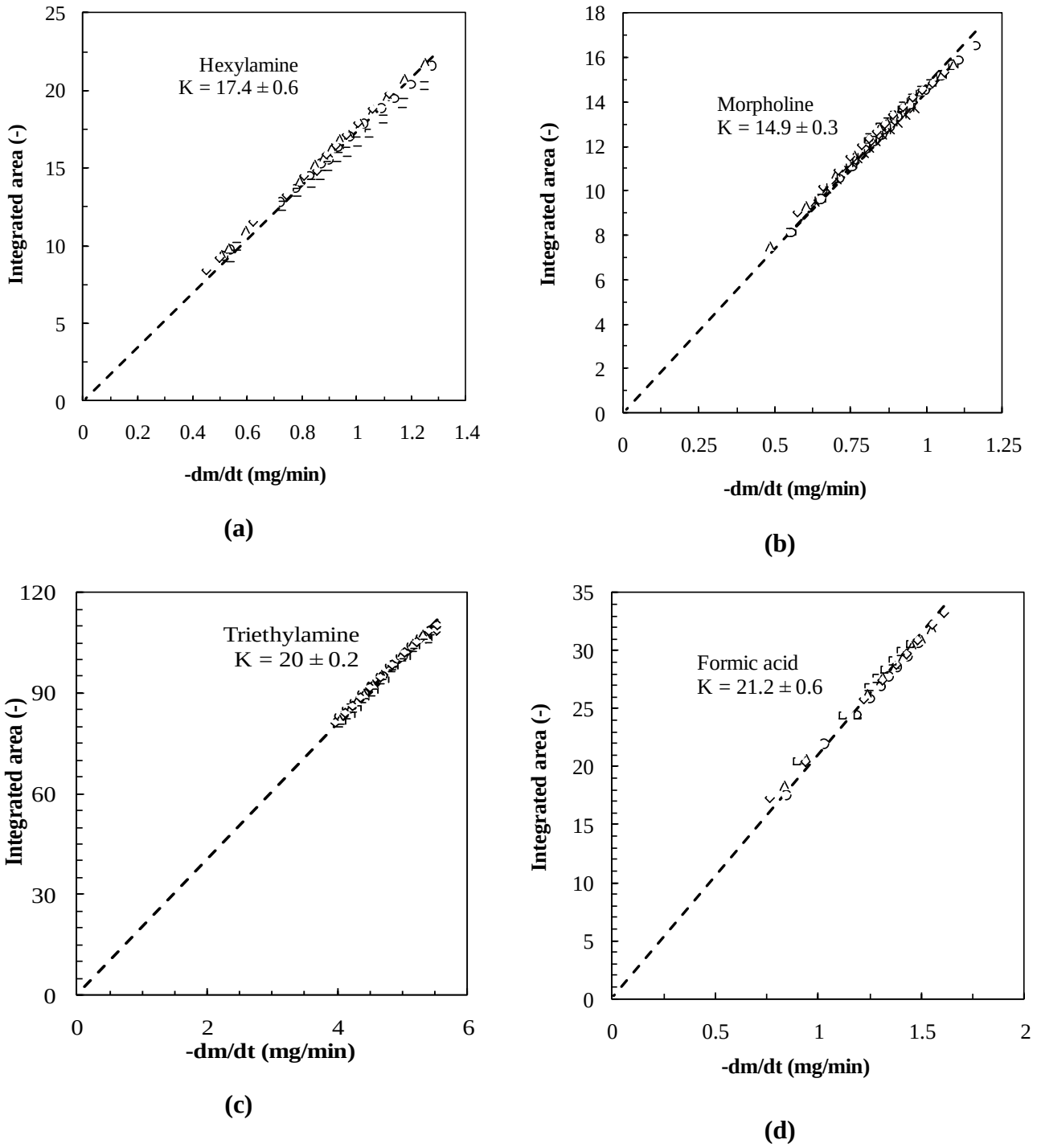

Figure D-1: Calibration curves of (a) pure hexylamine, (b) pure morpholine, (c) pure TEA and (d) formic acid

D-2: Calibration curves of pure acetic acid and pure propanoic acid

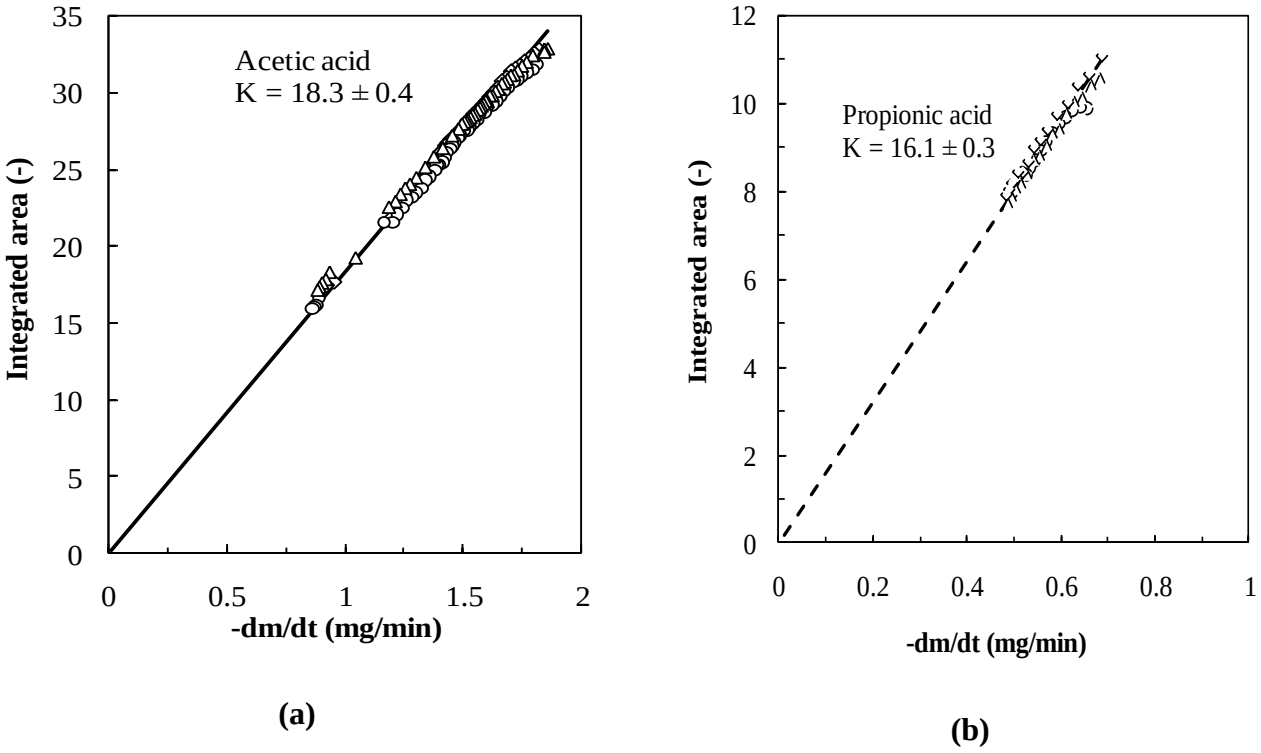

Figure D-2: Calibration curves of (a) pure acetic acid and (b) pure propanoic acid

Appendix E: Shape functions

E-1: Shape of pure components in comparison with the FTIR spectra

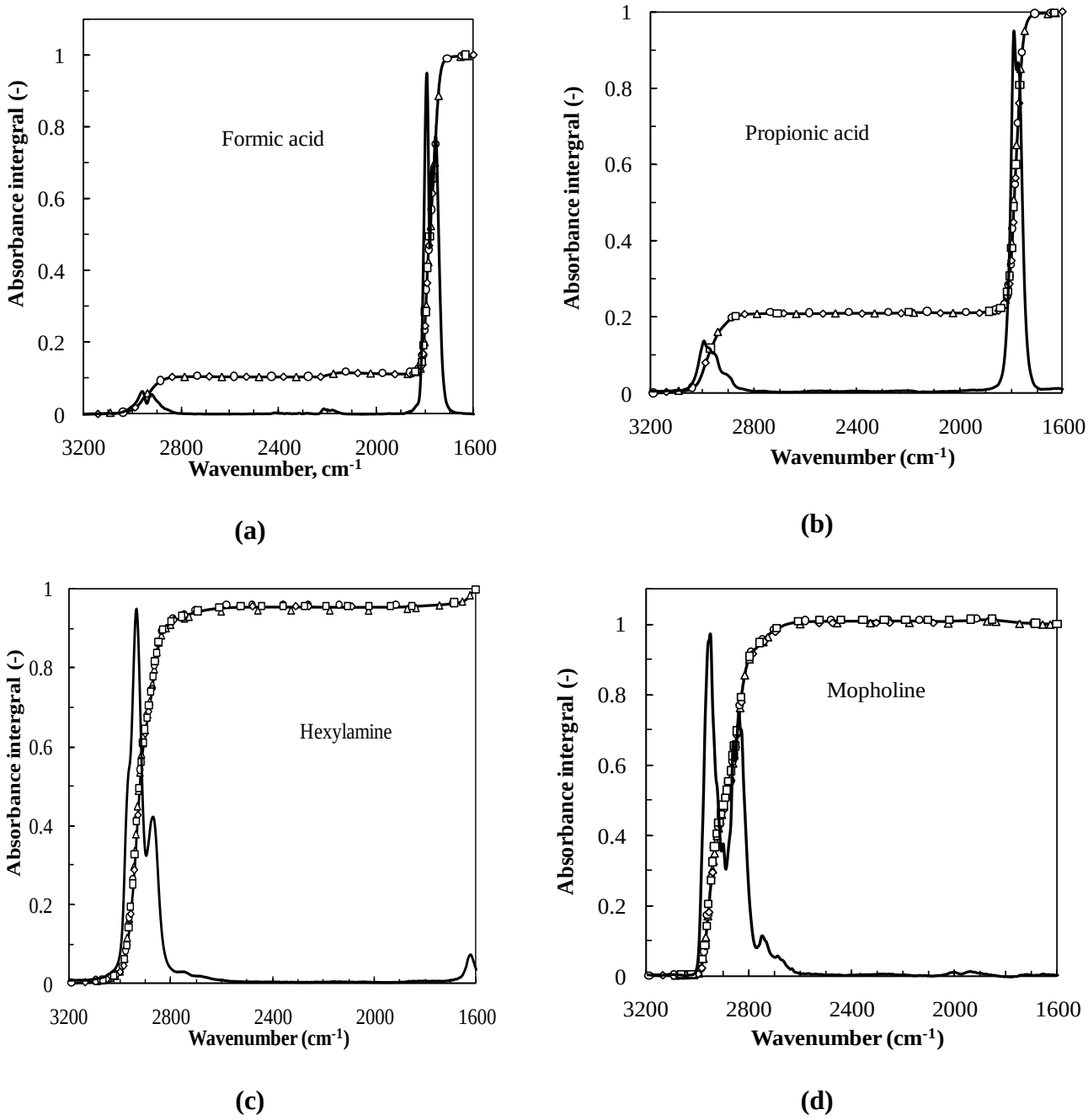

Figure E-1: Absorbance integrals and FTIR spectra of pure components

E-2: Shape of pure components in comparison with the mixtures

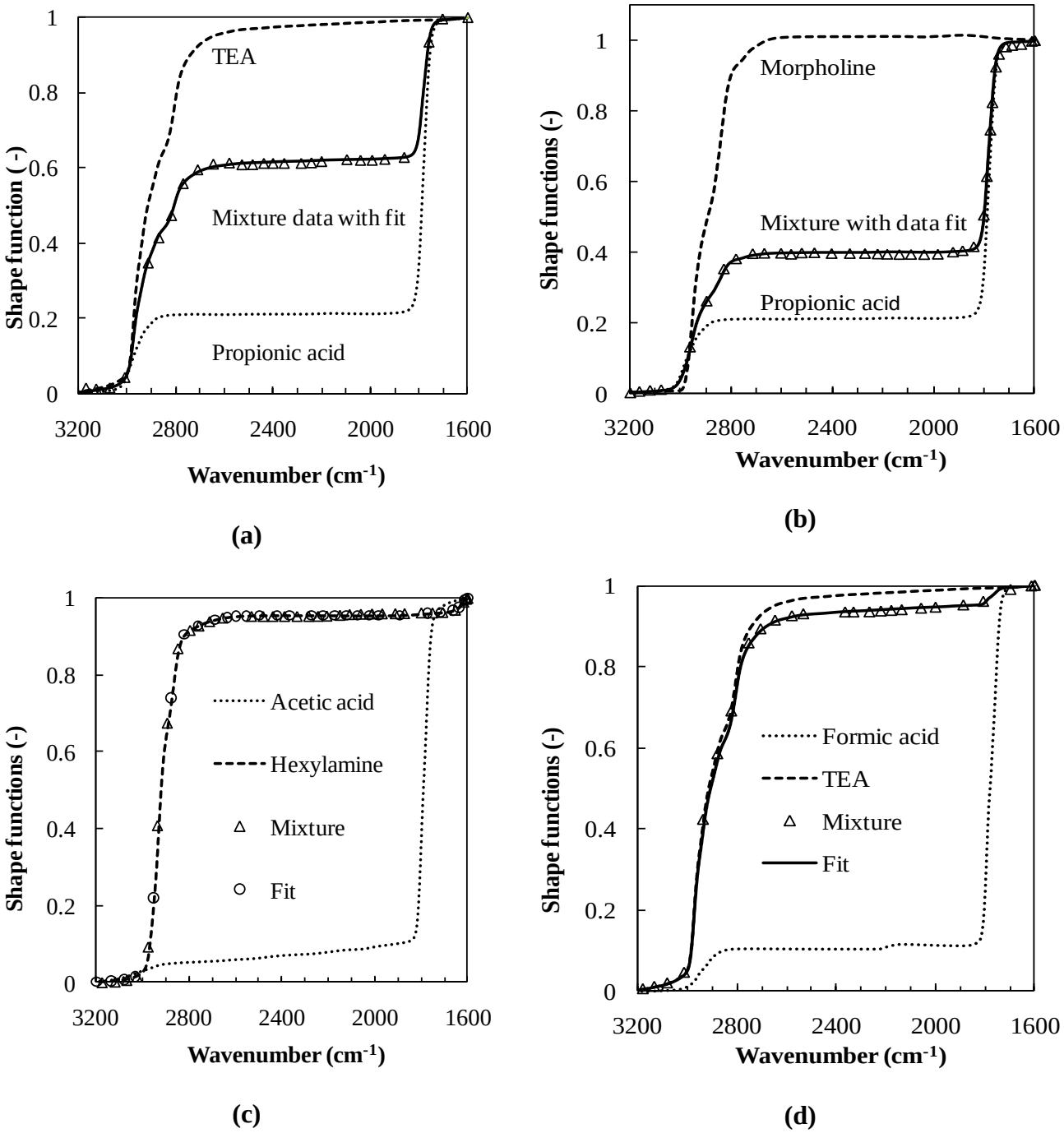

Figure E-2: Shape of pure components in comparison with the mixtures

Appendix F: PiD_{Ai} profiles of pure amines, pure carboxylic acids and their mixtures

F-1: P_iD_{Ai} profiles of pure components

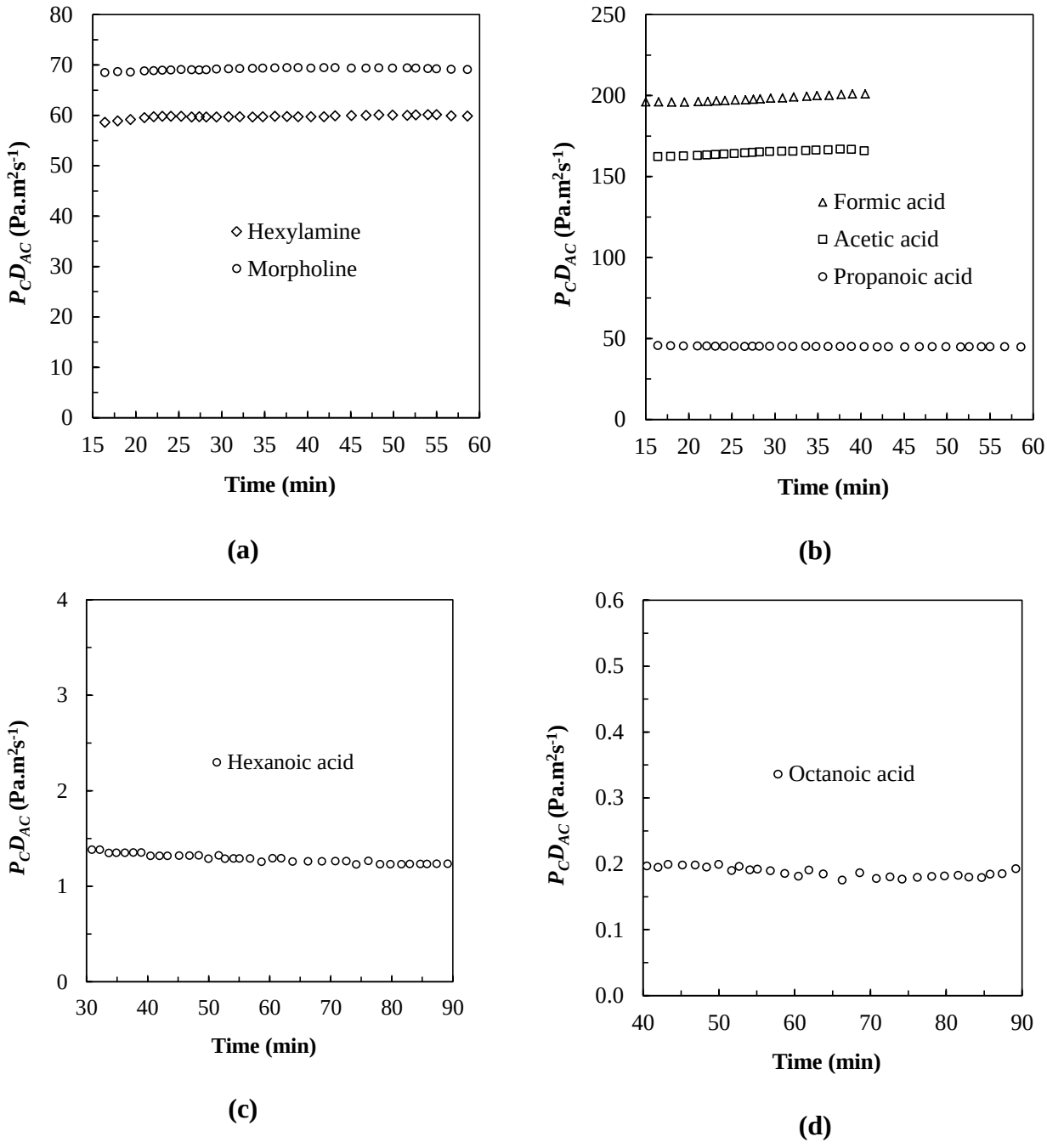

Figure F-1: P_iD_{Ai} profiles of pure (a) hexylamine and pure morpholine, (b) pure formic, acetic, and propanoic acids, (c) pure hexanoic acid and (d) pure octanoic acid

F-2: P_iD_{Ai} profiles of hexylamine-carboxylic acid binary mixtures

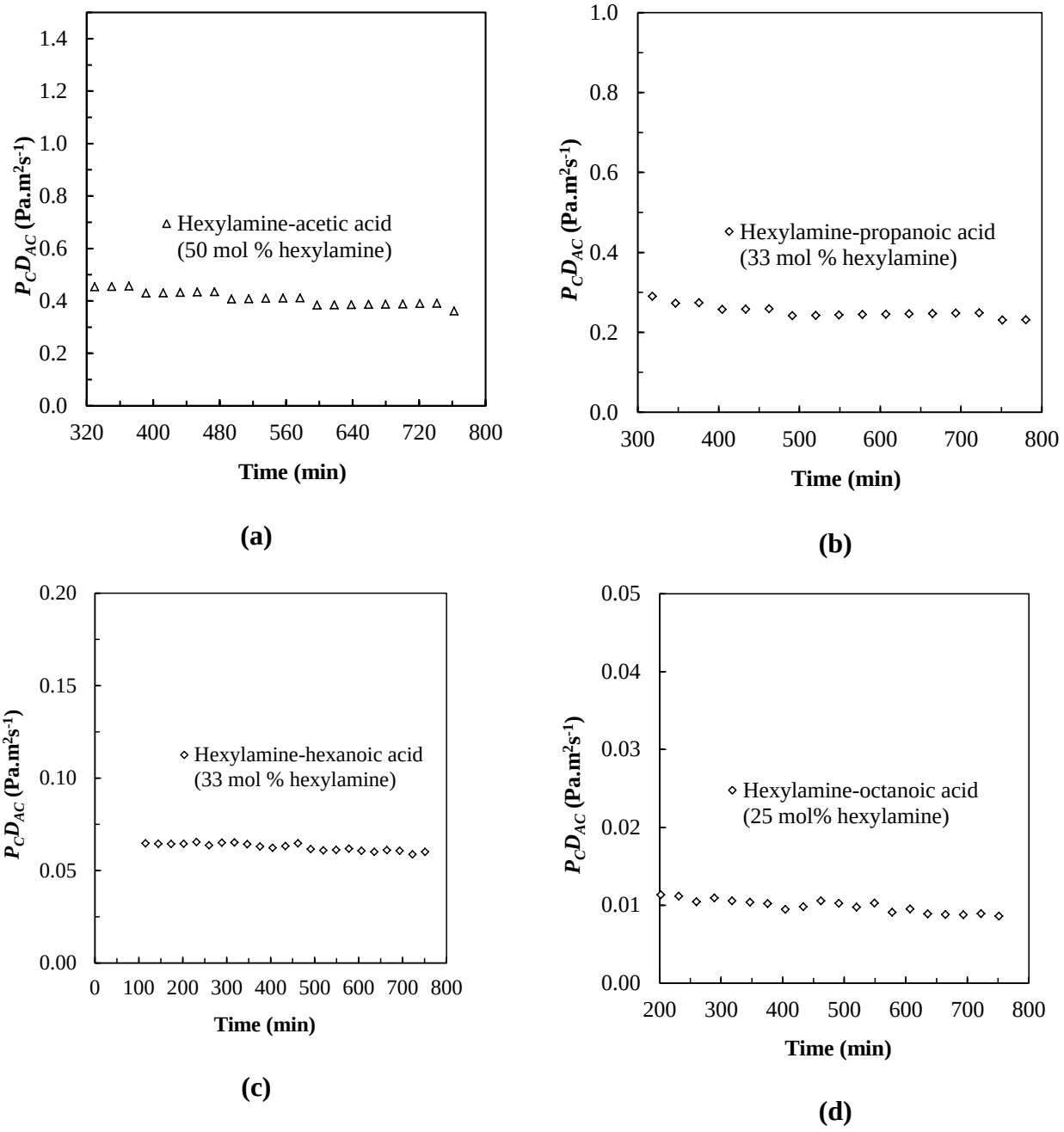

Figure F-2: P_iD_{Ai} profiles of hexylamine-carboxylic acid binary mixtures

F-3: P_iD_{Ai} profiles of morpholine-carboxylic acid binary mixtures

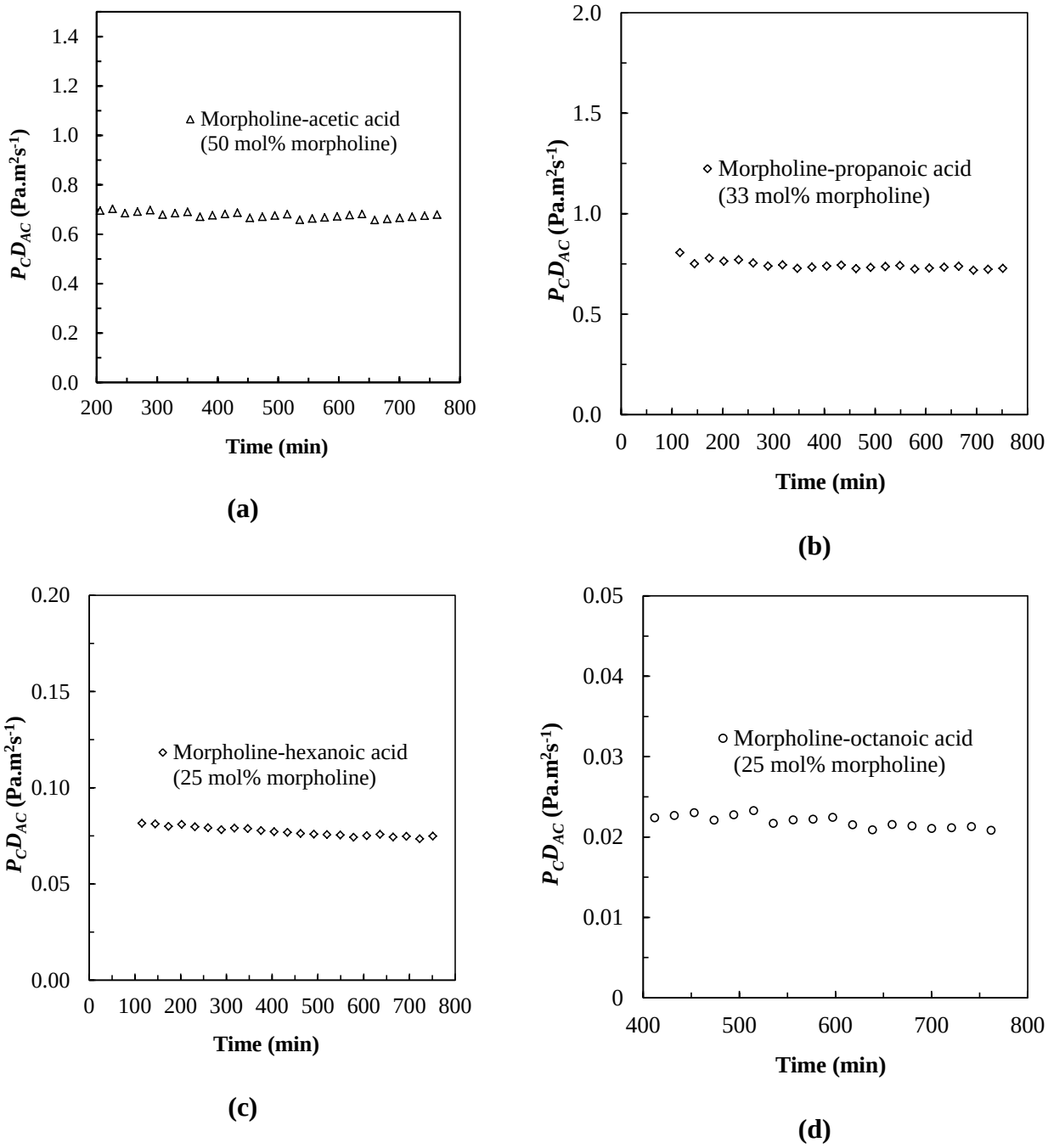

Figure F-3: P_iD_{Ai} profiles of morpholine-carboxylic acid binary mixtures

F-4: P_iD_{Ai} profiles of TEA-carboxylic acid binary mixtures

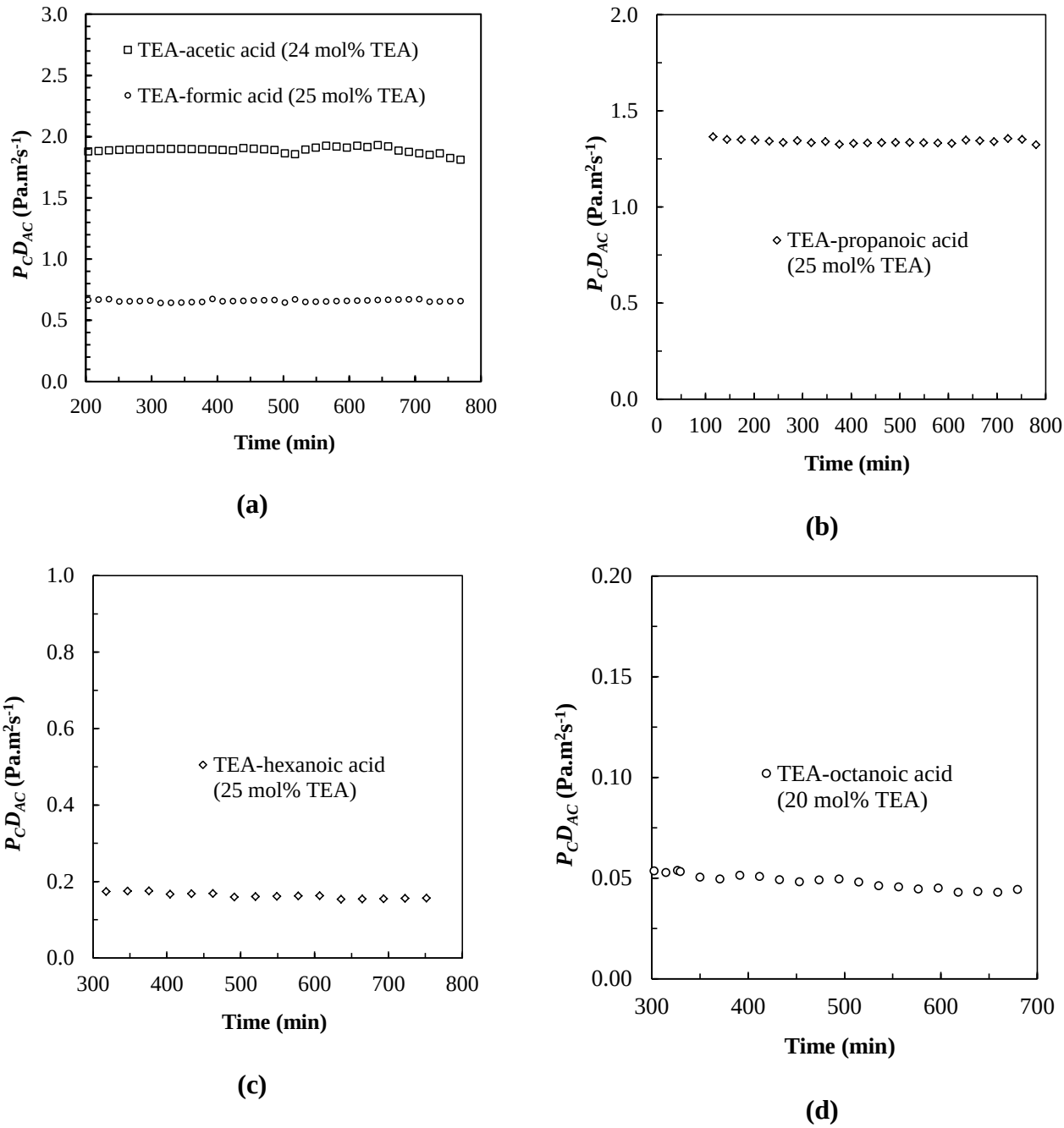

Figure F-4: P_iD_{Ai} profiles of TEA-carboxylic acid binary mixtures